Vapour-Phase Deposition of Functional Nanolayers

PhD thesis

Department of Chemistry
University of Durham
Thomas James Wood

March 2013

Statement of Copyright

Declaration

The work contained within this thesis was carried out at the Department of Chemistry, University of Durham between September 2009 and September 2012. It is the original work of this author (except when otherwise stated) and has not been submitted for a degree at this or any other higher education establishment.

Mikkel Larsen and Peter Lund (IRD Fuel Cells A/S, Denmark) performed ionic conductivity measurements at elevated temperatures in chapter 5. Dr. Wayne Schofield and Hayley Andrews resepectively deposited poly(4-vinylpyridine) and poly(dimethylaminoethyl acrylate) films used in chapter 5. Dr. Richard Thompson (Department of Chemistry, University of Durham) carried out the ion beam depth profiling experiments used in chapter 6. Tracey Davey (Electron Microscopy Services, University of Newcastle) performed all electron microscopy within this thesis (chapters 6–8). Philip Brown prepared the phospholipid-biotin and avidin-fluorescein solutions used in chapter 7.

List of Publications

Work in this thesis has been published, has been submitted for publication or is in preparation for publication as follows:

Articles

1. "Single Step Solventless Deposition of Highly Proton-Conducting Anhydride Layers" Wood, T. J.; Schofield, W. C. E.; Badyal, J. P. S. *J. Mater. Chem.* **2012**, *22*, 7831.

2. "Highly Proton Conducting Composite Sulfonic Acid–Carboxylic Acid Films" Wood, T. J.; Badyal J. P. S. *ACS Appl. Mater. Interfaces* **2012**, *4*, 1675.

3. "Highly Ion-Conducting Poly(Ionic Liquid) Layers" Wood, T. J.; Schofield, W. C. E.; Lund, P.; Larsen, M. J.; Badyal, J. P. S. *Chem. Commun.* **2012**, *48*, 10201.

4. "Ion- and Electron-Conducting, Platinum-Polymer, Nanocomposite Films" Wood, T. J.; Andrews, H. G.; Badyal, J. P. S. *ACS Appl. Mater. Interfaces* **2012**, *4*, 6747.

5. "Atomized Spray Plasma Deposition (ASPD) of Structurally Well-Defined Alkyl Functionalized Layers" Wood, T. J.; Badyal, J. P. S. *Surf. Coat. Technol.*, **2012**, *accepted for publication*.

6. "Anhydride Nanocoatings for Heavy Metal Cadmium Capture and Release" Wood, T. J.; Schofield, W. C. E.; Badyal, J. P. S. *in preparation*.

7. "Oxidative Atomized Spray Deposition of Electrically Conductive Poly(3,4-Ethylenedioxythiophene)" Wood, T. J.; Badyal, J. P. S. *in preparation*.

8. "Atomized Spray Plasma Deposition of Structurally Well-Defined Bioactive Coatings" Wood, T. J.; Ward, L. J.; Brown, P. S.; Schofield, W. C. E.; Badyal, J. P. S. *in preparation*.

9. "Super-Adhesive Polymer-Silica Nanocomposite Layers for Single Step In-Situ Bonding" Wood, T. J.; Ward, L. J.; Badyal, J. P. S. *in preparation*.

10. "Plasma Deposition of Lithium-Ion Conducting and Anti-Fouling Poly(Di(Ethylene Glycol) Ethyl Ether Acrylate) Films" Wood, T. J.; Schofield, W. C. E.; Ward, L. J.; Badyal, J. P. S. *in preparation*.

Patents

1. Wood, T. J.; Schofield, W. C. E.; Badyal, J. P. S. GB Patent Appl. No. 1006886.4, 2010.

2. Wood, T. J.; Badyal, J. P. S. GB Patent Appl. No. 1119867.8, 2011.

3. Wood, T. J.; Badyal, J. P. S. GB Patent Appl. No. 1116025.6, 2011.

4. Wood, T. J.; Badyal, J. P. S. GB Patent Appl. No. 1211393.2, 2012.

5. Wood, T. J.; Badyal, J. P. S. GB Patent Appl. No. 1222841.7, 2012.

6. Wood, T. J.; Badyal, J. P. S. GB Patent Appl. No. 1300409.8, 2013.

Acknowledgments

Many thanks to the following: Professor Jas Pal Badyal, my supervisor for three years of help and guidance (and supervision); all those at Lab 98 who contributed to the general good-natured atmosphere and shared ideas (to whit, Hayley, Phil, Suzanne, Alex, Matt, Olivia, Glenn, Alison and, of course Dr Wayne Schofield PhD DPhil); the technicians various who fixed things I broke (thinking particularly of Peter and Malcolm, the glassblowers, Neil in the mechanical workshop and Kelvin in the electrical workshop); Professor Mike Petty for the use of his impedance spectrometer for three years; Dr Chris Pearson for evaporating gold electrodes and showing me how the clean rooms worked; my wife, Libby, for putting up with chemistry chat and awkward hours kept.

Abstract

Vapour-phase deposition techniques have many advantages including being solventless and providing fine control (down to the nanometre level) of coating thickness. This thesis is about the use of both plasmachemical deposition and oxidative vapour-phase deposition to form functional coatings.

Chapter 1 provides brief reviews of proton exchange membrane fuel cells and vapour-phase deposition techniques as well as an overall introduction to the thesis.

Chapter 2 is a synopsis of the most commonly used experimental techniques used throughout this thesis (especial attention is focused on XPS and FTIR as they are used in every chapter).

Chapters 3–4 record the use of plasmachemical deposition to form proton-conducting coatings for potential use in fuel cells. The strategy described is the use of anhydride precursors in order to produce layers with a high density of carboxylic acids. In chapter 4 these layers themselves are used as initiators to graft sulfonic-acid containing polymer brushes for the enhancement of proton conductivity.

Chapter 5 describes the fabrication of poly(ionic liquid) layers by depositing an imidazole-containing precursor via pulsed plasmachemical deposition, which is subsequently quaternized via a vapour-phase reaction with 1-bromobutane. The resultant coatings show high values of ionic conductivity above 90 °C.

In chapter 6 plasma enhanced chemical vapour deposition of metal(II) hexafluoroacetylacetonate precursors is used in order to produce metal-containing nanocomposite layers. The retention of an organic matrix and its chemical rearrangement under plasma conditions leads to high ionic conductivities.

Chapters 7–8 utilize an atomized spray delivery system and plasma in conjunction with liquid precursor mixtures in order to form bioactive coatings (chapter 7) and nanocomposite layers (chapter 8) which show good adhesion and lithium-ion conductivity values.

Finally chapter 9 utilizes the atomized spray system to deliver high vapour pressures of 3,4-ethylenedioxythiophene in the presence of triflic anhydride which acts as an oxidant. The ensuing vapour-phase reaction yields a conducting polymer coating.

Contents

List of Schemes

List of Figures

List of Tables

Chapter 1

Literature Review and Introduction

1.1 Review: What are fuel cells?

Fuel cells are electrochemical conversion devices, which are supplied continuously by a fuel (normally hydrogen or methanol) and an oxidant (normally air or oxygen).[1] As global efforts are taking place to find alternatives to the combustion engine, fuel cells have emerged as a possibility for automotive, stationary or portable power applications.[2–5]

The reaction of hydrogen and oxygen at catalytic electrodes, separated by an electrolyte (sulfuric acid), resulting in an electric current was first noted, independently, by Grove and Schoenbein in 1839.[6] This effect was then developed by the former into the first functioning hydrogen/oxygen fuel cell (then named the gas voltaic battery), comprising alternating tubes of oxygen and hydrogen with platinum foil as a catalyst, submerged in dilute sulfuric acid, which served as the electrolyte, Figure 1.1.[7]

The first practical design for a fuel cell was invented in 1889, where a porous separator filled with dilute sulfuric acid was used in order to keep the catalyst layer of platinum black dry.[8] After this there was little commercial development until proton exchange membrane fuel cells (PEMFCs, also known as polymer electrolyte membrane fuel cells) were first developed in the early 1960s for use in the Gemini space programme. These first cells were very expensive to manufacture and had short lifetimes, due to their lack of oxidative stability.

A PEMFC consists of a membrane electrode assembly (MEA), which is supplied with fuel and oxidant, Figure 1.2. Hydrogen gas (or sometimes methanol in the case of a direct methanol fuel cell) is catalytically oxidised at the anode according to the following half-reaction: $H_2 \longrightarrow 2\,H^+ + 2\,e^-$. Oxygen is catalytically reduced at the cathode according to the half-reaction: $\frac{1}{2}\,O_2 + 2\,H^+ + 2\,e^- \longrightarrow H_2O$. This gives the overall reaction: $H_2 + \frac{1}{2}\,O_2 \longrightarrow H_2O$ ($E^0 = 1.229$ V). As a result of this chemical reaction a circuit is completed with the protons as the charge carriers across the PEM.

High performance proton exchange membranes therefore have the following requirements: (1) high proton conductivity, (2) low permeability to hydrogen (or methanol) and oxygen, (3)

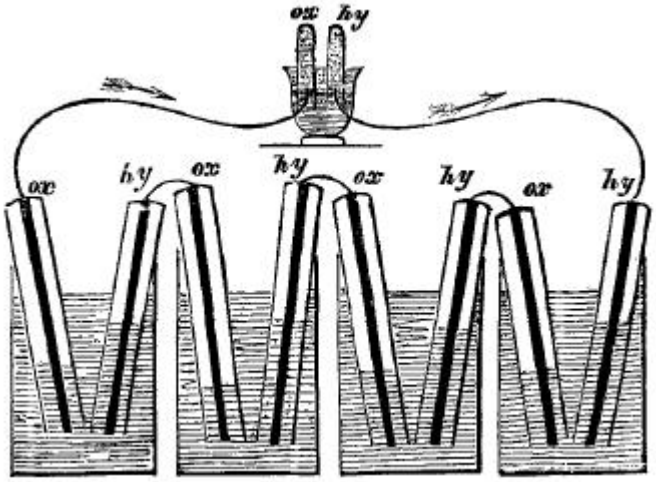

Figure 1.1: The first hydrogen/oxygen fuel cell design: tubes of oxygen and hydrogen alternately submerged in sulfuric acid solution are connected in series to drive the electrolytic separation of water; the thick dark lines represent platinum foil catalyst. Reproduced from reference 7.

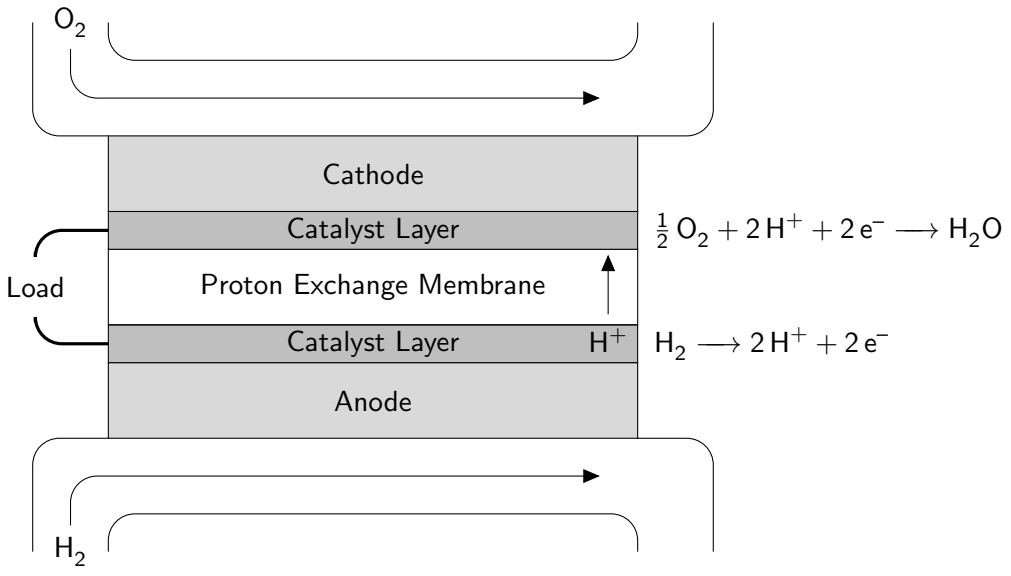

Figure 1.2: Schematic of a proton exchange membrane fuel cell.

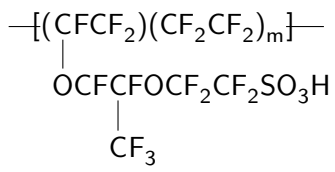

Figure 1.3: Chemical structure of Nafion, where m is usually around 14.

oxidative and hydrolytic stability, (4) adequate mechanical properties to deal with swelling and contracting and (5) low cost.[2] Nafion (a different proton conducting polymer to that used in the Gemini spacecraft) was commercialized later on that decade by the E. I. Dupont Company, primarily for use in the chlor-alkali industry.[9] Since then, it has become the benchmark against which other proton exchange membranes are compared.

Proton exchange membranes must also be able to bind with the catalyst effectively. The catalyst of choice in PEMFCs has been platinum supported on a carbon matrix (in order to increase surface area and allow the gas to permeate). The catalyst layer therefore consists of (i) the proton exchange membrane itself, (ii) platinum on a carbon matrix, (iii) sufficient porosity for gas diffusion. Catalyst is needed at both cathode and anode for the reduction of oxygen and the oxidation of hydrogen. The kinetics for the reduction of oxygen is orders of magnitude slower and so the oxygen reduction reaction is a source of voltage loss in the PEMFC.

1.1.1 Proton Exchange Membrane

Nafion

Whilst Nafion has a plethora of other applications including within the chlor-alkali industry,[9] and as a catalyst (due to its superacidity)[10] the greatest interest has been its use as as a proton exchange membrane. Both Nafion's chemical structure and its morphology in dry and hydrated states are important for understanding its ability to act as an effective proton exchange membrane.

Nafion is produced by the copolymerization of tetrafluoroethene with a perfluorinated vinyl ether monomer, which results in the structure given in Figure 1.3. Nafion films are described by equivalent weight (EW) which is the number of grams of dry Nafion per mole of sulfonic acid groups. The sulfonic acid groups are responsible for the proton conducting ability of the membranes by the proton hopping from one sulfonic acid group to the next: $RSO_3H + RSO_3^- \longrightarrow RSO_3^- + RSO_3H$. The perfluorinated structure of the polymer backbone means that Nafion films are resistant to chemical attack, giving oxidative and hydrolytic stability. The perfluorinated structure near the sulfonic acid groups means that Nafion is very acidic (pKa = -6),[11] and therefore the O−H bond is more labile, which gives good proton conductivity.

The proton conductivity of Nafion is dependent not only on the equivalent weight, but more importantly on the water content, with very low conductivity at low humidity.[12] The reason for this is that the chemical structure of a hydrophobic perfluorinated backbone, along with the

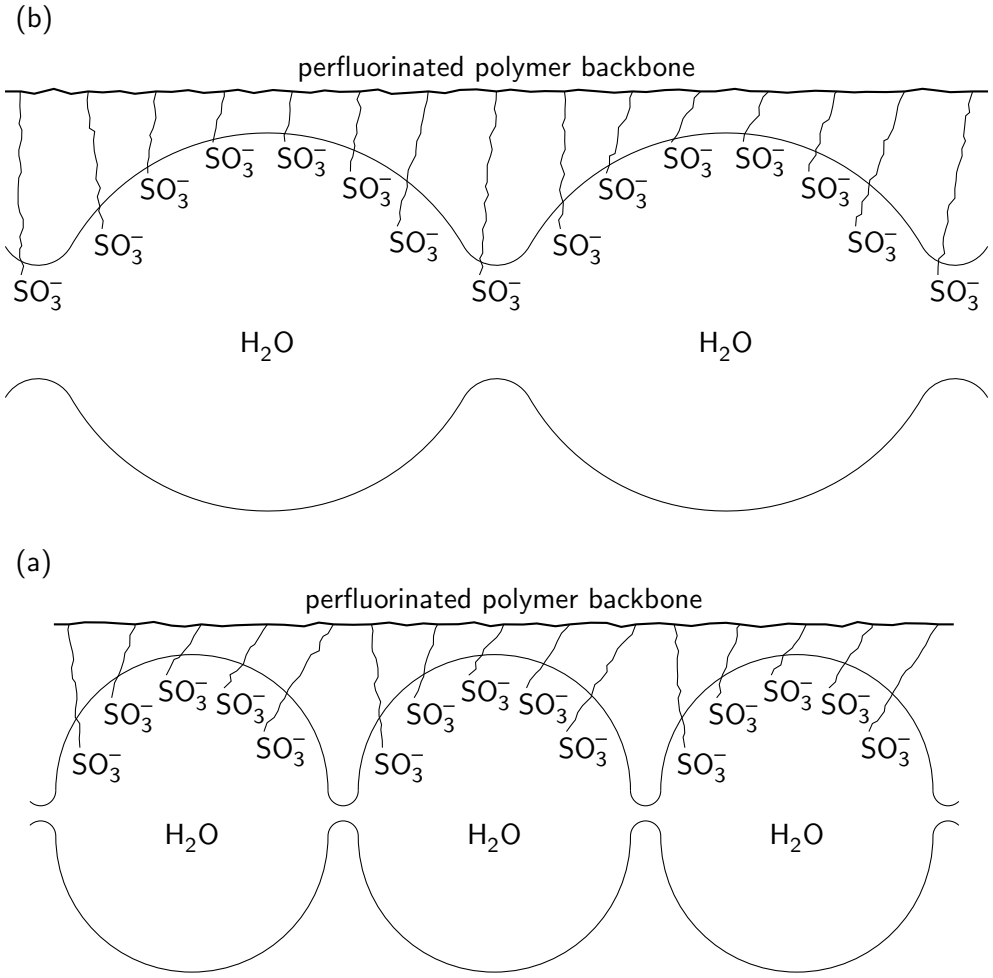

Figure 1.4: Evolution of larger clusters with increased hydration of Nafion from (a) low humidity to (b) high humidity. Adapted from reference 13.

hydrophilic ether group and sulfonic acid, means that there are different morphologies for different levels of water content.

The morphology of Nafion is responsible partly for its mechanical properties and also enables proton conduction across the entire membrane. The hydrophilic parts of the membrane cluster together to form an inverse micelle type structure. When dry, these micelle-like clusters have limited connectivity therefore the proton conductivity is very low. Conceptually, as the Nafion film swells and takes up water, the clusters enlarge and become more connected, Figure 1.4.[13]

Nafion is the benchmark for proton exchange membranes, because of its good conductivity, low permeability to hydrogen and oxygen and good mechanical properties. All these can be traced back to Nafion's chemical structure and changing morphology. The main weaknesses of Nafion are that it is expensive and has low conductivity at low humidity and elevated temperatures (above 80 °C).[14]

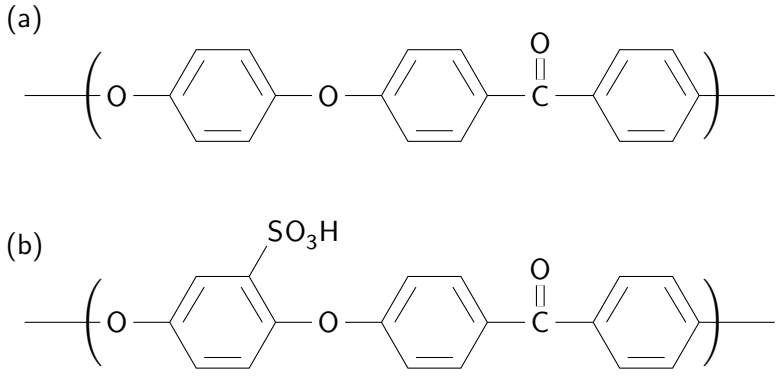

Figure 1.5: Chemical structures of (a) unsulfonated and (b) sulfonated poly(arylene ether ether ketone).

Alternatives to Nafion

With the high cost of Nafion and the other perfluorinated membranes, other polymers have been investigated as to whether a less expensive, viable alternative for proton exchange can be found. The aims of these have been to exclude perfluorination, which is expensive, and yet still retain good proton conductivity along with hydrolytic and oxidative stability.[3] The major alternative systems comprise those based on poly(styrene), poly(arylene ether)s, poly(imide)s and alternatives to sulfonic acid groups.

The advantage of basing polymer membranes on styrene is that styrene monomers are widely available and can be easily tailored to specific functions.[15] There are, at the moment, two commercially produced proton exchange membranes based on styrene: BAM from Ballard Advanced Materials Corporation[16] and a sulfonated styrene–ethylene–butylene–styrene (SEBS) membrane manufactured by Dais Analytic Corporation.[17] Other PEMs based on styrene have been developed, but none commercialized. The majority of these membranes have been made by grafting copolymers onto hydrophobic backbones in an attempt to produce Nafion-like structure, but with less expensive monomers.[18]

Given that perfluorination is expensive, as seen in the cost of Nafion and other perfluorinated membranes, there has been some interest in constructing polymer backbones out of wholly aromatic parts. This would also bypass the weakness of the styrene based membranes, which have shown themselves susceptible to oxidative attack and therefore lack the stability required for higher temperature applications. Whilst several structures have been reported, the most popular polymer used is poly(arylene ether ether ketone) (PEEK), Figure 1.5. Generally sulfonation is carried out after polymerization by using concentrated sulfuric acid.[19] Another possibility is to use sulfonated monomers and then copolymerize, which gives random (or statistical) copolymers.[20] These copolymers can give excellent conductivity as there is a high density of sulfonic acid moieties, but they can also swell (water uptakes of greater than 100 %), which gives inferior mechanical properties.[21]

Five-membered ring poly(imide)s are high performance materials, but when sulfonated they are particularly susceptible to hydrolytic attack and so are unstable within fuel cell applications. The hydrophobicity of the six-membered ring poly(imide)s has been used in conjunction with other sulfonated species (e.g. the sulfonated PEEK above) to form more stable membranes.[22] Part of the idea behind these block copolymers is to recreate the hydrophobic/hydrophilic domains that exist in Nafion, which give its proton conductivity and stability. Questions still remain over the stability of the six-membered ring poly(imide)s, however, and studies carried out have confirmed that the higher the degree of sulfonation of the poly(imide), the lesser the stability.[23]

Nafion and most other proton exchange membranes rely on sulfonic acid groups to conduct protons via exchange with water when the membrane is hydrated. This limits good conductivity in these membranes to below 100 °C, unless pressurized conditions are used. Phosphonic or phosphinic acid containing moieties have not been as well studied, largely due to a more limited breadth of synthetic procedures. However, it is known that phosphoric acid and some polymers with immobilized heterocycles conduct protons via a structure diffusion mechanism.[24] This means that their operation can be extended to temperatures far greater than the boiling point of water. The problems with phosphonic acid based proton exchange membranes is that, despite their improved stability, both chemical and thermal, they are not as acidic as their sulfonated counterparts, which in turn limits their conductivity.[2]

1.1.2 Fuel Cell Catalysts

The catalyst layers are critical in the efficient operation of a fuel cell (especially for the reduction of oxygen). Platinum loaded onto a carbon matrix is by far the most popular catalyst, but, because of the expense of platinum, alternatives have been sought. These can be broadly split into precious metal/alloy catalysts, polymer catalysts and carbon nanotubes.

Platinum and other metal catalysts

Platinum has been the benchmark of proton exchange membrane fuel cell catalysts for some years. It is used for both the oxidation of hydrogen at the anode and the reduction of oxygen at the cathode. Much research has gone into maximising the surface area of the platinum, in order to improve its catalytic ability and to reduce cost. The platinum is usually loaded onto a nanoporous carbon matrix (graphite-like), which ideally will allow the gas to permeate whilst maximising the surface area of platinum loaded onto it. These carbon matrices include carbon black,[25] and ordered hierarchical nanostructured carbon, which is specifically manufactured for the purpose of catalyst loading.[26] There have been many other attempts to increase the surface area and improve the oxidative stability of the carbon matrices by modifying the surface with an organic layer,[27] using carbon nanofibres,[28] and using a carbon black/ionomer/platinum particle ink to deposit catalyst layers.[29] The actual deposition of the platinum onto these carbon supports has been done by electrochemical deposition,[30] chemical bath deposition,[31] a combination of

the two,[31] and chemical vapour deposition.[32] The manufacture of platinum crystallites has also been accomplished along with the deposition of a carbonaceous material onto them (the reverse procedure).[33]

In order to reduce the cost of the platinum catalysts, there have been many alloys produced, especially with non-noble metals to produce core-shell nanoparticles. These are comprised of a core non-noble metal with a shell of platinum on the outside. If the same catalytic activity can be achieved without the need for as much platinum then the manufacturing cost of proton exchange membrane fuel cells will be significantly reduced. The most popular alloys are platinum with iron/copper,[34] ruthenium,[35] cobalt,[36] and ruthenium/nickel.[37]

Alternatives to Platinum

Whilst noble metal based catalysts have been the primary focus of improved catalysis in proton exchange membrane fuel cells, there has been research using polymers as catalysts, in order to overcome both the cost issues, and also the lack of tolerance of the noble metals to carbon monoxide (known as CO poisoning). Conductive polymers have been incorporated with traditional catalytic metal centres (such as platinum or cobalt) with varying degrees of success.[38] There has been recently reported a polymer thin film which displays oxygen reduction catalytic ability in and of itself.[39] At high acidity (pH $= 1$) the platinum is more catalytically active, but at neutral and alkaline conditions, the polymer electrode displays similar catalytic ability.

Carbon nanotubes have been more investigated for their porosity and ability to support a platinum catalyst rather than their intrinsic catalytic ability. Vertically aligned carbon nanotubes functionalized with nitrogen have been found to be better catalysts than platinum in fuel cells under alkaline conditions.[40] Whilst there is no problem with the availability of carbon (unlike platinum), the manufacture thereof into aligned carbon nanotubes is still costly and generally at high temperatures.

Other catalytic systems investigated have been the use of metal (iron or cobalt) porphyrins which display enhanced oxygen reduction catalytic ability when used in conjunction with conductive polymers[41] or carbon nanotubes.[42]

1.1.3 Conclusions about PEMFCs

Current barriers to wide-scale commercialization of PEMFCs in portable and stationary energy sectors are fuel difficulties (i.e. hydrogen is difficult to extract and store) and high cost. The future of the PEMFC within renewable energy will rely on cheaper alternatives to Nafion and platinum being found. These materials will not only be less costly, but very reliable/have long lifetimes.

1.2 Review: Methods for Vapour Deposition of Coatings

Vapour-phase deposition methods can be split into physical vapour deposition (PVD) and chemical vapour deposition (CVD) processes, both of which usually take place under vacuum conditions. The former utilize physical processes in order to effect coating manufacture whereas the latter use chemical reactions.

1.2.1 Physical Vapour Deposition Processes

Physical vapour deposition processes typically comprise one of the following: evaporation, electron beam PVD, pulsed laser ablation, cathodic arc deposition or rf magnetron sputtering. Evaporation is simply the heating of a material under low pressure such that a significant vapour pressure is obtained; the material then condenses on substrates to form a thin coating. Electron beam PVD involves a similar process whereby a focused electron beam is used to provide high enough energy such that the material in question is evaporated followed by coating.[43] Similarly, pulsed laser deposition utilizes a laser focused on a target such that the target material is ablated and coats substrates within the vicinity.[44] Cathodic arc deposition and rf magnetron sputtering both use plasma discharges in conjunction with a target in order to induce ionization in the case of the former[45] (due to the high powers used) and bombardment leading to material sputtering in the case of the latter[46] (and subsequent deposition in both cases). While physical vapour deposition techniques are well suited for forming thin films of inorganic coatings, they are generally not suited to less robust, organic coatings due to the high temperatures and harsh conditions created by the methods of vaporization.

1.2.2 Chemical Vapour Deposition Techniques

Chemical vapour deposition processes can be split into thermal CVD, plasma enhanced CVD, direct liquid injection CVD and aerosol assisted CVD.

Thermal chemical vapour deposition makes use of organometallic precursors (i.e. metal centres of interest with organic ligands) to provide a higher vapour pressure of the material in question. Depending on processing conditions, the organic ligands are removed by the high temperatures which leaves an inorganic coating, e.g. metal oxide.[47] Plasma enhanced chemical vapour deposition utilizes a similar setup to thermal CVD, but instead of requiring very high temperatures, the use of a plasma can yield the same effect of removing any organic ligands leaving an inorganic coating.[48]

Direct liquid injection and aerosol assisted chemical vapour deposition both utilize a form of liquid introduction to bypass problems to do with low vapour pressures/high temperatures. The former uses a liquid precursor mixed with a carrier gas (such as nitrogen) at temperatures under 200 °C in order to provide a high concentration of vapour.[49] The latter utilizes a precursor dissolved in a solvent which is introduced into the deposition chamber via an aerosol spray delivery

system.[50]

1.2.3 Other Vapour-Phase Deposition Methods

The above vapour-phase deposition coating techniques generally require high temperatures (i.e. above 100 °C), which are unsuitable for many substrates (e.g. textiles). These processing conditions are also not viable for the manufacture of organic-containing films. Vapour-phase processes that are carried out at low temperatures are comprised of plasmachemical deposition, oxidative chemical vapour deposition and initiated chemical vapour deposition.

Plasmachemical deposition is also known as plasma polymerization and involves introducing an organic precursor into a non-isothermal plasma such that excited organic species are formed, which then react at the surface of substrates to produce organic coatings.[51] This process is described in more detail in section 2.1 (page 27).

Oxidative chemical vapour deposition is most often used for the manufacture of conducting polymers such as poly(3,4-ethylenedioxythiophene). It entails introducing monomer vapour in the presence of an oxidant, which is either in vapour form or already deposited on the substrate. The redox reaction that takes place at the surface produces a polymer coating.[39,52–55]

Initiated chemical vapour deposition utilizes conventional organic monomer vapour in conjunction with initiator vapour. Both these are introduced into a chamber with heated filaments, which provide the energy to start the polymerization reaction. The substrate to be coated is cooled and so the initated monomers condense thereon producing polymeric coatings.[56]

1.2.4 Conclusions about Vapour-Phase Deposition

Vapour-phase deposition techniques have numerous advantages in that they are conformal, solventless and enable fine control over coating thickness (down to the angstrom range). There are some serious limitations, however, including the unsuitability of physical vapour deposition processes for producing organic-containing films (due to the harsh processing conditions) and the requirement of high temperatures or exotic precursors for several chemical vapour deposition processes. The utilization of low-temperature vapour-phase deposition techniques therefore can combine the advantages of low temperature and conventional precursors with conformal coatings without the need for solvents.

1.3 Introduction

This thesis is concerned with the use of vapour-phase deposition techniques in order to fabricate thin films for use in proton exchange membrane fuel cells. Chapter 3 expounds the use of pulsed plasmachemical deposition to create both carboxylic acid- and anhydride-containing films. Whilst the proton conductivity the maleic anhydride based films are good (on a par with Nafion under

similar conditions), in chapter 4, a sulfonate-bearing polymer (poly(sodium 4-styrenesulfonate)) is grafted from the anhydride-containing films in order to further improve the proton conductivity.

Such films which contain carboxylic acid and sulfonic acid groups rely on a proton hopping mechanism in the presence of water (as in the case of Nafion films). At higher temperatures than 90 °C, therefore these films are not able to conduct protons since there is no water present. In chapter 5 pulsed plasmachemical deposition is used to make imidazole-containing films which are subsequently quaternized by 1-bromobutane in the vapour phase. This results in a poly(ionic liquid)-like coating with positively charged imidazolium groups and negatively charged bromide ions. The resultant coatings show a high level of ionic conductivity above 90 °C with moderate conductivity up to that point. These films therefore could be advantageous for intermediate temperature fuel cells (100–200 °C), which have the added benefits of not requiring careful water/humidification management and more efficient catalysis.

The advantages of using vapour-phase deposition in order to fabricate proton exchange membranes are that the method is substrate-independent, conformal and there is no requirement for solvent removal post-manufacture. These advantages would be extended if other parts of the fuel cell could be deposited in the vapour phase. In chapter 6, therefore, metal containing precursors (copper(II) and platinum(II) hexafluoroacetylacetonate) are used to coat substrates with a hybrid nanocomposite layer, which has inorganic nanoparticles (copper or platinum) within an organic matrix. This organic matrix can conduct protons due to the formation of carboxylic acid species from the hexafluoroacetylacetonate under plasma conditions. In the case of platinum, the films can electrically conduct due to the percolation effect (where the nanoparticles are close enough to each other within the organic matrix for there to be a significant current due to electrons tunnelling through the potential barrier). These properties (proton and electronic conductivity) combined with platinum's known catalytic ability mean that these coatings could form fuel cell catalysis layers.

Whilst vapour-phase deposition provides many advantages (detailed above), it has significant limitations, none more important than the requirement for a precursor with a high enough vapour pressure. The films fabricated in chapters 3–6 are also limited in their deposition rates—6 nm min^{-1} is not conducive to scale up, since it would take a long time to build up a thick enough coating (nearly three hours per micron). As a result, the rest of the thesis is concerned with the development of a spray plasma deposition process, which combines the advantages of vapour-phase deposition with a much larger precursor feedthrough, thanks to the use of an ultrasonic nozzle introducing a fine mist into the reactor chamber. Using this method therefore allows for non-volatile precursors (including solid-liquid slurries) and yields larger deposition rates. By way of example, chapter 7 details the use of atomized spray plasma deposition (ASPD) to create bioactive coatings—those that immobilize biomolecules (alkyl-containing polymers) and those that are resistant to biomolecules. Within these examples is the deposition of a copolymer, which is enabled by dissolving a solid precursor (ocatadecyl acrylate) into a liquid precursor (dodecyl acrylate).

Further exemplification of the flexibility of the ASPD method is related in chapter 8, where methacryloyl functionalized silica particles are suspended in monomer precursors in order to improve the properties of the resultant polymer coating. This includes 2-hydroxyethyl methacrylate, which forms a strong adhesive bond between substrates when deposited. This bond is further strengthened by the addition of silica particles, which act as crosslinkers to make the polymeric film more robust. A different improvement is shown in the case of the di(ethylene glycol)-containing monomer, where the use of silica particles promotes amorphousness within the final film, which in turn enables ionic conductivity (due to a lithium salt also included in the precursor mixture).

Finally, in chapter 9, the atomized spray deposition process is used without plasma excitation, in order to produce a conductive polymer film (poly(3,4-ethylenedioxythiophene)), which could be used as an electrode for electrochemical devices (e.g. batteries and fuel cells) or in plastic electronics.

Thus, the use of vapour-phase deposition is shown to be a flexible technique for the formation of thin films and coatings with multiple properties, especially for use within proton exchange membrane fuel cells.

1.4 References

[1] Winter, M.; Brodd, R. J. *Chem. Rev.* **2004**, *104*, 4245.

[2] Hickner, M. A.; Ghassemi, H.; Kim, Y. S.; Einsla, B. R.; McGrath, J. E. *Chem. Rev.* **2004**, *104*, 4587.

[3] Steele, B. C. H.; Heinzel, A. *Nature* **2001**, *414*, 345.

[4] Service, R. F. *Science* **2002**, *296*, 1222.

[5] *2010 Annual Report*; Hydrogen and Fuel Cell Technical Advisory Committee, U.S. Department of Energy, 2011.

[6] (a) Grove, W. R. *Phil. Mag.* **1839**, *14*, 127; (b) Schoenbein, C. F. *Phil. Mag.* **1839**, *14*, 43.

[7] Grove, W. R. *Phil. Mag.* **1842**, *21*, 417.

[8] Mond, L.; Langer, C. *Proc. Roy. Soc., (London)* **1889**, *46*, 296.

[9] Connolly, D. J.; Gresham, W. F. U.S. Patent 3,282,875, 1966.

[10] Olah, G. A.; Prakash, G. K. S.; Iyer, P. S.; Tashiro, M.; Yamato, T. *J. Org. Chem.* **1987**, *52*, 1881.

[11] Pathapati, P. R.; Xue, X.; Tang, J. *Renew. Energy* **2005**, *30*, 1.

[12] Zawodzinski Jr., T. A.; Neeman, M.; Sillerud, L. O.; Gottesfeld, S. *J. Phys. Chem.* **1991**, *95*, 6040.

[13] Gierke, T. D.; Munn, G. E.; Wilson, F. C. *J. Polym. Sci.: Polym. Phys. Ed.* **1981**, *19*, 1687.

[14] Kim, Y.-T.; Song, M.-K.; Kim, K.-H.; Park, S.-B.; Min, S.-K.; Rhee, H.-W. *Electrochim. Acta* **2004**, *50*, 645.

[15] Yang, T.; Roelofs, M. G. U.S. Patent Appl. 20080032184, 2008.

[16] Wei, J.; Stone, C.; Steck, A. E. U.S. Patent No. 5,422,411, 1995.

[17] Ehrenberg, S. G.; Serpico, J. M.; Wnek, G. E.; Rider, J. N. U.S. Patent No. 5,679,482, 1997.

[18] Ding, J.; Chuy, C.; Holdcroft, S. *Chem. Mater.* **2001**, *13*, 2231.

[19] Bishop, M. T.; Karasz, F. E.; Russo, P. S.; Langley, K. H. *Macromolecules* **1985**, *18*, 86.

[20] Helmer-Metzmann, F.; Osan, F.; Schneller, A.; Ritter, H.; Ledjeff, K.; Nolte, R.; Thorwirth, R. U.S. Patent No. 5,438,082, 1995.

[21] Wang, F.; Hickner, M.; Kim, Y. S.; Zawodzinski, T. A.; McGrath, J. E. *J. Membr. Sci.* **2002**, *197*, 231.

[22] Wang, L.; Yi, B. L.; Zhang, H. M.; Xing, D. M. *J. Phys. Chem. B* **2008**, *112*, 4270.

[23] Fang, J.; Guo, X.; Harada, S.; Watari, T.; Tanaka, K.; Kita, H.; Okamoto, K. I. *Macromolecules* **2002**, *35*, 9022.

[24] Kreuer, K. D. *J. Membr. Sci.* **2001**, *185*, 29.

[25] Fang, B.; Chaudhari, N. K.; Kim, M.; Kim, J. H.; Yu, J. *J. Am. Chem. Soc.* **2009**, *131*, 15330.

[26] (a) Joo, S. H.; Choi, S. J.; Oh, I.; Kwak, J.; Liu, Z.; Terasaki, O.; Ryoo, R. *Nature* **2002**, *412*, 169; (b) Fang, B.; Kim, J. H.; Kim, M.; Yu, J. *Chem. Mater.* **2009**, *21*, 789.

[27] Yoshida, K.; Kitagawa, H. PCT Intl. Patent Appl. 2009119556, 2009.

[28] Sakamoto, H.; Asai, H.; Kurabayashi, K. Jpn Patent Appl. 2009211869, 2009.

[29] Zuber, R.; Kahli, R.; Knut, F.; Starz, K. U.S. Patent No. 6,156,449, 2000.

[30] Kim, H. Y.; Jeong, N. J.; Lee, S. J.; Song, K. S. Kor. Patent No. 726,237, 2007.

[31] Merzougui, B.; Kandoi, S. PCT Intl. Patent Appl. 2009120204, 2009.

[32] Yamaura, K.; Imazato, M.; Kanemitsu, T.; Sato, N.; Katori, K.; Shirai, K.; Tanaka, K. U.S. Patent No. 6,827,748, 2004.

[33] Jalan, V. M.; Bushnell, C. L. U.S. Patent No. 4,137,373, 1979.

[34] Itoh, T.; Kato, K. U.S. Patent No. 5,096,866, 1990.

[35] Oguri, M.; Inoue, H.; Sasaki, Y.; Asaki, T. Jpn. Patent Appl. 2002222655, 2002.

[36] Kato, M. Jpn. Patent Appl. 2001345107, 2001.

[37] Gorer, A. U.S. Patent No. 6,498,121, 2002.

[38] Bashyam, R.; Zelenay, P. *Nature* **2006**, *443*, 63.

[39] Winther-Jensen, B.; Winther-Jensen, O.; Forsyth, M.; MacFarlane, D. R. *Science* **2008**, *321*, 671.

[40] Gong, K.; Du, F.; Xia, Z.; Durstock, M.; Dai, L. *Science* **2009**, *323*, 760.

[41] Zhou, Q.; Li, C. M.; Li, J.; Cui, X.; Gervasio, D. *J. Phys. Chem. C* **2007**, *111*, 11216.

[42] Zhang, W.; Shaikh, A. U.; Tsui, E. Y.; Swager, T. M. *Chem. Mater.* **2009**, *21*, 3234.

[43] Singh, J.; Wolfe, D. E. *J. Mater. Sci.* **2005**, *40*, 1.

[44] Pappas, D. L.; Saenger, K. L.; Bruley, J.; Krakow, W.; Cuomo, J. J.; Gu, T.; Collins, R. W. *J. Appl. Phys.* **1992**, *71*, 5675.

[45] Sanders, D. M.; Anders, A. *Surf. Coatings Technol.* **2000**, *133–134*, 78.

[46] Tanemura, S.; Miao, L.; Wunderlich, W.; Tanemura, M.; Mori, Y.; Toh, S.; Kaneko, K. *Sci. Technol. Adv. Mater.* **2005**, *6*, 11.

[47] Taylor, C. J.; Gilmer, D. C.; Colombo, D. G.; Wilk, G. D.; Campbell, S. A.; Roberts, J.; Gladfelter, W. L. *J. Am. Chem. Soc.* **1999**, *121*, 5220.

[48] AuBuchon, J. F.; Daraio, C.; Chen, L.-H.; Gapin, A. I.; Jin, S. *J. Phys. Chem. B* **2005**, *109*, 24215.

[49] Li, Z.; Gordon, R. G.; Pallem, V.; Li, H.; Shenai, D. V. *Chem. Mater.* **2010**, *22*, 3060.

[50] Xu, C.; Hampden-Smith, M. J.; Kodas, T. T. *Chem. Mater.* **1995**, *7*, 1539.

[51] Yasuda, H. *Plasma Polymerization*; Academic Press: New York, 1985.

[52] Winther-Jensen, B.; West, K. *Macromolecules* **2004**, *37*, 4538.

[53] Im, S. G.; Gleason, K. K. *Macromolecules* **2007**, *40*, 6552.

[54] Im, S. G.; Olivetti, E. A.; Gleason, K. K. *Appl. Phys. Lett.* **2007**, *90*, 152112.

[55] Chelawat, H.; Vaddiraju, S.; Gleason, K. K. *Chem. Mater.* **2010**, *22*, 2864.

[56] Baxamusa, S. H.; Im, S. G.; Gleason, K. K. *Phys. Chem. Chem. Phys.* **2009**, *11*, 5227.

Chapter 2

Experimental Techniques

2.1 Plasmachemical Deposition

Plasmas consist of a partially ionized gas. They are often referred to as the fourth state of matter because of their differing properties to solids, liquids and gases. The term plasma was coined by Irving Langmuir, who noted that, although plasmas can electrically conduct (due to the significant concentration of charge carriers), the charges are balanced.[1]

Plasmachemical deposition, also known as plasma polymerization, refers to the deposition of polymeric materials/coatings under plasma conditions. The ability of many organic compounds to form waxy deposits when exposed to electrical discharge was for many years regarded as an unwanted by-product,[2] although the potential for forming new chemical species was realized very early on.[3] The waxy hydrocarbons produced, however, were difficult to characterize due to their reactivity (susceptibility to oxidation) and random structure, although average molecular weights above 400 were recorded.[4]

In the 1960s plasmachemical deposits were better characterized and the insoluble properties considered for wider applications.[5] The harsh conditions of a plasma means that chemical rearrangement can easily happen and very high weight, well defined polymers (like those formed by conventional polymerization processes) are difficult to obtain.[6] The next major advance was to pulse the plasma, which gives an unprecedented level of functionality retention. Several chemical functionalities have been put down this way including anhydride, organotin, perfluoroaryl, epoxide and cyano groups.[7–11]

Typically plasma polymerizations are performed under vaccuum (although atmospheric pressure glow discharge polymerization is known[12–14]) with pressures between 0.01 and 10 torr. The applied electric field transfers energy to free electrons in the chamber which are accelerated and collide with gas molecules to form electrons and ions. These electrons are then accelerated in their turn and a self-sustained plasma is formed.[15] Alternating current rf glow discharges can be initiated by a coil outside the reaction chamber. Above 500 kHz free electrons oscillate and gain energy from elastic collisions with gas molecules until they gain enough energy to make inelastic

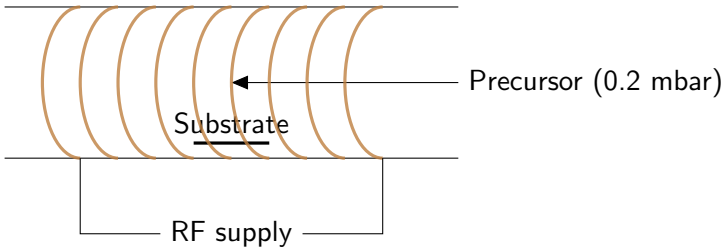

Figure 2.1: Plasma deposition process: precursor vapour is introduced under vacuum and rf is used to generate a plasma using copper coils surrounding the chamber, within which the substrate is located.

collisions, at which point the plasma is initiated.[15]

Typical plasma depositions in this thesis were carried out in an electrodeless cylindrical glass reactor (volume of 480 cm^3, base pressure of 3 x 10^{-3} mbar, and with a leak rate better than, 2 x 10^{-9} mol s^{-1}) surrounded by a copper coil (4 mm diameter, 10 turns), and enclosed in a Faraday cage, Figure 2.1. The chamber was pumped down using a 30 L min^{-1} rotary pump attached to a liquid nitrogen cold trap; a Pirani gauge was used to monitor system pressure. The output impedance of a 13.56 MHz radio frequency (rf) power supply was matched to the partially ionized gas load via an L-C matching unit connected to the copper coil. Prior to each deposition, the reactor was scrubbed using detergent, rinsed in propan-2-ol, and dried in an oven. A continuous wave air plasma was then run at 0.2 mbar pressure and 40 W power for 30 min in order to remove any remaining trace contaminants from the chamber walls. Precursor vapour was allowed to purge the reactor for 5 min at a pressure of 0.2 mbar prior to electrical discharge ignition. For pulsed plasma depositions optimum values for the on-time (t_{on}) and the off-time (t_{off}) were used. Upon plasma extinction, the precursor vapour was allowed to continue to pass through the system for a further 3 min, and then the chamber was evacuated back down to base pressure, prior to venting to atmosphere.

2.2 X-ray Photoelectron Spectroscopy

X-ray photoelectron spectroscopy (XPS) is a powerful technique for analysis of surfaces. Surfaces are irradiated with monoenergetic soft X-rays typically from a Mg Kα or Al Kα source (1253.6 eV and 1486.6 eV respectively). The X-ray photons interact with atoms on the sample surface causing electrons to be emitted via the photoelectric effect. The photoelectrons have measured kinetic energies given by:

$$KE = h\nu - BE - \phi_s \tag{2.1}$$

where hν is the energy of the photon, BE is the binding energy of the atomic orbital from which the electron is ejected, and ϕ_s is the workfunction of the spectrometer. The X-ray photon penetrates solid samples to distances up to between 1 and 10 μm, but since electrons have far

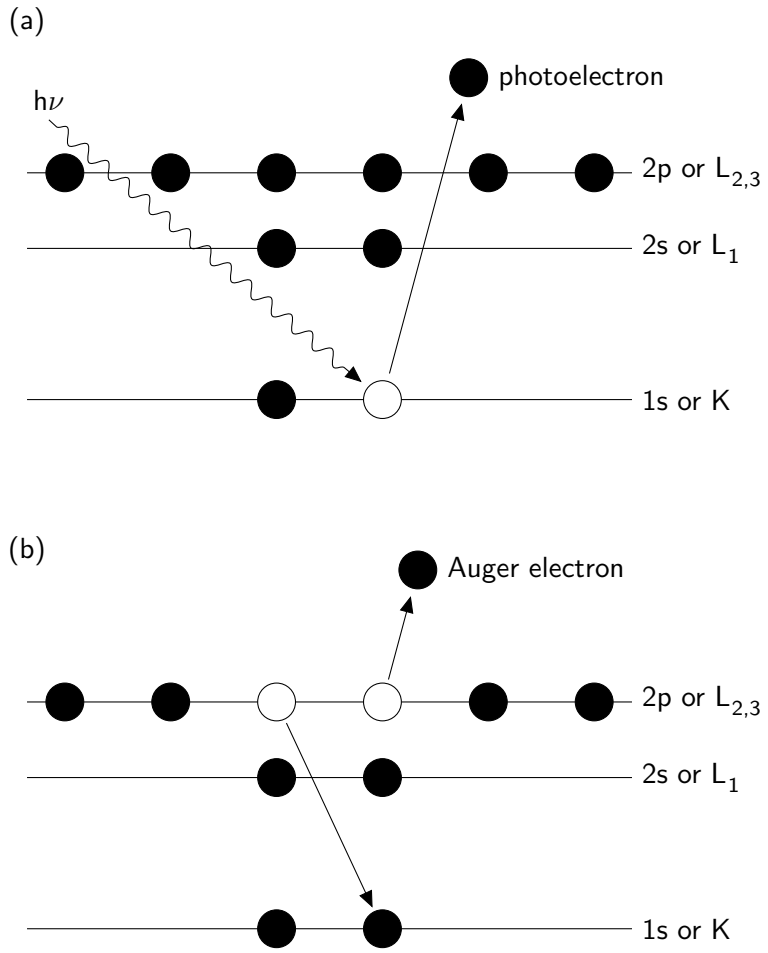

Figure 2.2: XPS emission processes for a model atom: (a) an incident photon causes the emission of a photoelectron from a core level and (b) the relaxation process resulting in emission of a $KL_{23}L_{23}$ electron. Adapted from reference 16.

less penetration, only the first 5 nm of a sample will emit electrons which are detectable.

Each element has its own set of binding energies, therefore XPS can be utilised to identify the individual elements on the surface. By using various standards a quantitative ratio of the elements on the surface can be calculated from XPS spectra. Also, because the binding energy changes with chemical environment, there are chemical shifts in the spectra which give additional information (e.g. the C(1s) peak is shifted by around 8 eV if attached to three fluorine atoms relative to a hydrocarbon-only polymer).[16]

As well as the photoemission process, Auger electrons may be emitted as part of the relaxation process, Figure 2.2. This occurs around 10^{-14} s after the photoemission. The competing relaxation process of X-ray fluorescence is a minor one in this energy range. Therefore, photoionization usually results in two electrons being emitted—a photoelectron and an Auger electron. Auger lines form complex patterns in the XPS spectra, because there are many different relaxation pathways (e.g. theoretically nine for the KLL relaxation process seen in Figure 2.2).

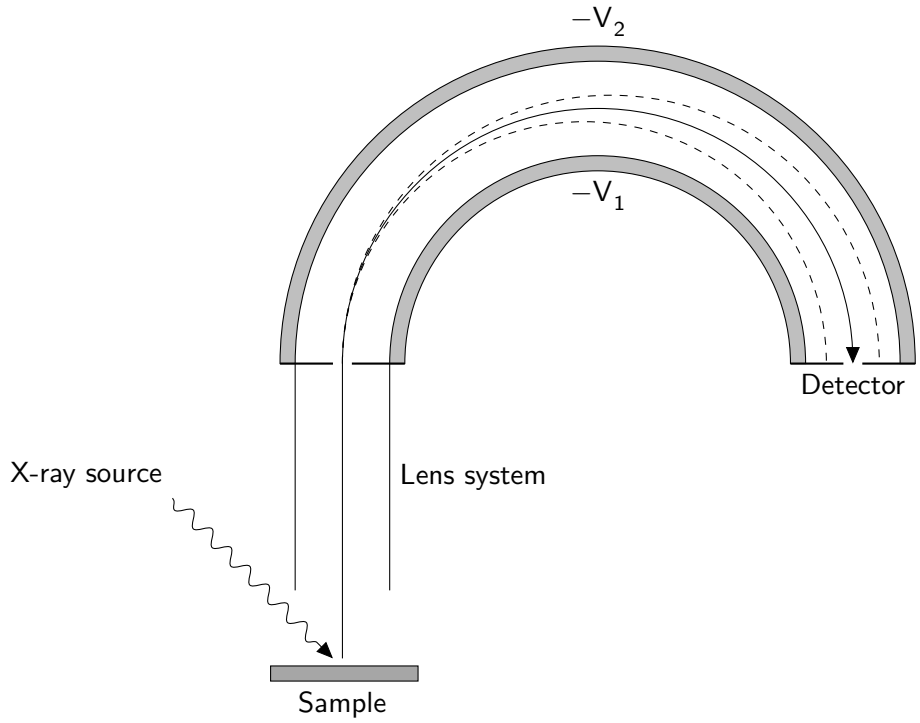

Figure 2.3: Schematic of a typical XPS experiment setup. The wavy line indicates the path of the incident X-ray photon, the solid line the path of the photoelectron (or Auger electron) and the dashed lines the paths of electrons with energy too great or small to be focused by the concentric hemispherical analyzer

An XPS experiment requires a X-ray source, a sample, an analyzer and a detector. One of the most popular analyzers is the concentric hemispherical analyzer (CHA) which has two stainless steel hemispheres of differing radii positioned concentrically, Figure 2.3. Negative potentials are applied to the two hemispheres with $V_2 > V_1$. This means that an incident electron with kinetic energy eV_0 (where V_0 is the equipotential surface between the two charged hemispheres) will follow the path shown and be focused at the detector. Electrons which have too great an energy or too small an energy will not be focused and therefore remain undetected. It is possible to run the CHA by varying the potential difference across the analyzer and thus obtain a spectrum; this is called constant retard ratio (CRR) operation. However, this would give differences in absolute resolution across the spectrum, which is generally undesirable. More commonly, therefore, the CHA is run under constant analyzer energy (CAE) operation where the potential difference is kept constant so only electrons with a certain pass energy (e.g. 20 or 50 eV) will be focused. It is then entirely the job of the lens system to retard the incoming electrons. This leads to a constant peak width resolution.

XPS analysis needs to be carried out under ultra high vacuum (UHV) conditions (i.e. $\sim 10^{-9}$ mbar) because otherwise there will still be an adsorbed gas layer on the surface from the atmosphere. Since XPS probes only 5 nm deep into the sample, adsorbed layers will significantly alter

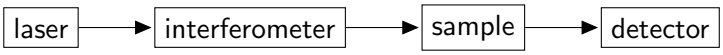

Figure 2.4: Scheme showing passage of light through an infrared spectrometer.

the spectrum, and so need to be eliminated. UHV conditions are achieved by using diffusion pumps and a series of chambers (insertion lock, preparation chamber and main chamber) in order to pump the sample down to the required pressure.

XPS characterizations within this thesis were carried out using a VG ESCALAB Mk II electron spectrometer equipped with a non-monochromated Mg Kα X-ray source (1253.6 eV) and a concentric hemispherical analyser. Photoemitted electrons were collected at a take-off angle of 20° from the substrate normal, with electron detection in the constant analyser energy mode (CAE, pass energy = 20 eV). Experimentally determined instrument sensitivity factors were used in order to calculate elemental ratios for samples characterized. All binding energies were referenced to the C(1s) hydrocarbon peak at 285.0 eV.

Data analysis of the XPS spectra included a linear background being subtracted from core level spectra, which were then fitted using Gaussian peak shapes with a constant full-width-half-maximum (fwhm).[17] Each Gaussian (bell-shaped) peak thus fitted corresponded to a unique chemical environment of that atom within the film. For example, the poly(alkyl acrylate) C(1s) peaks (Figure 7.1, page 104) may be fitted to three chemical environments, which correspond to the hydrocarbon alkyl chains (C_xH_y), the singly oxygenated carbon (C–O) and the doubly oxygenated carbon (O–C=O). For more complex curve shapes, where the diversity of chemical species could be large (e.g. the platinum-containing nanocomposite films in Figure 6.1, page 89), only specifically resolvable peaks were assigned (e.g. the CF_3 peak with a distinctive 7–8 eV shift from the hydrocarbon peak), with the fewest number of Gaussian peaks (of constant full-width-half-maximum) used to fit the rest of the spectrum.

2.3 Fourier Transform Infrared Spectroscopy

Infrared spectroscopy is widely used to analyze chemical compounds, mixtures and films. It utilizes the fact that molecules undergoing infrared irradiation can (at some frequencies) absorb it. This excites the molecule from one energy level (E_n) to another (E_m):

$$h\nu = E_n - E_m \tag{2.2}$$

where $h\nu$ is the energy of the absorbed photon. Satisfying equation 2.2 is not the only requisite for infrared absorption, since there must be a change in the vibrational quantum number of ± 1 (greater changes are formally forbidden). The other selection rule is that infrared light may only be absorbed when the electric dipole of the molecule changes as a result of the change in molecular vibrational state.[18]

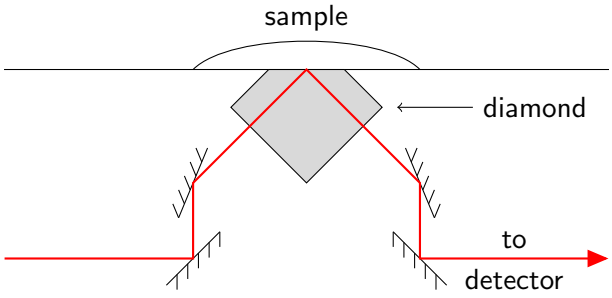

Figure 2.5: Diagram of an attenuated total reflection accessory.

Figure 2.4 shows the passage of light through a Fourier transform infrared spectrometer. Older techniques required each wavelength of light to be passed through the sample separately, which led to a very time-consuming process. Fourier transform infrared spectroscopy (FTIR) uses an interferometer, which utilizes a beamsplitter and a movable mirror. The beamsplitter causes half the light to go to a fixed mirror and half to a movable mirror. The beams then recombine at the beamsplitter to produce an interference spectrum, where every wavelength is represented. This inteference spectrum is passed through the sample, detected, and then decoded by applying a Fourier transform (a mathematical technique for analyzing the amount of each frequency that makes up a spectrum). This then gives a plot of percentage of light absorbed (as compared to a reference or background) versus the frequency of the light (usually measured in wavenumbers with units cm^{-1}).

FTIR spectra of thin films can be taken either using by coating them onto an infrared transparent material (such as a potassium bromide disc) and measuring the absorbance directly, or by using an attenuated total reflectance technique (ATR) or reflection-absorption infrared spectroscopy (RAIRS).

Figure 2.5 shows an ATR accessory. The beam enters the accessory where it is directed (by mirrors) into a diamond crystal at an angle such that it will undergo total internal reflection. The sample is placed above the crystal such that is in contact with the face where internal reflection is happening (pressure is applied if the sample is solid to ensure contact). When light is totally internally reflected, an evanescent wave (a product of the wave equation being non-zero at the diamond-sample interface) extends a few microns into the sample. This makes ATR a powerful tool for analyzing small amounts of liquid or thin solid samples.

RAIRS can also be used to obtain the infrared spectra of films deposited on silicon wafer. The incident light is bounced off the surface in question at a low angle (the grazing angle, 66° for silicon) and then put through a polarizer in order to remove the s-polarized component (that which is perpendicularly polarized relative to the surface).

Once the light has passed through (or reflected off) the sample, it goes to the detector. A popular detector is the mercury cadmium telluride (MCT) detector, which operates at liquid nitrogen temperatures (77 K). It is composed of an alloy of mercury telluride (a semimetal) and

cadmium telluride (a semiconductor). When exposed to infrared light its resistance decreases as there are a number of electrons promoted from the valence band into the conduction band. The increase in electrical conductivity is directly proportional to the number of charge carriers, which can then be used to calculate the intensity of the incident infrared radiation.

Infrared spectra within this thesis were acquired using a FTIR spectrometer (Perkin-Elmer Spectrum One) fitted with a liquid nitrogen cooled MCT detector operating at 4 cm^{-1} resolution across the 4000–700 cm^{-1} range. The instrument included a variable angle reflection-absorption accessory (Specac Ltd.) set to a grazing angle of 66° for silicon wafer substrates and adjusted for p-polarization as well as a golden gate attenuated total resonance accessory (Specac Ltd.).

2.4 Spectrophotometry

Spectrophotometry is a non-destructive method for measuring the thickness of thin films with high accuracy (up to ±5 nm). A monochromated UV-visible light source is shone at the surface and the reflected and transmitted light detected over a range of wavelengths (350–1000 nm). On encountering an interface of two different materials (e.g. air and sample) the incident ray of light will be reflected, transmitted or absorbed, Figure 2.6.

The two optical parameters that describe the way in which light acts on encountering a material are the refractive index, n, and the extinction coefficient, k. The refractive index, $\frac{n_i}{n_0} = \frac{c_i}{c_0}$, where n_i and n_0 are the refractive indices of light in medium, i, and in vacuum respectively, and c_i and c_0 are the speed of light in the medium and in vacuum. The extinction coefficient refers to the fraction of light that is absorbed by the material.

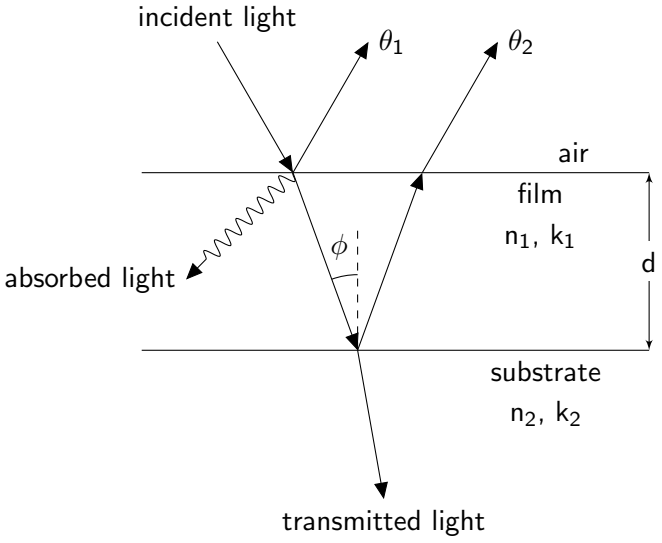

Figure 2.6: Scheme showing the possible pathways of incident light with regard to a thin polymer film (n_1, k_1) on a substrate (n_2, k_2).

When reflections from two separate interfaces (i.e. the air/film and film/substrate interfaces,

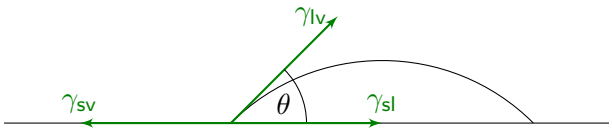

Figure 2.7: Surface tensions of a liquid droplet on a surface

denoted in Figure 2.6 by θ_1 and θ_2) recombine, they will interfere with each other. This interference will be constructive when

$$2nd = j\lambda cos\phi \qquad \text{(where j is an integer)} \tag{2.3}$$

and destructive when

$$2nd = (j + \tfrac{1}{2})\lambda cos\phi \tag{2.4}$$

From these equations, the intensity of the reflected light will oscillate over a range of wavelengths (the reflectance spectrum). A suitable mathematical model can be fitted to the data using an iterative method, which will give the thickness, d. The model is usually the Cauchy model, which assumes that k for polymers is approximately zero.

Film thicknesses were measured in this thesis using a spectrophotometer (nkd-6000, Aquila Instruments Ltd.). Transmittance-reflectance curves (350–1000 nm wavelength range) were acquired for each sample and fitted to a Cauchy material model using a modified Levenberg-Marquardt algorithm.[19]

2.5 Goniometry

Contact angle analysis (goniometry) is one of the simplest and most surface sensitive techniques available. A sessile drop is placed on a surface and the contact angle, θ, is measured by a goniometer. The goniometer takes a picture of the droplet, which then is analyzed by software to give θ. The contact angle on a smooth surface, θ, can be related to the surface tensions by Young's equation:

$$\gamma_{sv} = \gamma_{sl} + \gamma_{lv}cos\theta \tag{2.5}$$

where γ denotes surface tension, and the subscripts sv, sl and lv stand for solid-vapour, solid-liquid, and liquid-vapour respectively, Figure 2.7. A decrease in contact angle means that (all other things being equal) there is an increase in the surface tension of the solid-liquid interface.

Sessile drop water contact angle measurements in this thesis were performed at ambient temperature using a video capture apparatus in combination with a motorized syringe (VCA2500XE, A.S.T. Products Inc.) dispensing a 2 μL droplet size. High purity water (B.S. 3978 grade 1) was used as the probe liquid.

2.6 Impedance Spectroscopy

Impedance spectroscopy is a powerful technique for characterizing the electrical properties of materials and interfaces. Impedance, denoted by the character Z, is the alternating current analogue to resistance:

$$\mathrm{Z} = \mathrm{R} + \mathrm{jX} \tag{2.6}$$

where R is the resistance (real component, Re(Z)) and X is the reactance (jX is the imaginary component, Im(Z)).

Impedance spectroscopy entails applying a single-frequency voltage to the system and measuring the real and imaginary parts of the resulting current at that frequency. The impedance is thus measured over a frequency range (typically between 1 Hz and 1 MHz).

If a signal with a single frequency, $\nu(\mathrm{t}) = \mathrm{V_m sin}(\omega \mathrm{t})$, where $\nu \equiv \frac{\omega}{2\pi}$ is applied to a circuit, then the resulting current $\mathrm{i(t)} = \mathrm{I_m sin}(\omega \mathrm{t} + \theta)$ is measured. In this case θ is the phase difference between the voltage and the current. The response of the capacitive and inductive elements of the circuit is given by $\mathrm{i(t)} = \frac{\mathrm{d}\nu(\mathrm{t})}{\mathrm{dt}}\mathrm{C}$ and $\nu(\mathrm{t}) = \frac{\mathrm{di(t)}}{\mathrm{dt}}\mathrm{L}$ respectively. This leaves a complicated and sometimes intractable problem.[20]

Fortunately, the application of Fourier transformation to these differential equations gives (eventually) the relationship:

$$\mathrm{Z(j}\ \omega) = \frac{\mathrm{F}\{\nu(\mathrm{t})\}}{\mathrm{F}\{\mathrm{i(t)}\}} \tag{2.7}$$

where $\mathrm{F}\{\}$ denotes a Fourier transform. Equation 2.7 is the alternating current analogue of Ohm's law, but only applies when there is linearity, causality and stationarity of the system. Most systems are non-linear, however, but if the applied voltage $\mathrm{V_m}$ is less than the thermal voltage (which is about 25 mV at room temperature and pressure), then the system is linear to a good approximation.[20]

The typical shape of an impedance spectrum for a proton conducting film is shown in Figure 2.8, where the imaginary component of impedance (reactance) is plotted against the real component (the resistance). As the frequency, ω, increases the spectrum tends towards the origin (in the limiting case, $\omega = \infty$, then Z=0).

For proton conducting membranes, the bulk resistance of a membrane, R_S, can be obtained from fitting the high frequency arc and extrapolating to find its intercept with the real axis. The 45° line is due to the Warburg impedance, which reflects impedance due to charge carrier diffusion (in proton exchange membranes this is almost exclusively water).[21] This corresponds to a Randles circuit, which comprises a resistor (the membrane) and the Warburg impedance, W, in parallel with the double layer capacitance, C_{dl}, all in series with the resistance of the electrical contacts (R_∞), Figure 2.9. Impedance spectra within this thesis were acquired using an LF impedance analyser (HP 4192A) across the 10 Hz–13 MHz range. The formula $\sigma = l/R_S A$ was used to calculate proton conductivity, where σ is the membrane conductivity, R_S is the bulk membrane resistance, l is the distance between the electrodes, and A is the cross-sectional area of the film.[22]

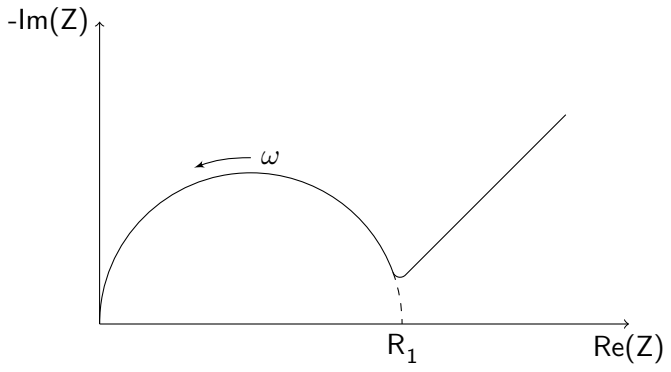

Figure 2.8: General shape of the impedance spectrum for a proton conducting film.

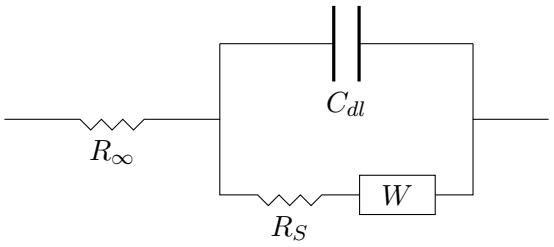

Figure 2.9: Randles circuit

2.7 Fluorescence Microscopy

Fluorescence spectroscopy utilizes an excitation source (light at a predetermined wavelength) in order to effect a transition in the molecule of interest, A, to an excited state, A*, via absorption of a photon. This takes the form $A + h\nu \longrightarrow A^*$ and when the excited state relaxes back to the ground state, a photon is emitted. The emitted photon is of a lower wavelength than the incident excitation since the excited molecule undergoes vibrational relaxation before emission.

Fluorescence microscopy is a simple variant whereby a surface (usually tagged with a fluorescent marker) is illuminated by light of a certain wavelength and a CCD is used in conjunction with optical objectives in order to gain an fluorescent image of the surface in question, Figure 2.10. Fluorescence microscopy in this thesis entailed use of a fluorescein tag, which has an absoprtion maximum at 494 nm and an emission maximum at 521 nm. An excitation source at 490 nm and detection at 528 nm is therefore used.

2.8 Bond Strength Testing

Adhesive bonds are tested using lap shear test which comprises two overlapping substrates bonded together with an adhesive. The two substrates are then subjected to shear forces (i.e. being pulled apart) of known magnitude and the distance moved is measured, Figure 2.11. The values obtained

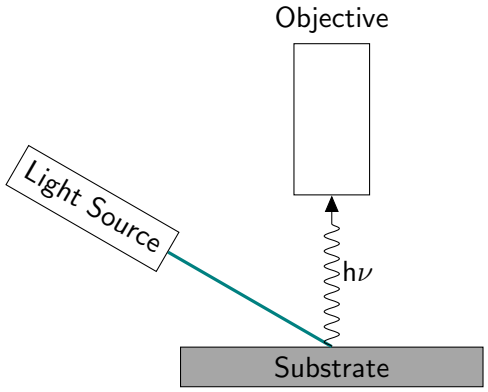

Figure 2.10: Schematic of a fluorescence microscope.

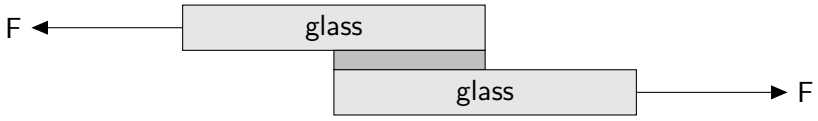

Figure 2.11: A lap shear test where two glass substrates joined by an adhesive are pulled apart thereby subjecting the bond to shear forces

enable a stress-strain curve to be plotted, where the stress is the force per unit area (measured in MPa) and the strain is the relative deformation of the adhesive (unitless), Figure 2.12. The curve shape takes the form of a linear section followed by a steep drop, where the adhesive has failed. This bond failure point is the measure of the shear bond strength, whereas the gradient of the linear section of the curve is the shear modulus (i.e. how stiff the adhesive is).

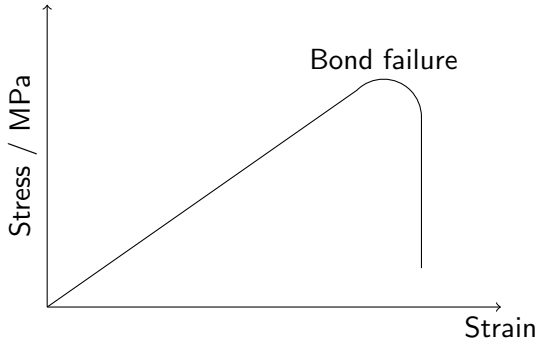

Figure 2.12: General shape of the stress-strain curve for the adhesives tested in this thesis.

2.9 References

[1] Langmuir, I. *Proc. Natl. Acad. Sci., U.S.A.* **1928**, *14*, 627.

[2] Schoepfle, C. S.; Connell, L. H. *Ind. Eng. Chem.* **1929**, *21*, 529.

[3] Collie, J. N. *J. Chem. Soc.* **1905**, *87*, 1540.

[4] Lind, S. C.; Glockler, G. *J. Am. Chem. Soc.* **1928**, *50*, 1767.

[5] (a) Arquette, G. J.; Reich, L. Insolubilization of coatings. U.S. Patent No. 3,061,458, 1962; (b) Stuart, M. *Nature* **1963**, *199*, 59.

[6] Yasuda, H. *Plasma Polymerization*; Academic Press: New York, 1985.

[7] Ryan, M. E.; Hynes, A. M.; Badyal, J. P. S. *Chem. Mater.* **1996**, *8*, 37.

[8] Chen, X.; Rajeshwar, K.; Timmons, R. B.; Chen, J.; Chyan, O. M. R. *Chem. Mater.* **1996**, *8*, 1067.

[9] Hynes, A. M.; Badyal, J. P. S. *Chem. Mater.* **1998**, *10*, 2177.

[10] Tarducci, C.; Kinmond, E. J.; Badyal, J. P. S.; Brewer, S. A.; Willis, C. *Chem. Mater.* **2000**, *12*, 1884.

[11] Tarducci, C.; Schofield, W. C. E.; Badyal, J. P. S.; Brewer, S. A.; Willis, C. *Chem. Mater.* **2001**, *13*, 1800.

[12] Sawada, Y.; Ogawa, S.; Kogoma, M. *J. Phys. D: Appl. Phys.* **1995**, *28*, 1661.

[13] Ward, L. J.; Schofield, W. C. E.; Badyal, J. P. S.; Goodwin, A. J.; Merlin, P. J. *Chem. Mater.* **2003**, *15*, 1466.

[14] Ward, L. J.; Schofield, W. C. E.; Badyal, J. P. S.; Goodwin, A. J.; Merlin, P. J. *Langmuir* **2003**, *19*, 2110.

[15] d'Agostino, R., Ed. *Plasma Deposition, Treatment, and Etching of Polymers*; Academic Press: London, 1990.

[16] Moulder, J. F.; Stickle, W. F.; Sobol, P. E.; Bomben, K. D. In *Handbook of X-ray Photoelectron Spectroscopy*; Chastain, J., Ed.; Perkin-Elmer Corporation: Minnesota, 1992.

[17] (a) Friedman, R. M.; Hudis, J.; Perlman, M. L. *Phys. Rev. Lett.* **1972**, *29*, 692; (b) Evans, J. F.; Gibson, J. H.; Moulder, J. F.; Hammond, J. S.; Goretzki, H. *Fresenius J. Anal. Chem.* **1984**, *841*, 319.

[18] Christy, A. A.; Ozaki, Y.; Gregoriou, V. G. In *Modern Fourier Transform Infrared Spectroscopy*, 1st ed.; Barcelo, D., Ed.; Comprehensive Analytical Chemistry; Elsevier, 2001.

[19] Lovering, D. *NKD-6000 Technical Manual*; Aquila Instruments: Cambridge, U.K., 1998.

[20] Barsoukov, E., Macdonald, J. R., Eds. *Impedance Spectroscopy: Theory, Experiment, and Applications*, 2nd ed.; John Wiley & Sons: Hoboken, NJ, 2005.

[21] Mikhailenko, S. D.; Guiver, M. D.; Kaliaguine, S. *Solid State Ionics* **2008**, *179*, 619.

[22] Zawodzinski Jr., T. A.; Neeman, M.; Sillerud, L. O.; Gottesfeld, S. *J. Phys. Chem.* **1991**, *95*, 6040.

Chapter 3

Pulsed Plasmachemical Deposition of Proton-Conducting Films

3.1 Introduction

Proton exchange membrane fuel cells (PEMFCs) are green energy devices for automotive, stationary, and portable power applications.[1–3] These electrochemical cells oxidise fuel (usually hydrogen gas or methanol) at the anode to produce protons, which travel across the proton exchange membrane and react at the cathode with an oxidant (oxygen gas or air). This completes an electrical circuit according to the overall reaction $H_2 + \frac{1}{2} O_2 \longrightarrow H_2O$ ($E^0 = 1.229$ V). The proton exchange membrane component of the PEMFC serves to separate the two electrodes, allowing protons to pass from anode to cathode, but not allowing reactant gases or electrons to traverse (thereby preventing a short circuit leading to loss of efficiency).[1] With widespread efforts aiming to cut global carbon emissions and move towards cleaner hydrogen-based energy sources, there exists a strong demand for cost-effective and efficient proton exchange membranes.[4,5]

The existing benchmark for proton exchange membranes is considered to be perfluorosulfonic acid containing polymers (e.g. Nafion[6]). Proton conductivity relies upon the sulfonic acid groups, yielding typical values of 80–90 mS cm^{-1} at 20 °C.[7–9] However, perfluorosulfonic acid membranes require toxic precursors (e.g. tetrafluoroethylene) and therefore their manufacture is considered to be expensive and environmentally unfriendly.[6,10] Alternative proton exchange membranes, which have been developed, include sulfonated styrene-based polymers,[11–13] sulfonated poly(arylene ether)s,[14,15] sulfonated poly(imides),[16–19] sulfonated poly(phosphazene)s,[20–22] phosphonated polymers[23,24] and carboxylated polymers.[25] Proton conductivities for these types of conventional polymer proton exchange membranes range between 0.05–110 mS cm^{-1} at room temperature when fully hydrated. However, preparation of such materials involves many steps,[16] and often requires dangerous precursors[3] and solvents,[24] or is limited by time-consuming separation and purification techniques.[24] Furthermore, this introduces the need for an additional fabrication step (such as solvent casting) during the manufacture of fuel cell membrane elec-

trode assemblies, which can lead to extra problems associated with controlling the thickness and conformality of the proton exchange membranes.[26]

In contrast to the aforementioned multi-step membrane fabrication techniques, plasma polymerization is a one-step, solventless methodology, which renders cross-linked, insoluble films.[27] Previous plasmachemically deposited acid-containing films for application in proton exchange membranes have suffered from low proton conductivity,[23,28–35] poor stability and cracking when hydrated[36,37] and the reliance upon having to feed precursor mixtures (which can lead to reproducibility issues).

The present study utilises pulsed plasmachemical deposition for the preparation of carboxylic acid- and anhydride-containing films, which display high proton conductivity values, Scheme 3.1. This is the first time that stable carboxylic acid-containing films with proton conductivities comparable to those of the state-of-the-art Nafion proton conducting membranes have been prepared using a single-step process entirely at ambient temperature.

3.2 Experimental

3.2.1 Preparation of Proton Exchange Layers

Precursors used for plasma deposition were acrylic acid (Aldrich Ltd.), 2-(trifluoromethyl)acrylic acid (Apollo Scientific Ltd.), maleic anhydride briquettes (+99%, Aldrich Ltd., ground into a fine powder) and (trifluoromethyl)maleic anhydride (+97%, Apollo Scientific Ltd.). All these were loaded into separate, sealable, glass tubes and thoroughly degassed via several freeze-pump-thaw cycles.

Plasma deposition was carried out in an electrodeless cylindrical glass reactor as detailed in section 2.1 (page 27). Substrates used for coating were silicon (100) wafer pieces (Silicon Valley Microelectronics Inc.) and polypropylene sheet (Lawson Mardon Ltd.) with two evaporated gold electrodes (5 mm length and 1.5 mm separation). Precursor vapour was allowed to purge the reactor for 5 min at a pressure of 0.2 mbar prior to electrical discharge ignition. Pulsed plasma deposition was performed using optimal duty cycles of 100 μs on-period and 4000 μs off-period in conjunction with 30 W peak power for the acid precursors, and 20 μs on-period and 1200 μs off-period in conjunction with a peak power of 5 W for the anhydride precursors.[38] Upon plasma extinction, the precursor vapour was allowed to continue to pass through the system for a further 3 min, and then the chamber was evacuated back down to base pressure, prior to venting to atmosphere.

The plasma deposited anhydride-containing films were subsequently hydrated in ultra high purity water (B.S. 3978 grade 1) at 20 °C for 16 h, and then allowed to dry in air at room temperature.

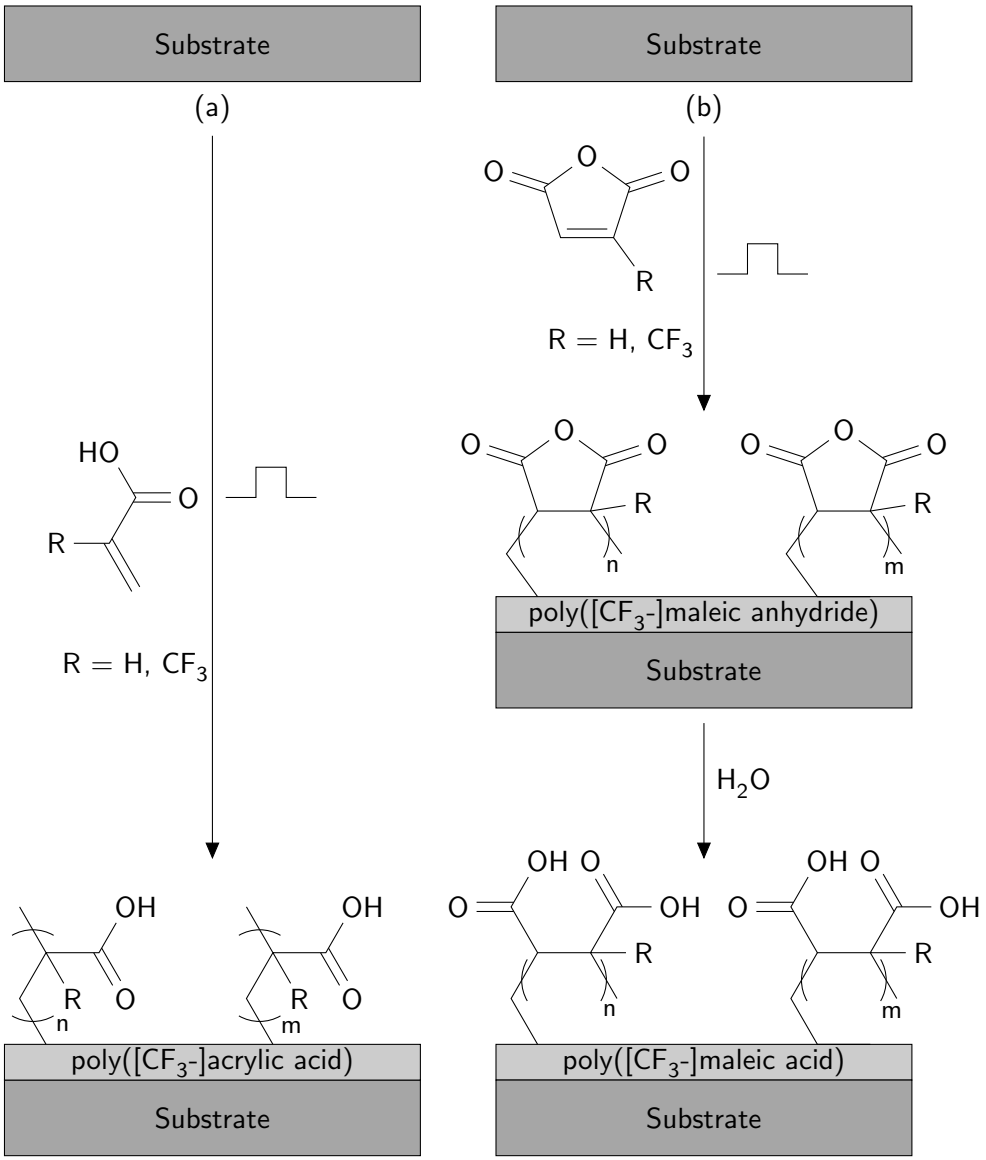

Scheme 3.1: Strategies to achieve films with a high density of acid groups: (a) pulsed plasmachemical deposition of acid-containing films and (b) pulsed plasmachemical deposition of anhydride-containing films followed by hydrolysis.

3.2.2 Film Characterization

Film thicknesses were measured using a spectrophotometer (nkd-6000, Aquila Instruments Ltd.) as detailed in section 2.4 (page 33).

Surface elemental compositions were determined by X-ray photoelectron spectroscopy (XPS) using a VG ESCALAB II electron spectrometer as detailed in section 2.2 (page 28). Experimentally determined instrument sensitivity (multiplication) factors were taken as C(1s): O(1s): F(1s) equals 1.00: 0.34: 0.26.

Infrared spectra were acquired using a FTIR spectrometer (Perkin-Elmer Spectrum One) as detailed in section 2.3 (page 31).

Sessile drop water contact angle measurements were performed at ambient temperature as detailed in section 2.5 (page 2.5).

Impedance measurements across the 10 Hz–13 MHz frequency range were carried out using an LF impedance analyser (HP 4192A) for plasma deposited layers on polypropylene substrates whilst submerged in ultra high purity water (B.S. 3978 grade 1) at room temperature (20 °C) as detailed in section 2.6 (page 35).

Optical inspection of the films to determine cracking (before and after hydration) was effected using an optical microscope (Olympus BX40) fitted with a x10 magnification lens.

3.3 Results

3.3.1 Pulsed Plasma Deposition of Carboxylic Acid Layers

In the case of pulsed plasma deposition of acrylic acid the resultant layers were found to be soluble in water at room temperature regardless of plasma parameters. Upon removal from the reactor immediate cracking within the film was observed. In contrast pulsed plasma deposited poly(2-(trifluoromethyl)acrylic acid) was stable in ambient conditions.

The absence of any Si(2p) XPS signal for pulsed plasma deposited poly(2-(trifluoromethyl)-acrylic acid) layers confirmed coverage of the silicon substrates. The layers displayed distinctive C(1s) component peaks at 289.9 eV corresponding to O−C=O acid carbon centres and at 292.5 eV which is characteristic of trifluoromethyl centres (CF_3), Figure 3.1.[39] This indicates that the acid group along with the trifluoromethyl group has been retained during the pulsed plasma deposition process.

The following infrared peaks were able to be assigned for the 2-(trifluoromethyl)acrylic acid monomer:[40] O−H broad stretch (around 3000 cm^{-1}), C=O acid dimer antisymmetric stretch (1708 cm^{-1}), C=C vinyl stretch (1635 cm^{-1}), C−OH in plane bend (1402 cm^{-1}) and OH···O carboxylic acid dimer wag (891 cm^{-1}), Figure 3.2. For the pulsed plasma deposited poly(2-(trifluoromethyl)acrylic acid) the vinyl C=C stretch at 1635 cm^{-1} disappeared which indicates conventional polymerization occurring at the C=C double bond. This was accompanied by a shift in the carboxylic acid C=O antisymmetric stretch to 1746 cm^{-1}, which, together with the loss

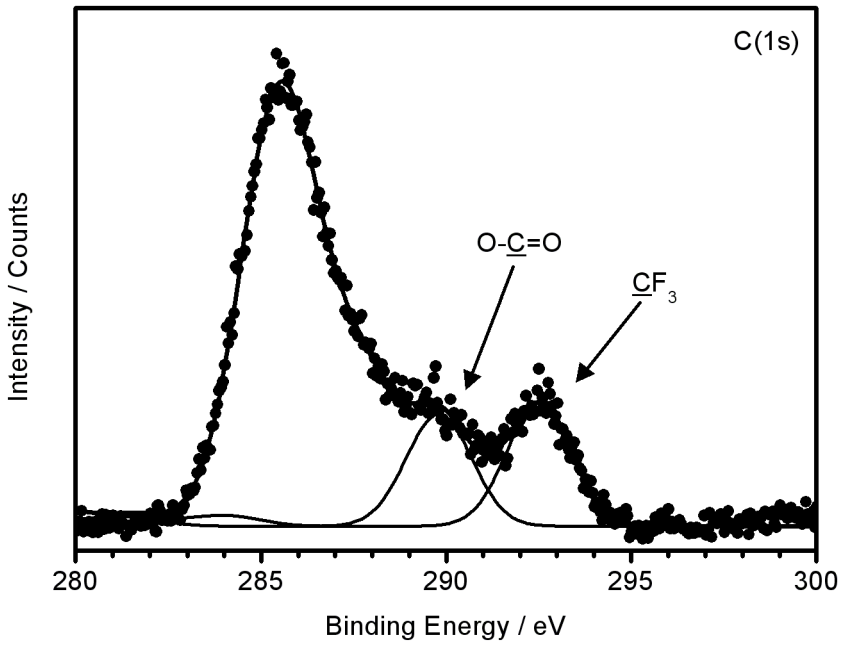

Figure 3.1: C(1s) X-ray photoelectron spectrum for pulsed plasma deposited poly(2-(trifluoromethyl)acrylic acid).

of the OH···O carboxylic acid dimer wag and retention of the C−OH in plane bend, confirms the move from a dimerized carboxylic acid system to single carboxylic acid groups (consistent with a change from liquid to solid). There was also the appearance of carboxylic anhydride C=O symmetric and antisymmetric stretches at 1876 cm^{-1} and 1810 cm^{-1} respectively, which infers some rearrangement of the monomer within plasma conditions.

3.3.2 Pulsed Plasma Deposition of Anhydride Layers

The absence of any Si(2p) XPS signal for pulsed plasma deposited poly(maleic anhydride) and poly((trifluoromethyl)maleic anhydride) layers confirmed coverage of the underlying silicon substrates. Pulsed plasma deposited poly(maleic anhydride) layers displayed a distinctive C(1s) component peak at 288.9 eV corresponding to anhydride carbon centres (O−C=O),[38] Figure 3.3. This peak was also evident for pulsed plasma deposited poly((trifluoromethyl)maleic anhydride), along with a component at 292.5 eV which is characteristic of trifluoromethyl (CF_3) centres.[39]

Infrared spectroscopy provided further evidence for anhydride group retention in both types of film, Figures 3.4 and 3.5. The infrared spectrum for pulsed plasma deposited poly(maleic anhydride) layers displays distinctive anhydride symmetric and antisymmetric C=O stretches at 1870 cm^{-1} and 1800 cm^{-1} respectively,[41] Figure 3.4 and Table 3.1. These anhydride C=O stretch vibrational bands are shifted to higher frequencies when compared to the maleic anhydride precursor molecule (1849 cm^{-1} symmetric and 1774 cm^{-1} antisymmetric). This is consistent with there

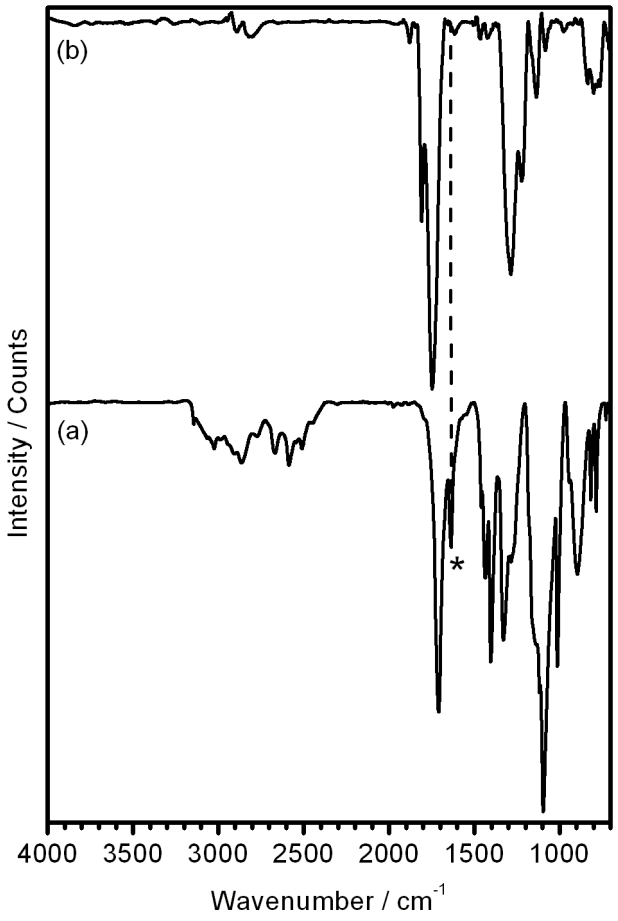

Figure 3.2: Infrared spectra of: (a) 2-(trifluoromethyl)acrylic acid monomer and (b) pulsed plasma deposited poly(2-(trifluoromethyl)acrylic acid) film. * Denotes characteristic vinyl C=C stretch.

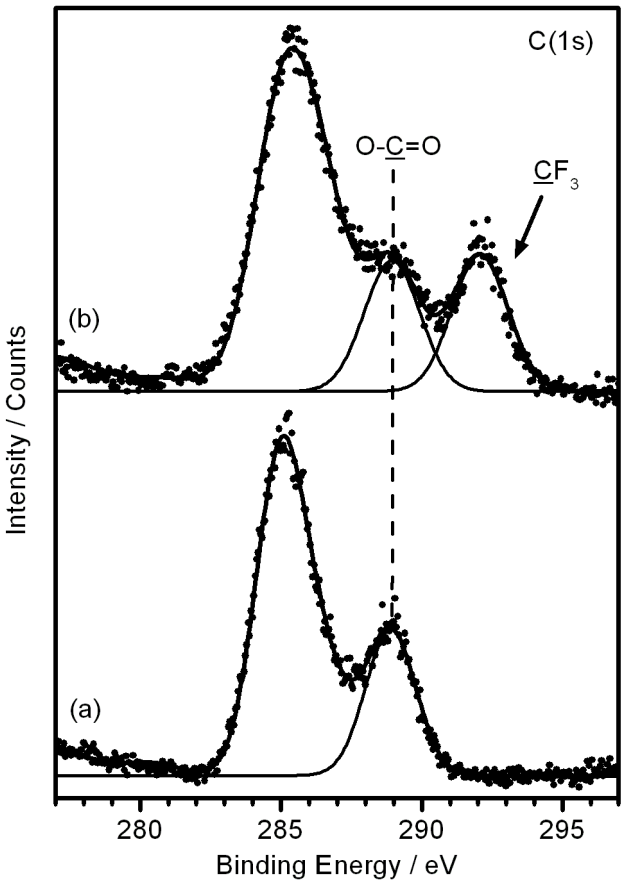

Figure 3.3: C(1s) X-ray photoelectron spectra for: (a) pulsed plasma deposited poly(maleic anhydride) and (b) pulsed plasma deposited poly((trifluoromethyl)maleic anhydride).

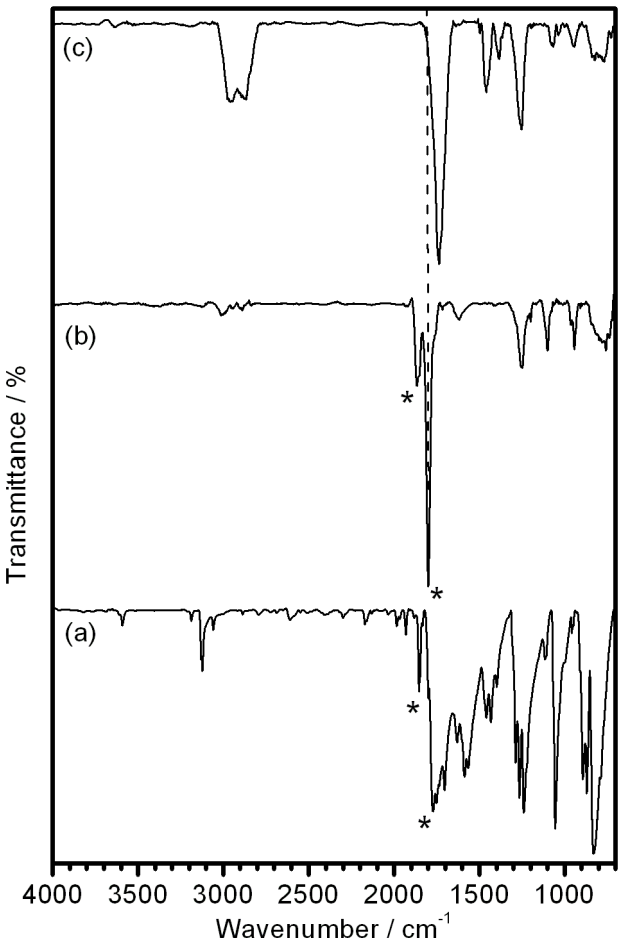

Figure 3.4: Infrared spectra of: (a) maleic anhydride monomer, (b) pulsed plasma deposited poly(maleic anhydride) film and (c) pulsed plasma deposited poly(maleic anhydride) film hydrolysed in water at 20 °C for 16 h. * Denotes characteristic anhydride C=O stretches.

being a change from a cyclic conjugated anhydride ring molecular structure to a cyclic unconjugated anhydride ring system (i.e. polymerization taking place at the C=C double bond).[41] Similar shifts towards higher C=O stretch vibrational frequencies were observed for the pulsed plasma deposited poly((trifluoromethyl)maleic anhydride) layers when compared to the (trifluoromethyl)-maleic anhydride precursor, which again can be attributed to polymerization of the C=C double bond, Figure 3.5 and Table 3.1. Furthermore, the anhydride symmetric and antisymmetric C=O stretches for both (trifluoromethyl)maleic anhydride monomer and corresponding pulsed plasma deposited layer are shifted to higher frequencies compared to their non-fluorinated maleic anhydride counterparts. This can be explained on the basis of the electron-withdrawing effect of the trifluoromethyl group attached to the anhydride ring in the case of the former,[40] Scheme 3.1.

Exposure of the pulsed plasma deposited poly(maleic anhydride) layers to water gave rise to a loss of anhydride infrared C=O stretches with the concurrent emergence of a single C=O stretch at 1735 cm^{-1}, which is signature of the carboxylic acid dimer C=O antisymmetric stretch (the

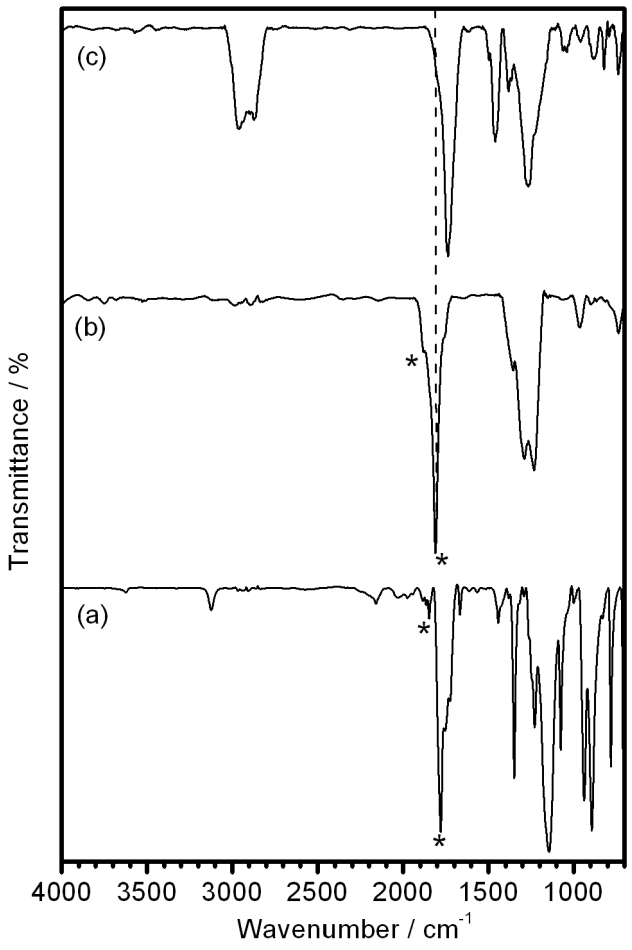

Figure 3.5: Infrared spectra of: (a) (trifluoromethyl)maleic anhydride monomer, (b) pulsed plasma deposited poly((trifluoromethyl)maleic anhydride) film and (c) pulsed plasma deposited poly((trifluoromethyl)maleic anhydride) film hydrolysed in water at 20 °C for 16 h. * Denotes characteristic anhydride C=O stretches.

Table 3.1: Infrared carbonyl stretching frequencies for anhydride precursor molecules and the corresponding pulsed plasma deposited layers

	C=O stretches / cm^{-1}		
Precursor/Film	Anhydride (symmetric)	Anhydride (antisymmetric)	Carboxylic Acid (antisymmetric)
Maleic anhydride	1849	1774	—
Pulsed plasma deposited poly(maleic anhydride)	1870	1800	—
Pulsed plasma deposited poly(maleic anhydride) after 16 h hydrolysis in water at 20 °C	—	—	1735
(Trifluoromethyl)maleic anhydride	1848	1782	—
Pulsed plasma deposited poly((trifluoromethyl)maleic anhydride)	1880	1809	—
Pulsed plasma deposited poly((trifluoromethyl)maleic anhydride) after 16 h hydrolysis in water at 20 °C	—	—	1739

symmetric stretch is not infrared-active[40]), Figure 3.4 and Table 3.1. In addition, a broad band for the carboxylic acid O−H stretch centred at 2910 cm^{-1} together with the carboxylic acid C−OH in-plane bend at 1459 cm^{-1}, provided further evidence for carboxylic acid formation. Similarly, for the case of the hydrolysed pulsed plasma deposited poly((trifluoromethyl)maleic anhydride) films, the anhydride C=O stretches disappeared, and were replaced by a carboxylic acid dimer C=O antisymmetric stretch at 1739 cm^{-1}, along with the appearance of the corresponding carboxylic acid O−H stretch and carboxylic acid COH in-plane bend vibrations at 2910 cm^{-1} and 1460 cm^{-1} respectively. Again this is consistent with conversion of anhydride functionalities to carboxylic acid during hydrolysis.

3.3.3 Proton Conductivity

In the case of the pulsed plasma deposited poly(2-(trifluoromethyl)acrylic acid) films, no proton conductivity was observed, which was due to the severe cracking of the films when hydrated, Table 3.2. The proton conductivity value for the fully hydrated pulsed plasma deposited poly(maleic anhydride) films was measured to be 50 mS cm^{-1}, Table 3.2. This arises from the high density of carboxylic acid groups present in the hydrolysed films, which yields a hydrophilic equilibrium water contact angle of 38°. However, such a large level of hydrophilicity for these pulsed plasma deposited poly(maleic anhydride) films gave rise to the formation of surface cracks upon exposure to water. In contrast, the pulsed plasma deposited poly((trifluoromethyl)maleic anhydride) films were not susceptible to surface cracking during hydrolysis, whilst the proton conductivity value was measured to be significantly greater at 90 mS cm^{-1}. Correspondingly, the equilibrium water contact angle in this case was more hydrophobic compared to its non-fluorinated counterpart, and can be attributed to the retention of hydrophobic trifluoromethyl functionalities throughout the film, Table 3.2. Moreover, as a result of this greater hydrophobicity, the pulsed plasma deposited poly((trifluoromethyl)maleic anhydride) films remained stable in water, and showed no signs of cracking following repeated hydration and drying cycles.

3.4 Discussion

Pulsed plasmachemical deposition of acrylic acid and 2-trifluoromethylacrylic acid precursors results in films which are unstable in water and therefore unsuitable for applications such as proton exchange membrane fuel cells, which require stability in water at high temperatures (around 80 °). Conversely, pulsed plasmachemical deposition of anhydride-containing films effectively provides a single-step process for preparing proton exchange membranes at ambient temperatures. The resultant hydrolysed membrane layers contain a high density of carboxylic acid functionalities, which underpin proton conductivity. Carboxylic acids are weaker acids compared to the more popular sulfonic acid groups (as used in the current benchmark perfluorosulfonic acid containing polymer membranes (Nafion)) and therefore have in the past been reported to yield low proton conductiv-

Table 3.2: Water uptake, proton conductivity, water contact angle, and stability in water at 20 °C of pulsed plasma deposited films

Hydrated Film	Mass Increase on Hydration/wt %	Proton Conductivity/mS cm^{-1}	Contact Angle/°	Optical Appearance
Poly(2-(trifluoromethyl)-acrylic acid)	152±9	—	65±2	Severe cracking
Poly(maleic anhydride)	167±7	50±5	38±1	Cracking
Poly((trifluoromethyl)-maleic anhydride)	143±3	90±5	84±1	No cracking

ities.[25] However, the present study demonstrates that hydrolysis of anhydride functionalities can lead to a high density of proton conducting carboxylic acid centres. For the case of pulsed plasma deposited poly(maleic anhydride) and poly(trifluoromethyl-maleic anhydride) films, the measured proton conductivities are on a par with Nafion (80–90 mS cm^{-1} at room temperature[7–9]), Table 3.2.

The high level of anhydride incorporation into these films (functional retention) stems from the underlying pulsed plasmachemical reaction pathway, which promotes conventional polymerization via the C=C double bond contained within the monomer during the prolonged duty cycle off-period[38] (in contrast to the structural damage normally associated with the more common continuous wave plasmas[27]).

A threefold beneficial effect is achieved by utilising a trifluoromethyl group substituted variant of maleic anhydride: firstly it provides stabilization of anhydride radicals within the electrical discharge[42] (thus enhancing rate of polymerization and suppressing ablation[43,44]); secondly its electron-withdrawing effect gives rise to a stronger carboxylic acid group;[45] and thirdly, it provides a degree of hydrophobicity which helps to avoid cracking (due to less hydrophilicity and therefore swelling/internal mechanical stress within the layers). Previous attempts made at utilising plasmachemical deposition for preparing proton conductive membranes have employed much higher average powers and continuous wave conditions, which lead to structural damage of the growing film.[23,28–35] Furthermore, they have needed to resort to mixing precursors which introduces inherent reproducibility issues.

The choice of precursors for pulsed plasmachemical deposition of acid-containing films is limited by the chemical and physical properties of available monomers. For example, sulfonic acid–containing precursors tend to be unstable with a double bond present (e.g. vinylsulfonic acid is commercially unavailable), sulfonate salts (which could be converted to acids by ion exchange)

have negligible vapour pressure, which is the same problem experienced for phosphonic acids. As a result, carboxylic acid containing monomers, which have good vapour pressure (sufficient for vapour-phase deposition) and do not autopolymerize (under room temperature conditions) were investigated. The use of conventional monomer types (i.e. those with carbon-carbon double bonds present) meant that relatively low plasma powers (relative to previous examples in the literature[23,28–35]) are able to be utilized. This in turn leads to better structural retention within the plasma polymer films as evidenced by the XPS and FTIR data.

Finding the right deposition conditions relies on compromising with plasma parameters. On the one hand, a higher plasma power will lead to more crosslinking in the film, which therefore enables it to be stable in water. Too high an input power, however, and the film will contain so many trapped radicals and reactive species (as caused by precursor ablation within the plasma itself) that exposure to atmosphere or water will cause the film to crack as it chemically reacts.[27] Another disadvantage of a large plasma input power is that the ablation of the monomer leads to less structural retention within the plasma polymer film, and therefore, in this case, a large reduction in the number of acid groups per unit volume, which in turn results in lower proton conductivity (for example, in the case of maleic anhydride, increasing the peak plasma power to 30 W yields more than a hundredfold decrease in conductivity). Conversely, if too low a plasma input power is used, then the film will either be soluble in water, or, in the extreme case, no deposition will occur. Therefore, with the anhydride films, a plasma input power and pulsing duty cycle was used at 5 W and 20 μs on, 1200 μs off, in order to maximise the anhydride density (and thus acid density) whilst maintaining sufficient crosslinking for stability under hydrated conditions.[38]

Given the rising demand for fuel cells, the drive towards miniaturised energy sources,[4,5] and the inherently high costs and environmental impact of Nafion proton exchange membrane manufacture,[10] the outlined single-step plasmachemical deposition approach offers a cost-effective and viable alternative. Furthermore, elimination of the need to actually handle individual fabricated membranes can be accomplished by plasmachemical deposition directly onto fuel cell components, which overcomes the conventional mindset for thicker membranes (lowering costs). Higher plasmachemical deposition rates and throughputs can be envisaged by incorporating an atomiser for precursor delivery[46] in combination with roll-to-roll processing.

3.5 Conclusions

Pulsed plasmachemical deposition using anhydride precursors yields structurally well-defined thin films with high levels of functional retention. Subsequent hydrolysis of the anhydride centres produces a large concentration of carboxylic acid groups which give rise to high proton conductivity values. This conformal approach offers a range of benefits which include the ability to coat both two- and three-dimensional proton exchange fuel cell components, thereby negating the requirement for handling thicker conventional membranes, as well as low environmental impact.

3.6 References

[1] Winter, M.; Brodd, R. J. *Chem. Rev.* **2004**, *104*, 4245.

[2] Steele, B. C. H.; Heinzel, A. *Nature* **2001**, *414*, 345.

[3] Hickner, M. A.; Ghassemi, H.; Kim, Y. S.; Einsla, B. R.; McGrath, J. E. *Chem. Rev.* **2004**, *104*, 4587.

[4] Service, R. F. *Science* **2002**, *296*, 1222.

[5] *2010 Annual Report*; Hydrogen and Fuel Cell Technical Advisory Committee, U.S. Department of Energy, 2011.

[6] Connolly, D. J.; Gresham, W. F. U.S. Patent 3,282,875, 1966.

[7] Mikhailenko, S. D.; Guiver, M. D.; Kaliaguine, S. *Solid State Ionics* **2008**, *179*, 619.

[8] Fontanella, J. J.; Wintersgill, M. C.; Chen, R. S.; Wu, Y.; Greenbaum, S. G. *Electrochim. Acta* **1995**, *40*, 2321.

[9] Mauritz, K. A.; Moore, R. B. *Chem. Rev.* **2004**, *104*, 4535.

[10] Costamagna, P.; Srinivasan, S. *J. Power Sources* **2001**, *102*, 242.

[11] Tsang, E. M. W.; Zhang, Z.; Shi, Z.; Soboleva, T.; Holdcroft, S. *J. Am. Chem. Soc.* **2007**, *129*, 15106.

[12] (a) Serpico, J. M.; Ehrenberg, S. G.; Fontanella, J. J.; Jiao, X.; Perahia, D.; McGrady, K. A.; Sanders, E. H.; Kellogg, G. E.; Wnek, G. E. *Macromolecules* **2002**, *35*, 5916; (b) Won, J.; Park, H. H.; Kim, Y. J.; Choi, S. W.; Ha, H. Y.; Oh, I.; Kim, H. S.; Kang, Y. S.; Ihn, K. J. *Macromolecules* **2003**, *36*, 3228; (c) Xu, K.; Li, K.; Khanchaitit, P.; Wang, Q. *Chem. Mater.* **2007**, *19*, 5937.

[13] Chen, S.; Benziger, J. B.; Bocarsly, A. B.; Zhang, T. *Ind. Eng. Chem. Res.* **2005**, *44*, 7701.

[14] Miyatake, K.; Chikashige, Y.; Higuchi, E.; Watanabe, M. *J. Am. Chem. Soc.* **2007**, *129*, 3879.

[15] (a) Bae, B.; Yoda, T.; Miyatake, K.; Uchida, H.; Watanabe, M. *Angew. Chem., Int. Ed.* **2010**, *49*, 317; (b) Liu, B.; Robertson, G. P.; Kim, D.; Guiver, M. D.; Hu, W.; Jiang, Z. *Macromolecules* **2007**, *40*, 1934; (c) Matsumoto, K.; Higashihara, T.; Ueda, M. *Macromolecules* **2008**, *41*, 7560; (d) Reinholdt, M. X.; Kaliaguine, S. *Langmuir* **2010**, *26*, 11184;

(e) Marani, D.; D'Epifanio, A.; Traversa, E.; Miyayama, M.; Licoccia, S. *Chem. Mater.* **2010**, *22*, 1126.

[16] Yamazaki, K.; Kawakami, H. *Macromolecules* **2010**, *43*, 7185.

[17] Bin Hasan Susan, M. A.; Kaneko, T.; Noda, A.; Watanabe, M. *J. Am. Chem. Soc.* **2005**, *127*, 4976.

[18] (a) Essafi, W.; Gebel, G.; Mercier, R. *Macromolecules* **2004**, *37*, 1431; (b) Park, C. H.; Lee, C. H.; Sohn, J.; Park, H. B.; Guiver, M. D.; Lee, Y. M. *J. Phys. Chem. B* **2010**, *114*, 12036.

[19] Asano, N.; Aoki, M.; Shinsuke, S.; Miyatake, K.; Uchida, H.; Watanabe, M. *J. Am. Chem. Soc.* **2006**, *128*, 1762.

[20] Allcock, H. R.; Hofmann, M. A.; Ambler, C. M.; Morford, R. V. *Macromolecules* **2002**, *35*, 3484.

[21] Hofmann, M. A.; Ambler, C. M.; Maher, A. E.; Chalkova, E.; Zhou, X. Y.; Lvov, S. N.; Allcock, H. R. *Macromolecules* **2002**, *35*, 6490.

[22] Guo, Q.; Pintauro, P. N.; Tang, H.; O'Connor, S. *J. Membr. Sci.* **1999**, *154*, 175.

[23] Danilich, M. J.; Gervasio, D.; Burton, D. J.; Marchant, R. E. *Macromolecules* **1995**, *28*, 5567.

[24] (a) Parvole, J.; Jannasch, P. *Macromolecules* **2008**, *41*, 3893; (b) Lee, Y. J.; Bingol, B.; Murakhtina, T.; Sebastiani, D.; Meyer, W. H.; Wegner, G.; Spiess, H. W. *J. Phys. Chem. B* **2007**, *111*, 9711.

[25] Poppe, D.; Frey, H.; Kreuer, K. D.; Heinzel, A.; Mulhaupt, R. *Macromolecules* **2002**, *35*, 7936.

[26] Berron, B. J.; Payne, P. A.; Jennings, G. K. *Ind. Eng. Chem. Res.* **2008**, *47*, 7707.

[27] Yasuda, H. *Plasma Polymerization*; Academic Press: New York, 1985.

[28] Inagaki, N.; Tasaka, S.; Horkawa, Y. *J. Polym. Sci., Part A: Polym. Chem.* **1989**, *27*, 3495.

[29] Inagaki, N.; Tasaka, S.; Kurita, T. *Polym. Bull.* **1989**, *22*, 15.

[30] Ogumi, Z.; Uchimoto, Y.; Takehara, Z. *J. Electrochem. Soc.* **1990**, *137*, 3319.

[31] Ogumi, Z.; Uchimoto, Y.; Yasuda, K.; Takehara, Z. I. *Chem. Lett.* **1990**, 953.

[32] Inagaki, N.; Tasaka, S.; Chengfei, Z. *Polym. Bull.* **1991**, *26*, 187.

[33] Brumlik, C. J.; Parthasarathy, A.; Chen, W. J.; Martin, C. R. *J. Electrochem. Soc.* **1994**, *141*, 2273.

[34] Finsterwalder, F.; Hambitzer, G. *J. Membr. Sci.* **2001**, *185*, 105.

[35] Roualdes, S.; Topala, I.; Mahdjoub, H.; Rouessac, V.; Sistat, P.; Durand, J. *J. Power Sources* **2006**, *158*, 1270.

[36] Thery, J.; Martin, S.; Faucheux, V.; Le Van Jodin, L.; Truffier-Boutry, D.; Martinent, A.; Laurent, J. Y. *J. Power Sources* **2010**, *195*, 5573.

[37] Jiang, Z.; Jiang, Z.; Meng, Y. *J. Membr. Sci.* **2011**, *372*, 303.

[38] Ryan, M. E.; Hynes, A. M.; Badyal, J. P. S. *Chem. Mater.* **1996**, *8*, 37.

[39] Holmes, S. A.; Thomas, T. D. *J. Am. Chem. Soc.* **1975**, *97*, 2337.

[40] Lin-Vien, D.; Colthup, N. B.; Fateley, W. G.; Grasselli, J. G. *The Handbook of Infrared and Raman Characteristic Frequencies of Organic Molecules*; Academic Press: London, U.K., 1991.

[41] (a) Dauben, W. G.; Epstein, W. W. *J. Org. Chem.* **1959**, *24*, 1595; (b) Mirone, P.; Chiorboli, P. *Spectrochim. Acta* **1962**, *18*, 1425.

[42] Parsons, A. F. *An Introduction to Free Radical Chemistry*; Blackwell Science Ltd: Oxford, U.K., 2000.

[43] Mayo, F. R.; Lewis, F. M.; Walling, C. *J. Am. Chem. Soc.* **1948**, *70*, 1529.

[44] Griese, B. *Angew. Chem., Int. Ed.* **1983**, *22*, 753.

[45] Dippy, J. F. J. *Chem. Rev.* **1939**, *25*, 151.

[46] Ward, L. J.; Schofield, W. C. E.; Badyal, J. P. S.; Goodwin, A. J.; Merlin, P. J. *Chem. Mater.* **2003**, *15*, 1466.

Chapter 4

Proton Conducting Polymer Grafts from Plasmachemical Films

4.1 Introduction

In chapter 3, the use of plasma deposition in order to manufacture acid-containing coatings was detailed. As discussed in section 3.4, the use of vapour-phase deposition techniques entails a precursor with significant vapour pressure. This requirement precludes sulfonic acid or sulfonate containing monomers, which would be desirable for proton exchange membranes given their strong acid groups. A way to incorporate strong sulfonic acid groups into the plasma polymer film (aside from drastic methods such as boiling in sulfuric acid, which would likely cause severe degradation to the polymer) could be to use the chemical properties of plasma polymers themselves. Plasmachemically deposited films have radicals trapped within them even under the relatively gentle plasma conditions used in chapter 3.[1] These radicals survive only a short time (a matter of minutes) when the polymer is exposed to air, but could potentially be used to initiate conventional radical polymerization from the surface of the films. Since such graft polymerizations would be done in the solution/liquid phase, the number of available monomers is vastly increased and includes sulfonate bearing moieties. This chapter expounds the use of the trapped radical phenomenon in order to improve the proton conductivity of plasmachemically deposited thin films.

Current global efforts targeting the reduction of carbon emissions are aiming towards cleaner hydrogen-based energy sources as one viable solution. In this context, proton exchange membrane fuel cells (PEMFCs) are under development for automotive, stationary, and portable power applications.[2–4] These electrochemical cells oxidise fuel (usually hydrogen gas or methanol) at the anode to produce protons, which travel across the proton exchange membrane and react at the cathode with an oxidant (oxygen gas or air).[2] PEMFCs are particularly attractive when utilized in combination with energy storage media such as lithium ion batteries (which also require efficient ion conducting membranes).[5,6] Therefore there exists a strong demand for cost-effective and high performance proton exchange membranes.[7,8]

Nafion is the current industry benchmark for proton conducting membranes. It consists of perfluorosulfonic acid groups pendant off a poly(tetrafluoroethylene) backbone, and yields a proton conductivity of around 80–90 mS cm^{-1} at room temperature when fully hydrated.[9–12] The inherently high costs and environmental impact of Nafion proton exchange membrane manufacture means that there is an impetus for the development of alternative highly proton conducting membranes which are stable in water and easy to manufacture.[13] Some potential candidates have included poly(styrene),[14,15] poly(imide),[16] poly(aryl ether),[17,18] or poly(phosphazene)[19,20] hydrophobic backbones, which are either copolymerized with a hydrophilic acid-containing moiety,[16 17] sulfonated post polymerization,[21] or have hydrophilic acid-containing polymer chains grafted onto the hydrophobic backbone.[22,23] Amongst these polymer backbone functionalisation methods, grafting is particularly attractive since it can yield higher proton conductivity values.[22,23] Such graft polymerization techniques can be divided into either graft-from methods, where free radical creation within the polymer backbone is induced by radiation followed by growth of acid-containing polymer;[24] or graft-to approaches, where polymer brushes are synthesized beforehand and then attached to the polymer backbone via a reactive moiety (e.g. a double bond).[22] However, both ways suffer from various shortfalls: radiation-induced grafting-from can cause damage to the polymer backbone,[24] whereas graft-to requires multi-step syntheses prolonged reaction times.[22]

In contrast to the aforementioned complex membrane fabrication techniques, plasma polymerization is a much more straightforward and solventless methodology.[1] Previous plasma deposited proton exchange membranes have suffered from low proton conductivity[25–34] and susceptibility towards cracking when hydrated.[35,36]

In this investigation, anhydride-containing films are prepared by pulsed plasmachemical deposition, which are then activated by reaction with propylamine (aminolysis). This derivatisation with by propylamine leads to swelling of the anhydride layers, which provides greater access to subsurface free radicals trapped within the plasmachemical films.[37] These free radicals are then able to act as initiator sites for graft polymerization of styrene or sodium 4-styrenesulfonate (which is easily converted into sulfonic acid groups), Scheme 4.1.

This is the first time that carboxylic acid–containing polymer backbone films with intrinsic proton conductivity have been combined with grafted sulfonic acid–containing polymer brushes, and found to display high proton conductivity. Furthermore, the measured proton conductivities are greater than or equal to Nafion, and these layers exhibit good stability in water.

4.2 Experimental

4.2.1 Preparation of Polymer Graft Layers

Plasma deposition of the poly(anhydride) layers was carried out according to the method in section 2.1 (page 27). Substrates used for coating were silicon (100) wafer pieces (Silicon Valley Microelectronics Inc.) and polypropylene sheet (Lawson Mardon Ltd.) with two evaporated gold

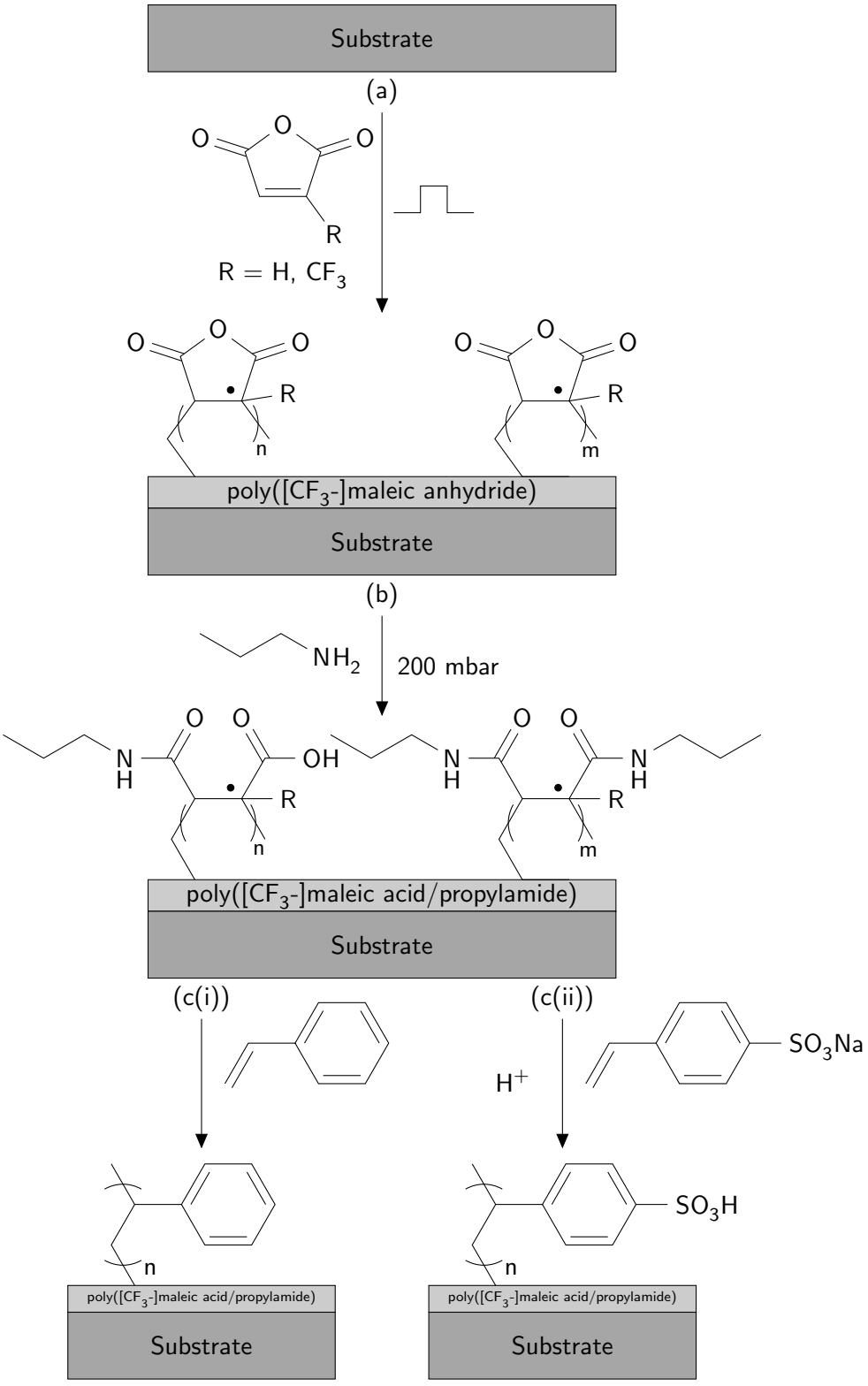

Scheme 4.1: (a) Pulsed plasmachemical deposition of anhydride-containing films followed by (b) aminolysis and (c) subsequent thermal graft-from polymerization of (i) styrene or (ii) sodium 4-styrenesulfonate.

electrodes (5 mm length and 1.5 mm separation) for proton conductivity testing. Borosilicate glass slides (VWR Ltd.) were used for radical density quantification measurements. Maleic anhydride briquettes (+99%, Aldrich Ltd., ground into a fine powder) and (trifluoromethyl)maleic anhydride (+97%, Apollo Scientific Ltd.) were loaded into separate sealable glass tubes and degassed using multiple freeze-pump-thaw cycles. Pulsed plasma deposition utilized an optimal duty cycle of 20 μs on-period and 1200 μs off-period in conjunction with a peak power of 5 W.[38]

The plasma deposited anhydride-containing films were subsequently derivatised by exposure to propylamine vapour at a pressure of 200 mbar for 30 min, followed by evacuation of the system back down to base pressure.

Next, the propylamine derivatised anhydride-containing films were placed into a sealable glass tube together with either 1 mL of styrene (+99%, Aldrich Ltd.) or 18 wt % sodium 4-styrenesulfonate (Aldrich Ltd.) solution in water. These mixtures were subjected to several freeze-pump-thaw cycles until fully degassed, whereupon the tube was placed into an oil bath (at 90 °C for styrene and at 50 °C for sodium 4-styrenesulfonate) to initiate graft-from polymerization. Upon completion of the styrene polymerization, the substrates were washed by a dichloromethane soxhlet for 16 h in order to remove unattached polymer. Upon completion of the sodium 4-styrenesulfonate polymerization, substrates were washed in high purity water (pH = 7.0) and aqueous acetic acid (Fisher Scientific Ltd.) solution (pH = 3.7) in order to effect ion exchange between Na^+ and H^+. Finally, the samples were allowed to dry in air at room temperature.

4.2.2 Film Characterization

Surface elemental compositions were determined by X-ray photoelectron spectroscopy (XPS) using a VG ESCALAB II electron spectrometer as described in section 2.2 (page 28). Experimentally determined instrument sensitivity (multiplication) factors were taken as C(1s): O(1s): F(1s): N(1s): Na(1s): S(2p) equals 1.00: 0.34: 0.26: 0.66: 0.05: 0.55.

Infrared spectra were acquired using a FTIR spectrometer (Perkin-Elmer Spectrum One) as described in section 2.3 (page 2.3). The instrument included a variable angle reflection-absorption accessory (Specac Ltd) set to a grazing angle of 66° for silicon wafer substrates and adjusted for p-polarization.

The concentration of radical sites present in the films was determined using 2,2-diphenyl-1-picrylhydrazyl (DPPH, 95%, Aldrich Ltd).[39] A borosilicate glass coverslip slide coated with the plasmachemical films was placed into a glass tube containing 1×10^{-4} mol dm^{-3} solution of DPPH in toluene (which had been thoroughly degassed using multiple freeze-pump-thaw cycles). The tube was then heated to 50 °C for 30 min. The DPPH molecules consumed by surface radicals were quantified using a spectrophotometer (Philips Scientific Ltd, PU 8625) by measuring the difference in absorbance at 520 nm between the starting solution and following immersion of each coated sample.

Film thicknesses were measured using a spectrophotometer (nkd-6000, Aquila Instruments Ltd.) as described in section 2.4 (page 33).

Proton conductivity values were obtained by undertaking impedance measurements across the 10 Hz-13 MHz frequency range using an LF impedance analyser (Hewlett-Packard, 4192A) for coated polypropylene substrates whilst submerged in ultra high purity water at room temperature (20 °C) as described in section 2.6 (page 35).

4.3 Results

Pulsed plasma deposited poly(maleic anhydride) layers display a distinctive XPS C(1s) component peak at 288.9 eV (O−C=O) corresponding to anhydride carbon centres, Figure 4.1.[38] Following reaction with propylamine, this feature shifts to 288.0 eV (N−C=O), which is consistent with aminolysis having taken place.[40] This is accompanied by an increase in the hydrocarbon (C_xH_y) component peak at 285.0 eV attributable to the alkyl chain of propylamine. Subsequent graft polymerizations of either styrene or sodium 4-styrenesulfonate resulted in the loss of the anhydride/amide shoulder peak to leave the predominant hydrocarbon (C_xH_y) feature. This is consistent with there being complete coverage by poly(styrene) or poly(sodium 4-styrenesulfonate) of the poly(maleic anhydride) initiator layer. A low intensity $\pi \rightarrow \pi^*$ shake-up feature at 291.0 eV characteristic of the phenyl centres is also observed.[40]

A similar series of reactions was shown to occur for pulsed plasma deposited poly((trifluoromethyl)maleic anhydride) layers, which initially display the distinctive anhydride component peak at 288.9 eV (O−C=O) as well as a feature at 292.5 eV characteristic of trifluoromethyl (CF_3) centres,[41] Figure 4.2. This trifluoromethyl peak remains following aminolysis, but disappears upon coverage by the grafted poly(styrene) or poly(4-styrenesulfonate) layers.

For both types of anhydride initiator layer, the absence of any Si(2p) XPS signal from the underlying silicon substrate confirmed surface coverage. For the propylamine derivatized films, carbon, oxygen and nitrogen signals were detected (along with fluorine in the case of pulsed plasma deposited poly((trifluoromethyl)maleic anhydride)) confirming reaction of the propylamine with the anhydride functionalities, Table 4.1. The N:O ratio for the propylamine derivatized pulsed plasma deposited poly(maleic anhydride) films was 1.0:2.4, whilst a much higher ratio of 1.0:1.1 was measured for the propylamine-derivatized pulsed plasma deposited poly((trifluoromethyl)-maleic anhydride) layers. This is indicative of the anhydride rings being more susceptible towards complete aminolysis for the latter and is supported by the accompanying N(1s) XPS region which shows a single component peak at 399.8 eV (corresponding to amide O=C−N(H)−C group formation);[40] in the case of pulsed plasma deposited poly(maleic anhydride) there is an extra smaller peak at 401.6 eV (assigned to $C-NH_3^+$ centres and hence only partial aminolysis[40]), Figure 4.3. Elemental XPS concentrations for both thermally grafted poly(styrene) and poly(sodium 4-styrenesulfonate) films show good agreement with the predicted theoretical polymer structure, Table 4.1. The cationic sodium content is measured to be less as a consequence of some ion

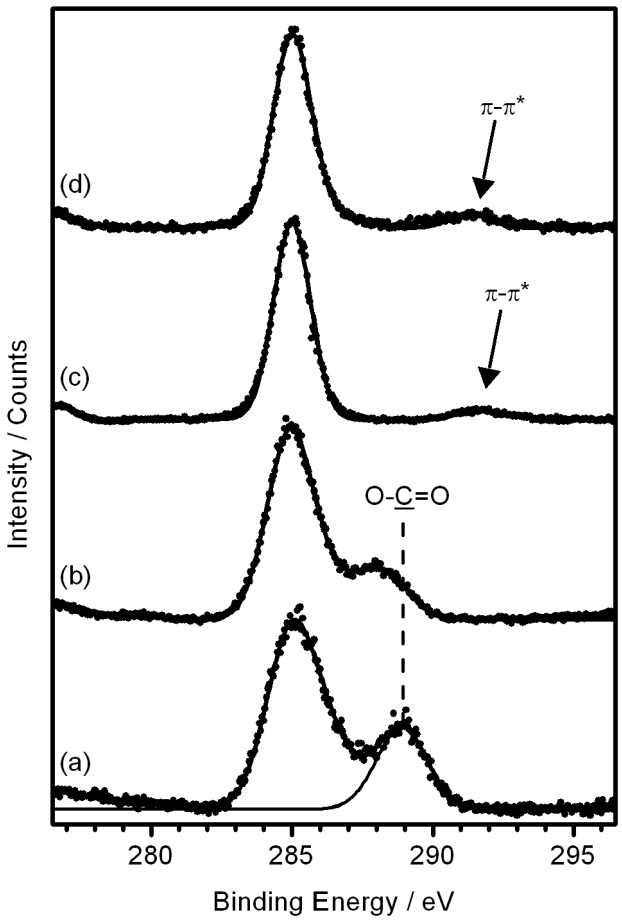

Figure 4.1: C(1s) XPS spectra for: (a) pulsed plasma deposited poly(maleic anhydride), (b) propylamine-derivatized pulsed plasma deposited poly(maleic anhydride), (c) poly(styrene) grafted from propylamine-derivatized pulsed plasma poly(maleic anhydride) and (d) poly(sodium 4-styrenesulfonate) grafted from propylamine-derivatized pulsed plasma poly(maleic anhydride).

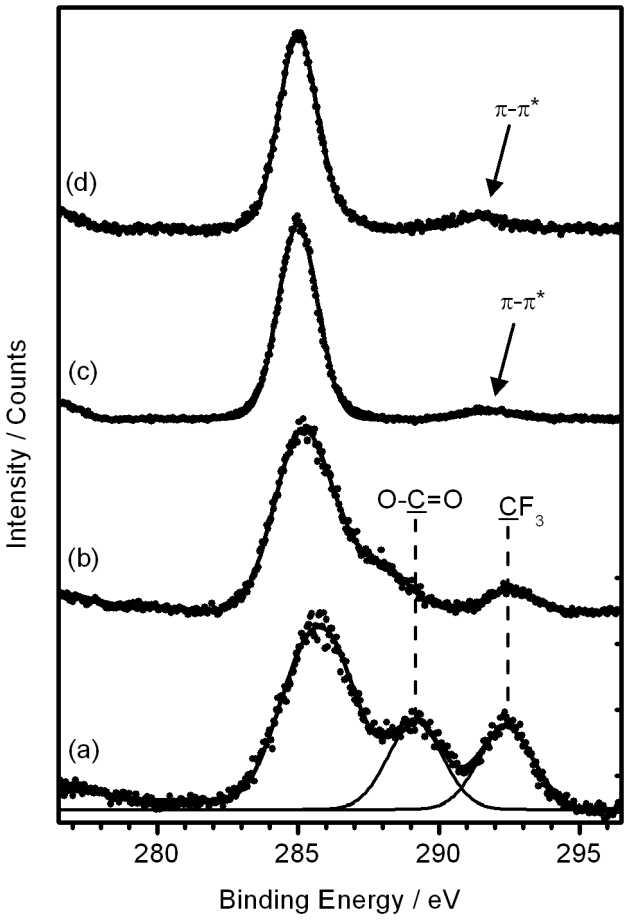

Figure 4.2: C(1s) XPS spectra for: (a) pulsed plasma deposited poly((trifluoromethyl)-maleic anhydride), (b) propylamine-derivatized pulsed plasma deposited poly((trifluoromethyl)-maleic anhydride), (c) poly(styrene) grafted from propylamine-derivatized pulsed plasma poly((trifluoromethyl)maleic anhydride) and (d) poly(sodium 4-styrenesulfonate) grafted from propylamine-derivatized pulsed plasma poly((trifluoromethyl)maleic anhydride).

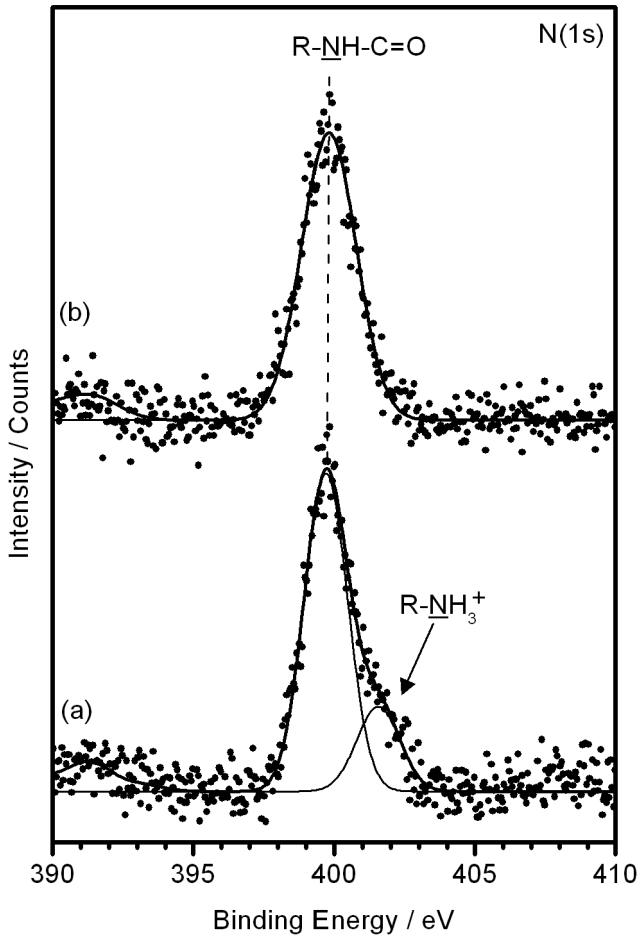

Figure 4.3: N(1s) XPS spectra following propylamine derivatization of: (a) pulsed plasma deposited poly(maleic anhydride) and (b) pulsed plasma deposited poly((trifluoromethyl)maleic anhydride).

exchange with H^+ having taken place during the cleaning step with water and aqueous acetic acid following graft polymerization. This was proven by deliberately soaking in pH = 3.7 acetic acid solution, which gave rise to the complete disappearance of the sodium XPS signal, whilst other elements remained, thus confirming that ion exchange of Na^+ for H^+ can take place.

Infrared spectra for the pulsed plasma deposited poly(maleic anhydride) films show fingerprint anhydride symmetric (1870 cm^{-1}) and antisymmetric (1800 cm^{-1}) C=O stretches,[38] Figure 4.4. Propylamine derivatization causes attenuation of the anhydride peak (1800 cm^{-1}) with the concurrent appearance of a carboxylic acid antisymmetric C=O stretch (1711 cm^{-1}), amide C=O stretch (1656 cm^{-1}, amide I) and amide C−N−H stretch bend (1577 cm^{-1}, amide II). Alkyl group features are also evident with CH_3 antisymmetric stretch (2966 cm^{-1}), CH_2 antisymmetric stretch (2936 cm^{-1}) and CH_3 symmetric stretch (2874 cm^{-1}), along with a broad band corresponding to the amide N−H stretch (3250 cm^{-1}). After thermal grafting of styrene the following bands appeared:[42] C−H aromatic ring stretches (3100–3000 cm^{-1}), CH_2 antisymmetric and symmetric

Layer	%C	%O	%F	%N	%Na	%S
Pulsed plasma poly(maleic anhydride)	67±1	33±1	—	—	—	—
Pulsed plasma poly((trifluoromethyl)maleic anhydride)	52±1	15±1	33±1	—	—	—
Propylamine-derivatized pulsed plasma poly(maleic anhydride)	69±1	2±1	—	9±1	—	—
Propylamine-derivatized pulsed plasma poly(trifluoromethylmaleic anhydride)	63±1	10±1	19±1	9±1	—	—
Poly(styrene) thermally grafted from propylamine-derivatized pulsed plasma poly(maleic anhydride)	100	—	—	—	—	—
Poly(styrene) thermally grafted from propylamine-derivatized pulsed plasma poly((trifluoromethyl)maleic anhydride)	100	—	—	—	—	—
Theoretical poly(sodium 4-styrenesulfonate)	62	23	—	—	8	8
Poly(sodium 4-styrenesulfonate) thermally grafted from propylamine-derivatized pulsed plasma poly(maleic anhydride)	67±1	22±1	—	—	3±1	9±1
Poly(sodium 4-styrenesulfonate) thermally grafted from propylamine-derivatized pulsed plasma Poly((trifluoromethyl)maleic anhydride)	66±1	22±1	—	—	4±1	9±1

Table 4.1: XPS elemental concentrations

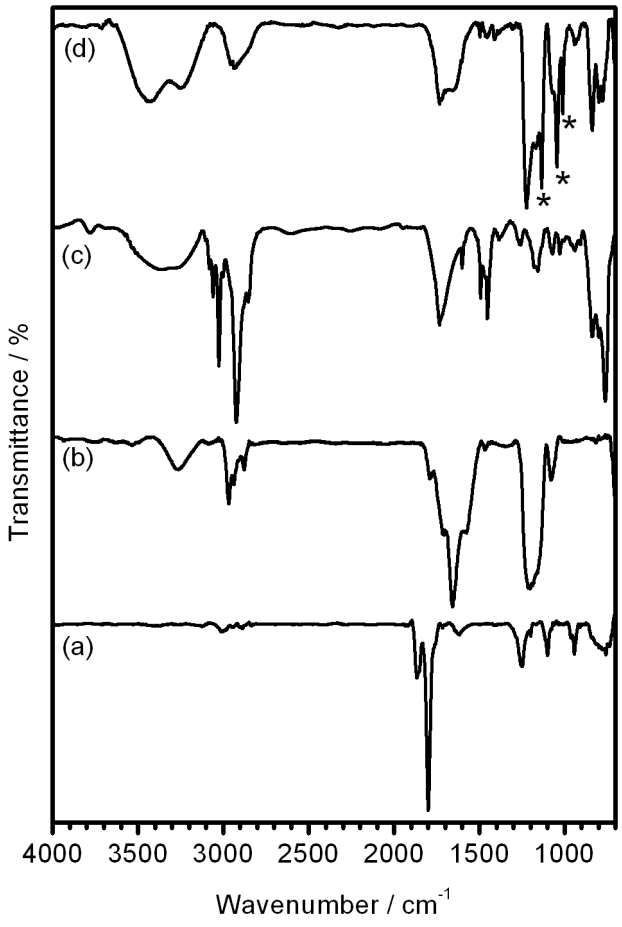

Figure 4.4: Infrared spectra of: (a) pulsed plasma deposited poly(maleic anhydride), (b) propylamine-derivatized pulsed plasma deposited poly(maleic anhydride) layer, (c) poly(styrene) grafted from propylamine-derivatized pulsed plasma deposited poly(maleic anhydride) and (d) poly(sodium 4-styrenesulfonate) layer grafted from propylamine-derivatized pulsed plasma deposited poly(maleic anhydride). * Denotes characteristic benzenesulfonate peaks.

stretches (2921 cm^{-1} and 2850 cm^{-1} respectively), ring quadrant stretches (1600 cm^{-1} and 1582 cm^{-1}) and ring semicircle stretches (1493 cm^{-1} and 1452 cm^{-1}). Subsequent graft polymerization of sodium 4-styrenesulfonate gave rise to the appearance of the SO_3 symmetric stretch (1045 cm^{-1}), together with the phenyl ring in-plane skeleton vibration (1134 cm^{-1}) and in-plane bending vibration (1012 cm^{-1}), Figure 4.4.[43]

In the case of pulsed plasma deposited poly((trifluoromethyl)maleic anhydride) films, the infrared spectra display similar changes, with there being initially characteristic anhydride C=O symmetric (1880 cm^{-1}) and antisymmetric (1809 cm^{-1}) peaks, Figure 4.5. These completely disappear upon propylamine derivatization, thereby confirming complete reaction throughout the plasma deposited layer, whilst graft polymerization of styrene gave rise to the appearance of the C−H aromatic ring stretches at 3100–3000 cm^{-1}, CH_2 antisymmetric and symmetric stretches (2921 cm^{-1} and 2850 cm^{-1} respectively), ring quadrant stretches (1600 cm^{-1} and 1582 cm^{-1})

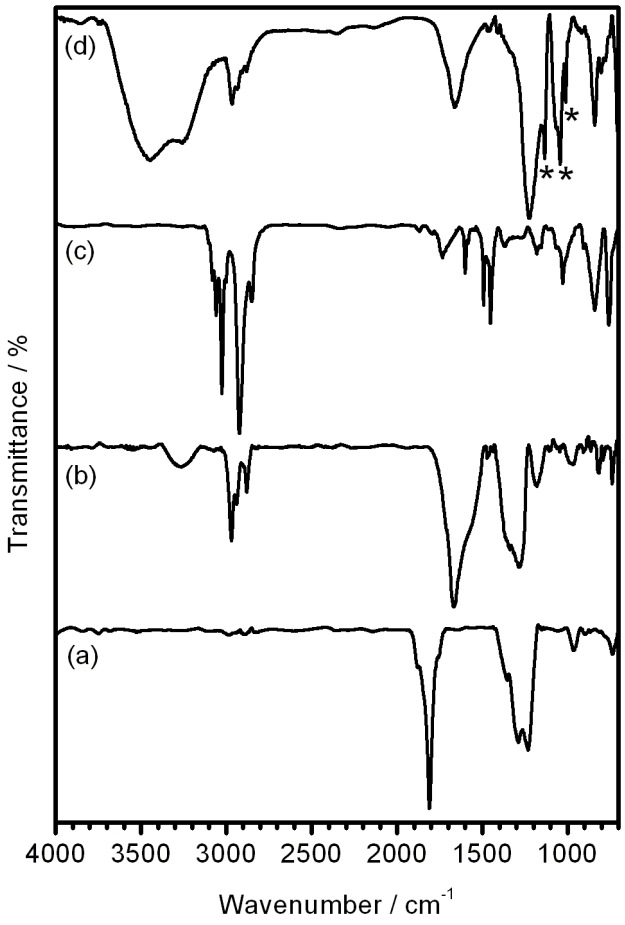

Figure 4.5: Infrared spectra of: (a) pulsed plasma deposited poly(trifluoromethyl)maleic anhydride), (b) propylamine-derivatized pulsed plasma deposited poly(trifluoromethyl)maleic anhydride) layer, (c) poly(styrene) grafted from propylamine-derivatized pulsed plasma deposited poly(trifluoromethyl)maleic anhydride) and (d) poly(sodium 4-styrenesulfonate) layer grafted from propylamine-derivatized pulsed plasma deposited poly(trifluoromethyl)maleic anhydride). * Denotes characteristic benzenesulfonate peaks.

and ring semicircle stretches (1493 cm^{-1} and 1452 cm^{-1}). Graft polymerization of sodium 4-styrenesulfonate similarly gave rise to the appearance of the characteristic SO_3 symmetric stretch (1045 cm^{-1}), along with the phenyl ring in-plane skeleton vibration (1134 cm^{-1}) and in-plane bending vibration (1012 cm^{-1}), Figure 4.5.

Free radical density assays show that the radical density for the pulsed plasma poly((trifluoromethyl)maleic anhydride) is greater by a factor of ten compared to pulsed plasma poly(maleic anhydride), which can be attributed to the stabilizing effect of the electron withdrawing trifluoromethyl group, Table 4.2. Derivatization by propylamine gives rise to a much higher density of accessible surface radicals for both types of anhydride-containing layer, whereas the number of radicals measured was below the detection limit after the poly(sodium 4-styrenesulfonate) grafting step.

Film	Thickness/ nm	Radical density/ 10^{-9} mol cm^{-2}	Water uptake/ wt %
Pulsed plasma poly(maleic anhydride)	98±4	2.6±0.2	167±7
Pulsed plasma poly((trifluoromethyl)maleic anhydride)	101±5	31±2	143±3
Propylamine-derivatized pulsed plasma poly(maleic anhydride)	197±7	37±2	120±10
Propylamine-derivatized pulsed plasma poly((trifluoromethyl)-maleic anhydride)	211±8	52±4	90±10
Poly(styrene) thermally grafted onto propylamine-derivatized pulsed plasma poly(maleic anhydride), 1h	490±30	0.0±0.1	—
Poly(styrene) thermally grafted onto propylamine-derivatized pulsed plasma poly((trifluoromethyl)maleic anhydride), 1h	700±30	0.0±0.1	—
Poly(sodium 4-styrenesulfonate) thermally grafted onto propylamine-derivatized pulsed plasma poly(maleic anhydride), 1 h	248±9	0.0±0.1	140±10
Poly(sodium 4-styrenesulfonate) thermally grafted onto propylamine-derivatized pulsed plasma poly((trifluoromethyl)maleic anhydride), 1 h	292±9	0.0±0.1	120±10

Table 4.2: Film thickness, radical density and water uptake of deposited films.

Film thickness measurements for both types of plasma deposited anhydride containing layers showed approximately 100% swelling upon propylamine derivatization, which can be attributed to the aminolysis reaction,[37] Table 4.2. Subsequent graft polymerization of both poly(styrene) and poly(sodium 4-styrenesulfonate) films was found to be more rapid for the propylamine derivatized plasma deposited poly((trifluoromethyl)maleic anhydride) films compared to their maleic anhydride analogue, which is consistent with there being a higher concentration of radicals. Film thicknesses did not significantly increase beyond 1 h grafting time, which can be attributed to termination reactions taking place due to the non-controlled nature of the polymerization.[44]

Proton conductivity values of 50 $\pm$ 5 mS cm^{-1} and 90 $\pm$ 5 mS cm^{-1} were measured for pulsed plasma deposited poly(maleic anhydride) and poly((trifluoromethyl)maleic anhydride) films respectively, Figure 4.6. These proton conductivities were drastically reduced for both films upon aminolysis (10 and 20 mS cm^{-1} respectively), which can be attributed to the loss of free carboxylic acid centres due to reaction taking place with propylamine. Subsequent thermal graft polymerization of sodium 4-styrenesulfonate gave rise to a significant increase in proton conductivity exceeding the values for the parent films (95 and 125 mS cm^{-1} respectively). The higher proton conductivity of the poly(4-styrenesulfonic acid) films grafted from the propylamine derivatized pulsed plasma deposited poly((trifluoromethyl)maleic anhydride) layers can be attributed to the more extensive grafting, and therefore greater density of sulfonic acid groups (which are known to underpin proton conductivity). Control samples in the absence of propylamine derivatisation did not show this enhanced proton conductivity behaviour following graft polymerization of poly(sodium 4-styrenesulfonate). Furthermore, no cracking in the films upon hydration was observed.

4.4 Discussion

Pulsed plasma deposition of anhydride-containing films effectively provides a single-step process for preparing proton exchange membranes at ambient temperatures. Upon exposure to water, the inherent high density of carboxylic acid functionalities gives rise to proton conductivity. Propylamine derivatization leads to a drop in proton conduction, which can be explained on the basis of a loss of proton conducting carboxylic acid centres due to their consumption in the aminolysis reaction, Scheme 4.1. Grafting of poly(sodium 4-styrenesulfonate) layers from these aminolysed carboxylic anhydride membranes leads to a large enhancement in conductivity yielding 125 mS cm^{-1} at room temperature for the trifluoromethyl variant, Figure 4.6. This compares favourably to the current benchmark standard, Nafion, which has a proton conductivity of 80–90 mS cm^{-1} under similar test conditions.[12] These propylamine derivatized carboxylic anhydride films are sufficiently robust to allow growth of sulfonic acid-containing polymer brushes as well as being stable afterwards in water. This is in marked contrast with previous plasma polymer proton exchange membranes which suffer from a lack of stability upon hydration.[35,36]

A threefold beneficial effect is observed for the trifluoromethyl group substituted variant of

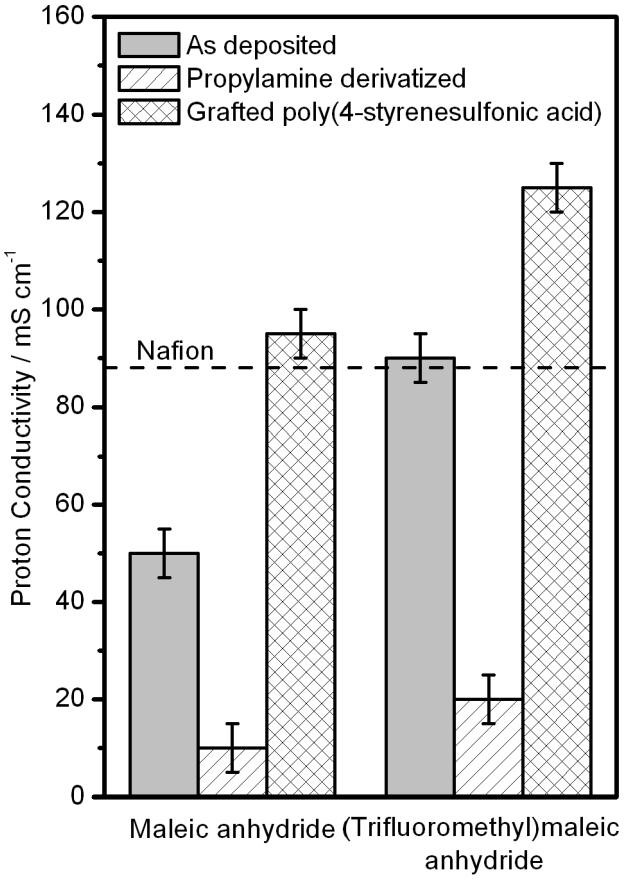

Figure 4.6: Proton conductivity upon immersion in water at 20 °C for pulsed plasma-deposited anhydride films: as deposited; after reaction with propylamine; and subsequent grafting of poly(sodium 4-styrenesulfonate) followed by proton exchange. No enhanced proton conductivity behaviour was observed following graft polymerization of poly(sodium 4-styrenesulfonate) in the absence of propylamine derivatization.

maleic anhydride precursor: firstly it stabilizes anhydride radicals within the electrical discharge[45] (thus enhancing polymer chain growth during the plasma duty cycle off-period, and also increases the density of radicals contained within the film which can act as initiation centres during the subsequent grafting step of styrene or sodium 4-styrenesulfonate[46,47]); secondly, its electron-withdrawing effect makes the carboxylic acid group more acidic (therefore higher proton conductivity);[48] and finally it makes the carbonyl centre more susceptible towards nucleophilic attack,[49] thus maximizing the extent of aminolysis, which helps to enhance the density of radicals contained in the functional layer.[37] Anhydride rings are known to be particularly good at stabilizing radicals due to resonance effects enabled by the cyclic conjugated anhydride structure.[50]

Free radical polymerizations can be split into controlled and uncontrolled reactions. The former include nitroxide mediated polymerization (NMP), atom transfer radical polymerization (ATRP) and reversible addition-fragmentation chain-transfer (RAFT) polymerization. All of these use some method of trapping the radicals present in the growing polymer brushes such that the concentration of any terminating species is reduced (for example, ATRP uses a copper catalyst and the equilibrium between copper(I) and copper(II) to control the polymerization reaction). In controlled radical polymerizations therefore, since there is a relatively low concentration of radicals which are reactive, the polymerization from the surface is slow, but has the advantage of producing polymer brushes with a low polydispersity index (i.e. of similar length).

In the case of growing polymer brushes from the surfaces of plasma polymer films in order to improve their proton conductivity, however, the use of controlled radical polymerization would only be advantageous if it directly enabled a greater density of acid groups within the polymer brushes. For poly(sodium 4-styrenesulfonate) brushes which have been grown from the surface of different plasma polymer films via controlled radical polymerization (ATRP), however, the maximum thickness attainable is around 50 nm.[51] The brushes do have the advantage of being a similar length, but in the current case, the grafting of poly(sodium 4-styrenesulfonate) brushes which have similar length is unnecessary, since this offers no improvement to the conductive properties of the films. Add to this the disadvantages of either needing an expensive polymerization agents (NMP and RAFT) or an extensive number of washing steps to remove copper catalyst (ATRP).

By contrast, thermal polymerization reaction, which simply utilizes the radicals within the plasma polymer films as an initiator, gives a similar thickness film (in the case of poly(sodium 4-styrenesulfonate)) but without the extra steps involved in controlled radical polymerizations. Additionally, many commercial polymerizations are based on thermal free radical reactions, whereas there are none to date which use controlled radical polymerization therefore engineering barriers to industry scaleup are minimized.

The outlined plasmachemical deposition process followed by propylamine derivatization, and the grafting of sulfonic acid containing polymer brushes, is simple, quick to manufacture, and utilizes water as a solvent (minimal environmental impact in marked contrast to Nafion).[52] Additionally, plasmachemical deposition provides a single-step deposition directly onto fuel cell com-

ponents (such as platinum loaded carbon black particles), which enables ease of manufacture by avoiding solvent casting techniques which inherently give rise to lack of conformality.[53] These advantages in the use of graft polymerization of polyelectrolytes from carboxylic acid–containing layers also have potential applications as lithium ion batteries or gas sensors.[6,54]

4.5 Conclusions

Pulsed plasmachemical deposition using maleic anhydride precursors yields structurally well-defined thin films. Subsequent aminolysis at the anhydride centres using propylamine causes swelling, which provides access to initiator free radical centres for the grafting of sulfonic-acid containing polymer brushes. The resultant functional layers yield proton conductivity values exceeding or on a par with Nafion. The inherent capability to conformally coat device components with highly proton conducting membranes offers advantage in term of lower cost, ease of manufacture, and avoidance of environmentally unfriendly non-aqueous processing.

4.6 References

[1] Yasuda, H. *Plasma Polymerization*; Academic Press: New York, 1985.

[2] Winter, M.; Brodd, R. J. *Chem. Rev.* **2004**, *104*, 4245.

[3] Hickner, M. A.; Ghassemi, H.; Kim, Y. S.; Einsla, B. R.; McGrath, J. E. *Chem. Rev.* **2004**, *104*, 4587.

[4] Steele, B. C. H.; Heinzel, A. *Nature* **2001**, *414*, 345.

[5] Crittenden, J. C.; White, H. S. *J. Am. Chem. Soc.* **2010**, *132*, 4503.

[6] Kerr, R. L.; Miller, S. A.; Shoemaker, R. K.; Elliott, B. J.; Gin, D. L. *J. Am. Chem. Soc.* **2009**, *131*, 15972.

[7] Service, R. F. *Science* **2002**, *296*, 1222.

[8] *2010 Annual Report*; Hydrogen and Fuel Cell Technical Advisory Committee, U.S. Department of Energy, 2011.

[9] Mikhailenko, S. D.; Guiver, M. D.; Kaliaguine, S. *Solid State Ionics* **2008**, *179*, 619.

[10] Spry, D. B.; Goun, A.; Glusac, K.; Moilanen, D. E.; Fayer, M. D. *J. Am. Chem. Soc.* **2007**, *129*, 8122.

[11] Fontanella, J. J.; Wintersgill, M. C.; Chen, R. S.; Wu, Y.; Greenbaum, S. G. *Electrochim. Acta* **1995**, *40*, 2321.

[12] Mauritz, K. A.; Moore, R. B. *Chem. Rev.* **2004**, *104*, 4535.

[13] Costamagna, P.; Srinivasan, S. *J. Power Sources* **2001**, *102*, 242.

[14] Chen, S.; Benziger, J. B.; Bocarsly, A. B.; Zhang, T. *Ind. Eng. Chem. Res.* **2005**, *44*, 7701.

[15] Bertran, O.; Curco, D.; Torras, J.; Ferreira, C. A.; Aleman, C. *Macromolecules* **2010**, *43*, 10521.

[16] Asano, N.; Aoki, M.; Shinsuke, S.; Miyatake, K.; Uchida, H.; Watanabe, M. *J. Am. Chem. Soc.* **2006**, *128*, 1762.

[17] Schmeisser, J.; Holdcroft, S.; Yu, J.; Ngo, T.; McLean, G. *Chem. Mater.* **2005**, *17*, 387.

[18] Miyatake, K.; Chikashige, Y.; Higuchi, E.; Watanabe, M. *J. Am. Chem. Soc.* **2007**, *129*, 3879.

[19] Allcock, H. R.; Hofmann, M. A.; Ambler, C. M.; Morford, R. V. *Macromolecules* **2002**, *35*, 3484.

[20] Hofmann, M. A.; Ambler, C. M.; Maher, A. E.; Chalkova, E.; Zhou, X. Y.; Lvov, S. N.; Allcock, H. R. *Macromolecules* **2002**, *35*, 6490.

[21] (a) Di Vona, M. L.; Sgreccia, E.; Licoccia, S.; Khadhraoui, M.; Denoyel, R.; Knauth, P. *Chem. Mater.* **2008**, *20*, 4327; (b) Kim, S. Y.; Park, M. J.; Balsara, N. P.; Jackson, A. *Macromolecules* **2010**, *43*, 8128.

[22] (a) Ding, J.; Chuy, C.; Holdcroft, S. *Macromolecules* **2002**, *35*, 1348; (b) Li, N.; Wang, C.; Lee, S. Y.; Park, C. H.; Lee, Y. M.; Guiver, M. D. *Angew. Chem., Int. Ed.* **2011**, *50*, 9158.

[23] Tsang, E. M. W.; Zhang, Z.; Shi, Z.; Soboleva, T.; Holdcroft, S. *J. Am. Chem. Soc.* **2007**, *129*, 15106.

[24] (a) Gupta, B.; Scherer, G. G. *J. Appl. Polym. Sci.* **1993**, *50*, 2129; (b) Yamaki, T.; Asano, M.; Maekawa, Y.; Morita, Y.; Suwa, T.; Chen, J.; Tsubokawa, N.; Kobayashi, K.; Kubota, H.; Yoshida, M. *Radiat. Phys. Chem.* **2003**, *67*, 403; (c) Holmberg, S.; Holmlund, P.; Nicolas, R.; Wilen, C.; Kallio, T.; Sundholm, G.; Sundholm, F. *Macromolecules* **2004**, *37*, 9909.

[25] Inagaki, N.; Tasaka, S.; Horkawa, Y. *J. Polym. Sci., Part A: Polym. Chem.* **1989**, *27*, 3495.

[26] Inagaki, N.; Tasaka, S.; Kurita, T. *Polym. Bull.* **1989**, *22*, 15.

[27] Ogumi, Z.; Uchimoto, Y.; Takehara, Z. *J. Electrochem. Soc.* **1990**, *137*, 3319.

[28] Ogumi, Z.; Uchimoto, Y.; Yasuda, K.; Takehara, Z. I. *Chem. Lett.* **1990**, 953.

[29] Inagaki, N.; Tasaka, S.; Chengfei, Z. *Polym. Bull.* **1991**, *26*, 187.

[30] Brumlik, C. J.; Parthasarathy, A.; Chen, W. J.; Martin, C. R. *J. Electrochem. Soc.* **1994**, *141*, 2273.

[31] Finsterwalder, F.; Hambitzer, G. *J. Membr. Sci.* **2001**, *185*, 105.

[32] Roualdes, S.; Topala, I.; Mahdjoub, H.; Rouessac, V.; Sistat, P.; Durand, J. *J. Power Sources* **2006**, *158*, 1270.

[33] Danilich, M. J.; Gervasio, D.; Burton, D. J.; Marchant, R. E. *Macromolecules* **1995**, *28*, 5567.

[34] Mahdjoub, H.; Roualdès, S.; Sistat, P.; Pradeilles, N.; Durand, J.; Pourcelly, G. *Fuel Cells* **2005**, *5*, 277.

[35] Thery, J.; Martin, S.; Faucheux, V.; Le Van Jodin, L.; Truffier-Boutry, D.; Martinent, A.; Laurent, J. Y. *J. Power Sources* **2010**, *195*, 5573.

[36] Jiang, Z.; Jiang, Z.; Meng, Y. *J. Membr. Sci.* **2011**, *372*, 303.

[37] Teare, D. O. H.; Schofield, W. C. E.; Garrod, R. P.; Badyal, J. P. S. *Langmuir* **2005**, *21*, 10818.

[38] Ryan, M. E.; Hynes, A. M.; Badyal, J. P. S. *Chem. Mater.* **1996**, *8*, 37.

[39] Suzuki, M.; Kishida, A.; Iwata, H.; Ikada, Y. *Macromolecules* **1986**, *19*, 1804.

[40] Beamson, G.; Briggs, D. *High Resolution XPS of Organic Polymers*; Wiley: Chichester, U.K., 1992.

[41] Holmes, S. A.; Thomas, T. D. *J. Am. Chem. Soc.* **1975**, *97*, 2337.

[42] Lin-Vien, D.; Colthup, N. B.; Fateley, W. G.; Grasselli, J. G. *The Handbook of Infrared and Raman Characteristic Frequencies of Organic Molecules*; Academic Press: London, U.K., 1991.

[43] Yang, J. C.; Jablonsky, M. J.; Mays, J. W. *Polymer* **2002**, *43*, 5125.

[44] Iddon, P. D.; Robinson, K. L.; Armes, S. P. *Polymer* **2004**, *45*, 759.

[45] Parsons, A. F. *An Introduction to Free Radical Chemistry*; Blackwell Science Ltd: Oxford, U.K., 2000.

[46] Mayo, F. R.; Lewis, F. M.; Walling, C. *J. Am. Chem. Soc.* **1948**, *70*, 1529.

[47] Griese, B. *Angew. Chem., Int. Ed.* **1983**, *22*, 753.

[48] Dippy, J. F. J. *Chem. Rev.* **1939**, *25*, 151.

[49] Nozaki, K.; Sato, N.; Ikeda, K.; Takaya, H. *J. Org. Chem.* **1996**, *61*, 4516.

[50] Teare, D. O. H.; Schofield, W. C. E.; Roucoules, V.; Badyal, J. P. S. *Langmuir* **2003**, *19*, 2398.

[51] Morsch, S.; Schofield, W. C. E.; Badyal, J. P. S. *Langmuir* **2011**, *27*, 14151.

[52] ten Brink, G.-J.; Arends, I. W. C. E.; Sheldon, R. A. *Science* **2000**, *287*, 1636.

[53] Berron, B. J.; Payne, P. A.; Jennings, G. K. *Ind. Eng. Chem. Res.* **2008**, *47*, 7707.

[54] van der Wal, P. D.; de Rooij, N. F.; Koudelka-Hep, M. *Sens. Actuators, B* **1996**, *35*, 119.

Chapter 5

Pulsed Plasmachemical Deposition of Ion-Conducting Poly(Ionic Liquid) Layers

5.1 Introduction

Chapters 3–4 were concerned with the plasmachemical deposition of proton conducting carboxylic acid-containing films (from anhydride precursors) and the enhancement in proton conductivity afforded by the grafting of sulfonic acid-containing polymer brushes from said films. Both types of films (pure carboxylic and carboxylic-sulfonic hybrid) rely on the presence of water for proton conductivity, however, and, as such, reach a maximum operating temperature of close to 100 °C after which the water present in the membranes will boil away. A similar problem is reported for Nafion which shows optimum proton conductivity at around 90 °C. Higher temperatures are quite desirable for use in proton exchange membrane fuel cells, however, since they improve the kinetics of the catalytic oxidation and reduction reactions at the electrodes as well as removing any need for water management (e.g. humidification of the fuel cell gas supply lines in order to balance osmotic water movement through the membrane). The use of liquid proton conductors such as phosphoric acid and ionic liquids, which conduct protons independent of water presence, is prevalent, but they need solid supports for mechanical reasons and a large membrane thickness in order to minimize gas crossover. Both these requirements lead to a higher membrane resistance with accompanying voltage loss (and therefore a fall in efficiency). In this chapter a poly(ionic liquid) film is deposited using a combination of vapour-phase techniques—the polymeric nature of the film solves the problems associated with liquid electrolytes and the ionic species within the polymer give rise to excellent ionic conduction.

Ionic liquids are organic salts which are molten at or near to room temperature. They typically consist of bulky organic cations, e.g. ammonium,[1,2] imidazolium[3] or phosphonium,[4] in combination with an appropriate anion (typically bis(trifluoromethane)sulfonylimide,[2,3] triflate[1] or

halide[5]). Poly(ionic liquid)s can be prepared from ionic liquids containing polymerizable moieties (e.g. acrylates or vinyl groups), and offer the advantage of superior mechanical properties.[6] Like their monomeric counterparts, they have found application in chromatography,[7] gas separation,[8] carbon dioxide absorption,[9] synthesis of intrinsically conducting polymers[10] and nanoparticles,[11] thermochromic dyes,[12] light emitting electrochemical cells,[13] lithium-ion batteries,[6] dye-sensitized solar cells[14,15] and supercapacitors.[16] In the case of electrolyte layers in fuel cells,[17] metal-air batteries[18] and humidity sensors,[19] good ionic conductivity at elevated temperatures and humidity is highly sought after (the current industrial benchmark, Nafion, starts to significantly lose ionic conductivity above 90 °C[20]). However, poly(ionic liquid)s have previously been reported to exhibit poor ionic conductivities compared to their parent monomers, which has been primarily attributed to a lack of polymer chain flexibility.[21,22] Normally this is redressed by doping with ionic liquids or other electrolytes,[23] but this occurs at the expense of a deterioration in mechanical properties.[24] Furthermore, the manufacture of such poly(ionic liquid)s typically relies upon wet chemical approaches, which have inherent disadvantages, including the requirement for solvent extraction and a separate casting step for application to solid surfaces.

In this chapter pulsed plasmachemical deposition is used to produce thin films with a high density of imidazole groups, which are subsequently quaternized using vapour-phase reaction with 1-bromobutane, Scheme 5.1. The resultant films show increasing ionic conductivity with rising temperature reaching values of 93.6 mS cm^{-1} at 100 °C (which is in marked contrast to the widely cited benchmark, Nafion, whose ionic conductivity starts to drop at elevated temperatures[25]).

5.2 Experimental

5.2.1 Deposition of Poly(ionic liquid) Layers

Pulsed plasmachemical deposition was carried out in an electrodeless cylindrical glass reactor (volume of 480 cm^3, base pressure of 3×10^{-3} mbar, and with a leak rate better than 2×10^{-9} mol s^{-1}) as described in section 2.1 (page 27). Substrates used for coating were silicon (100) wafer pieces (Silicon Valley Microelectronics Inc.) and polypropylene sheet pieces (Lawson Mardon Ltd.) which had two evaporated gold electrodes (5 mm length and 1.5 mm separation) for ion conductivity testing. 1-Allylimidazole (+97%, Acros Organics Ltd.) was loaded into a sealable glass tube and degassed using several freeze-pump-thaw cycles. Precursor vapour was allowed to purge the reactor for 5 min at a pressure of 0.18 mbar prior to electrical discharge ignition. Pulsed plasma deposition utilized an optimal duty cycle of 20 μs on-period and 1200 μs off-period in conjunction with a peak power of 30 W. Upon plasma extinction, the precursor vapour was allowed to continue to pass through the system for a further 3 min, and then the chamber was evacuated back down to base pressure. Imidazole ring quaternization entailed exposure of the deposited layers at 70 °C to 1-bromobutane vapour (99%, Sigma-Aldrich Ltd, degassed using several freeze-pump-thaw cycles) at a pressure of 4 mbar for 4.5 h. Subsequently, the reactor was

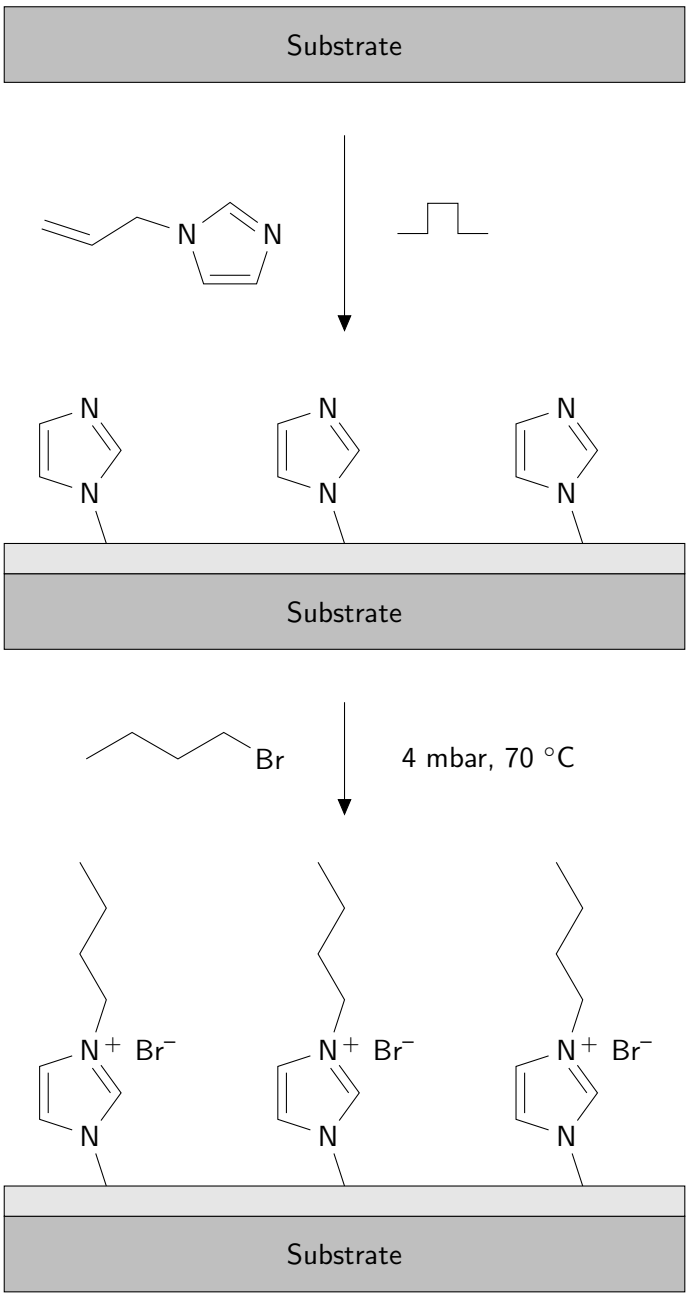

Scheme 5.1: Pulsed plasmachemical deposition of poly(1-allylimidazole) films followed by vapour-phase quaternization using 1-bromobutane at 70 °C.

evacuated to base pressure prior to venting to atmosphere.

Anion exchange experiments were carried out in the vapour phase by exposing the quaternized films to trifluoroacetic acid (Fluorochem Ltd) vapour for 300 s at room temperature before evacuating the reactor to base pressure prior to venting to atmosphere.

5.2.2 Film Characterization

Film thicknesses were measured using a spectrophotometer (nkd-6000, Aquila Instruments Ltd.) as described in section 2.4 (page 33). Typical deposition rates and film thicknesses were 16±2 nm min^{-1} and 580 nm respectively.

Infrared spectra were acquired using a FTIR spectrometer (Perkin-Elmer Spectrum One) as described in section 2.3 (page 31).

Surface elemental compositions were determined by X-ray photoelectron spectroscopy as described in section 2.2 (page 28). Experimentally determined instrument sensitivity (multiplication) factors were taken as C(1s): N(1s): Br(3d) equals 1.00: 0.66: 0.36.

Impedance measurements across the 700 Hz–13 MHz frequency range were carried out using an LF impedance analyser (Hewlett-Packard, 4192A) for coated polypropylene substrates as described in section 2.6 (page 35). Saturated salts of sodium chloride (+99%, Sigma-Aldrich Ltd.) and potassium sulfate (+99%, Sigma-Aldrich Ltd.) were used to create relative humidities of 75.5% and 97.6% at room temperature.[26] Ionic conductivity measurements at higher temperatures were carried out by Mikkel Larsen and Peter Lund of IRD Fuel Cells A/S, Denmark.

5.3 Results

Fourier-transform infrared spectroscopy of the pulsed plasma deposited poly(1-allylimidazole) films confirmed good structural retention of the precursor functionality, Figure 5.1. Characteristic imidazole ring absorbances include C=C−H ring stretch at 3107 cm^{-1}, C=N ring stretch at 1504 cm^{-1} and an in-plane bend N=C−H ring vibration at 1107 cm^{-1}.[27,28] Following quaternization of these imidazole rings with vapour-phase 1-bromobutane at 70 °C, a shift was observed in the imidazole ring vibrations to 3133 cm^{-1}, 1561 cm^{-1} and 1162 cm^{-1} respectively, which is consistent with the formation of an imodazolium cation.[29] Furthermore, the appearance of new C−H stretches at 2960 cm^{-1}, 2935 cm^{-1} and 2873 cm^{-1} along with the out of plane HCH deformation at 1463 cm^{-1} corresponds to the butyl chain belonging to 1-bromobutane. Broad peaks at 3500–3100 cm^{-1} and 1630 cm^{-1} can be attributed to water stretches, which is consistent with the hydrophilic nature of imidazole based polymers.[28] Compared to previously deposited pulsed plasma poly(1-allylimidazole) films,[27] the absence of C≡N stretches at 2230 cm^{-1} stems from the milder (more controlled) duty cycle employed in the present study.

X-ray photoelectron spectroscopy (XPS) analysis of the pulsed plasma deposited poly(1-allylimidazole) layer shows two N(1s) peaks at 398.9 eV and 400.7 eV corresponding to N−C

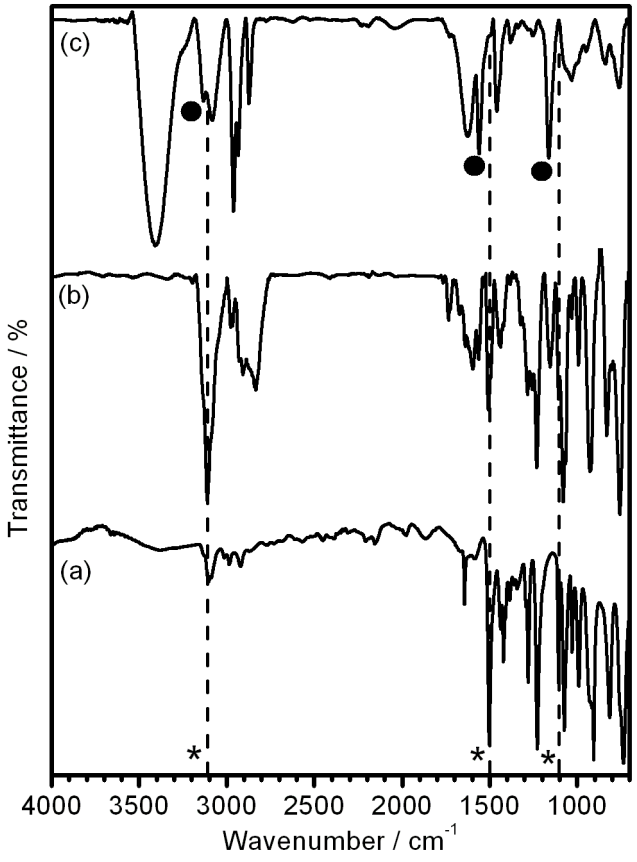

Figure 5.1: Fourier transform infrared spectra of (a) 1-allylimidazole monomer, (b) pulsed plasma deposited poly(1-allylimidazole) and (c) pulsed plasma deposited poly(1-allylimidazole) quaternized with 1-bromobutane. * Denotes imidazole ring absorbances. • Denotes imidazolium ring absorbances.

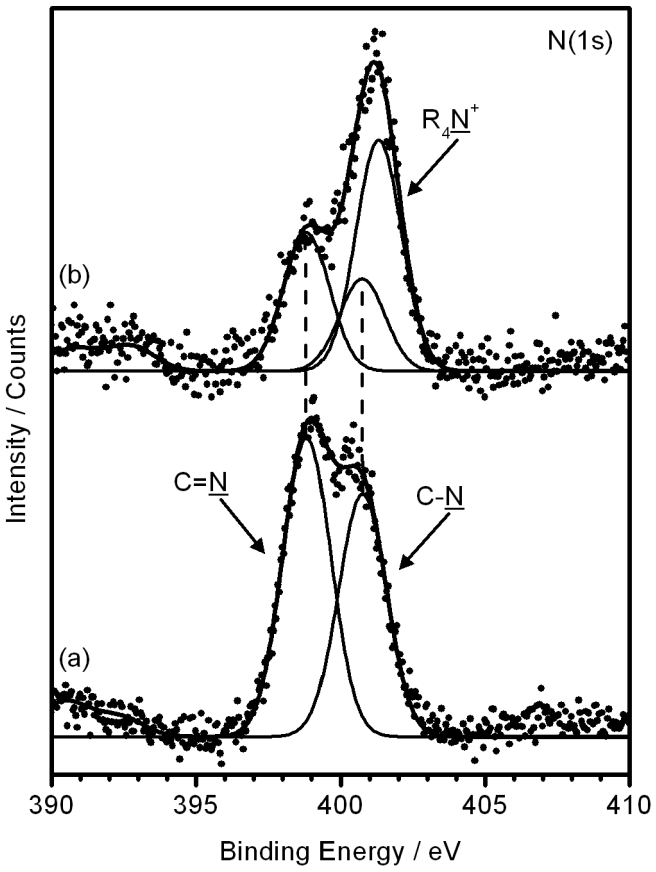

Figure 5.2: X-ray photoelectron N(1s) spectra of (a) pulsed plasma deposited poly(1-allylimidazole) and (b) pulsed plasma deposited poly(1-allylimidazole) quaternized with 1-bromobutane.

and N=C centres respectively,[30] Figure 5.2. Following quaternization of the imidazole ring, the XPS N(1s) spectrum shows a new, larger peak at 401.4 eV, which denotes quaternized, positively charged nitrogen centres.[30] The elemental XPS ratio of bromine to nitrogen was measured to be 1.0:3.1, which corresponds to 65% of the imidazole rings being quaternized to imidazolium.

Vapour-phase bromobutane quaternization also gives rise to a swelling in film thickness by approximately 10%, which, together with the infrared data, indicates that reaction has occurred throughout the plasmachemically deposited films.

Electrochemical impedance spectroscopy was used to measure the ionic conductivity of the films. Control samples of pulsed plasma deposited poly(1-allylimidazole) displayed no ionic conductivity, regardless of conditions. In contrast, at room temperature (20 °C), the quaternized poly(1-allylimidazole) films showed ionic conductivity of 0.7 mS cm^{-1} at 75.5% relative humidity, which increased to 1.0 mS cm^{-1} at 97.6% relative humidity. This rise in ionic conductivity with relative humidity is similar to that reported for imidazolium-based ionic liquids.[31] Furthermore, at higher temperatures of 60 °C and 80 °C (at 75% relative humidity) the ionic conductivity improves further to 6.9 mS cm^{-1} and 13.0 mS cm^{-1} respectively. Upon raising the temperature to 100 °C

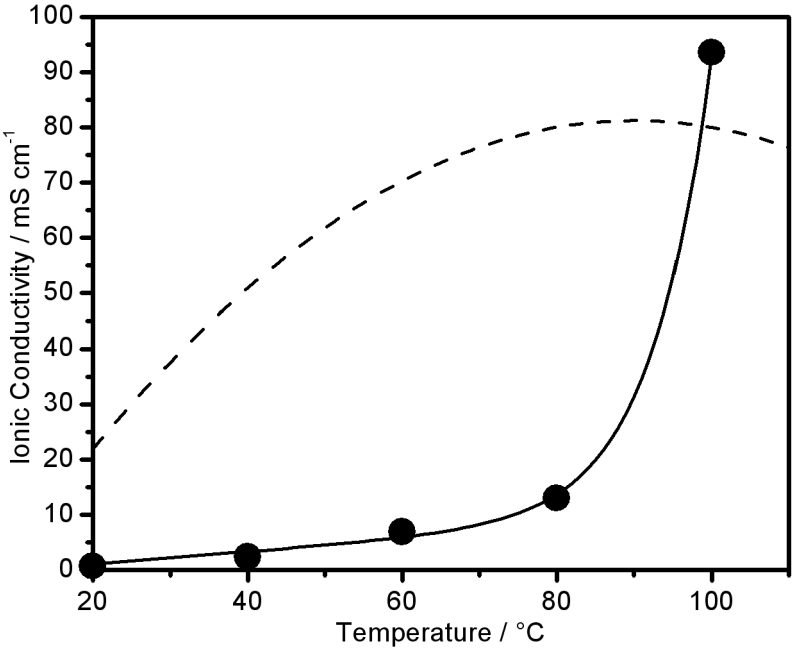

Figure 5.3: Ionic conductivity of pulsed plasma deposited poly(1-allylimidazole) quaternized with 1-bromobutane at 75% relative humidity (dashed line depicts performance of Nafion under similar conditions, extrapolated from references 25 and 32).

(relative humidity 75%), there is a sharp increase in the ionic conductivity of the films to 93.6 mS cm^{-1}, which is comparable to the performance of Nafion films under similar test conditions,[25,32] Figure 5.3.

5.4 Discussion

The source of ionic conductivity for the poly(ionic liquid) membranes is the bromide ions which act as charge carriers with the imidazolium groups anchored to the polymer backbone.[21] These conductivities are lower than those reported for bulk imidazolium ionic liquids due to the lack of free cationic charge carriers and the reduced mobility of the ions within the film.[33] The rise in ionic conductivity with relative humidity is similar to that reported for other imidazolium-based poly(ionic liquid)s, which can be attributed to the shielding effect of hydration shells around the ions within the polymer.[31] Polymer mobility is also known to be important for ionic conductivity since it lowers the energy barrier for anion movement throughout the film.[21,22] Therefore the large increase in ionic conductivity between 80 and 100 °C can be attributed to a T_g-like transition, which is responsible for increases in conductivity in conventional polymers due to enhanced segmental motion.[34] The behaviour of conductivity also relied on the nature of the anion, since after anion exchange with trifluoroacetate was carried out, the resultant films showed lower conductivities (0.33 and 0.68 mS cm^{-1} at room temperature, 75.5% and 97.6% relative humidity

respectively) and no significant change at higher temperatures.

In conventional ionic liquids there are many factors which affect ionic conductivity (that is, ionic mobility) including viscosity, melting point, ion size and humidity. Given this multitude of factors, there have been a large number of ionic liquids manufactured in order to optimize conductivity (and the other chemical properties in which ionic liquids excel, as solvents and catalysts etc.). Of all of these, imidazolium-based ionic liquids yield the highest ionic conductivity, particularly when combined with bulky anions (in the present study, however, the reverse is true, since the anion represents the major charge carrier).[31]

Similar attempts were made at creating poly(ionic liquid) films via pulsed plasmachemical deposition using 4-vinylpyridine, 1-vinylpyrrolidone and dimethylaminoethyl acrylate. All of the resultant polymers showed good structural retention upon plasma deposition, but the poly(4-vinylpyridine) layers were the only ones which reacted with 1-bromobutane at 70 °C. This can be attributed to the higher energy barrier to quaternization for non-aromatic nitrogen moieties (and indeed steric hindrance is increased in these cases). The quaternized poly(4-vinylpyridine) layers showed no significant ionic conductivity, however, which is in keeping with the superior conductive properties of imidazolium-containing (as opposed to pyridinium-containing) ionic liquids.

5.5 Conclusions

In conclusion, this plasmachemical deposition approach combined with vapour-phase quaternization yields poly(ionic liquid) films, which display very high ionic conductivities (exceeding 90 mS cm^{-1} at 100 °C and 75% relative humidity). In principle, this conformal and solventless technique could be applied directly to components employed in electrochemical devices (including fuel cells).

5.6 References

[1] Lu, W.; Fadeev, A. G.; Qi, B.; Smela, E.; Mattes, B. R.; Ding, J.; Spinks, G. M.; Mazurkiewicz, J.; Zhou, D.; Wallace, G. G.; MacFarlane, D. R.; Forsyth, S. A.; Forsyth, M. *Science* **2002**, *297*, 983.

[2] Zheng, H.; Zhang, Y.; Fu, Y.; Abe, T.; Ogumi, Z. *J. Phys. Chem. B* **2005**, *109*, 13676.

[3] Laforge, F. O.; Kakiuchi, T.; Shigematsu, F.; Mirkin, M. V. *J. Am. Chem. Soc.* **2004**, *126*, 15380.

[4] Evans, R. G.; Klymenko, O. V.; Saddoughi, S. A.; Hardacre, C.; Compton, R. G. *J. Phys. Chem. B* **2004**, *108*, 7878.

[5] Huang, J.; Sun, I. *Chem. Mater.* **2004**, *16*, 1829.

[6] Pont, A.-L.; Marcilla, R.; De Meatza, I.; Grande, H.; Mecerreyes, D. *J. Power Sources* **2009**, *188*, 558.

[7] Anderson, J. L.; Armstrong, D. W. *Anal. Chem.* **2005**, *77*, 6453.

[8] Bara, J. E.; Lessmann, S.; Gabriel, C. J.; Hatekeyama, E. S.; Noble, R. D.; Gin, D. L. *Ind. Eng. Chem. Res.* **2007**, *46*, 5397.

[9] Tang, J.; Sun, W.; Tang, H.; Radosz, M.; Shen, Y. *Macromolecules* **2005**, *38*, 2037.

[10] Marcilla, R.; Ochoteco, E.; Pozo-Gonzalo, H.; Grande, H.; Pomposo, J. A.; Mecerreyes, D. *Macromol. Rapid Commun.* **2005**, *26*, 1122.

[11] Mu, X.-D.; Meng, J.-Q.; Li, Z.-C.; Kou, Y. *J. Am. Chem. Soc.* **2005**, *127*, 9694.

[12] Tollan, C. M.; Marcilla, R.; Pomposo, J. A.; Rodriguez, J.; Aizpurua, J.; Molina, J.; Mecerreyes, D. *ACS Appl. Mater. Interfaces* **2009**, *1*, 348.

[13] Marcilla, R.; Mecerreyes, D.; Winroth, G.; Brovelli, S.; del Mar Rodriguez Yebra, M.; Cacialli, F. *Appl. Phys. Lett.* **2010**, *12*, 1916.

[14] Kawano, R.; Katakabe, T.; Shimosawa, H.; Nazeeruddin, M. K.; Grätzel, M.; Matsui, H.; Kitamura, T.; Tanabe, N.; Watanabe, M. *Phys. Chem. Chem. Phys.* **2010**, *12*, 1916.

[15] Wang, G.; Wang, L.; Zhuo, S.; Fang, S.; Lin, Y. *Chem. Commun.* **2011**, *47*, 2700.

[16] Kim, T. Y.; Lee, H. W.; Stoller, M.; Dreyer, D. R.; Bielawski, C. W.; Ruoff, R. S.; Suh, K. S. *ACS Nano* **2011**, *5*, 436.

[17] Noda, A.; Susan, M. A. B. H.; Kudo, K.; Mitsushima, S.; Hayamizu, K.; Watanabe, M. *J. Phys. Chem. B* **2003**, *107*, 4024.

[18] Kuboki, T.; Okuyama, T.; Ohsaki, T.; Takami, N. *J. Power Sources* **2005**, *146*, 766.

[19] Feng, C.-D.; Sun, S.-L.; Wang, H.; Segre, C. U.; Stetter, J. R. *Sens. Actuators, B* **1997**, *40*, 217.

[20] Kim, Y.-T.; Song, M.-K.; Kim, K.-H.; Park, S.-B.; Min, S.-K.; Rhee, H.-W. *Electrochim. Acta* **2004**, *50*, 645.

[21] Ohno, H.; Yoshizawa, M. *ACS Symp. Ser.* **2003**, *902*, 159.

[22] Lee, M.; Choi, U. H.; Colby, R. H.; Gibson, H. W. *Chem. Mater.* **2010**, *22*, 5814.

[23] Matsumi, N.; Sugai, K.; Miyake, M.; Ohno, H. *Macromolecules* **2006**, *39*, 6924.

[24] Marcilla, R.; Alcaide, F.; Sardon, H.; Pomposo, J. A.; Pozo-Gonzalo, C.; Mecerreyes, D. *Electrochem. Commun.* **2006**, *8*, 482.

[25] Ramani, V.; Kunz, H. R.; Fenton, J. M. *J. Membr. Sci.* **2004**, *232*, 31.

[26] Rockland, L. B. *Anal. Chem.* **1960**, *32*, 1375.

[27] Han, L. M.; Timmons, R. B.; Bogdal, D.; Pielichowski, J. *Chem. Mater.* **1998**, *10*, 1422.

[28] Kumagai, M.; Tsuchida, K.; Ogino, Y.; Hansen, J.; Ishida, H. *Polymer* **1995**, *36*, 535.

[29] Buffeteau, T.; Grondin, J.; Danten, Y.; Lassègues, J.-C. *J. Phys. Chem. B* **2010**, *114*, 7587.

[30] Beamson, G.; Briggs, D. *High Resolution XPS of Organic Polymers*; Wiley: Chichester, U.K., 1992.

[31] Ye, Y.; Elabd, Y. A. *Macromolecules* **2011**, *44*, 8494.

[32] (a) Alberti, G.; Costantino, U.; Casciola, M.; Ferroni, S.; Massinelli, L.; Staiti, P. *Solid State Ionics* **2001**, *145*, 249; (b) Bauer, F.; Willert-Porada, M. *J. Power Sources* **2005**, *145*, 101; (c) Mura, F.; Silva, R. F.; Pozio, A. *Electrochim. Acta* **2007**, *52*, 5824.

[33] Kim, D. W.; Chi, D. Y. *Angew. Chem., Int. Ed.* **2004**, *43*, 483.

[34] Watanabe, M.; Sanui, K.; Ogata, N.; Kobayashi, T.; Ohtaki, Z. *J. Appl. Phys.* **1985**, *57*, 123.

Chapter 6

Plasmachemical Deposition of Metal-Containing Nanocomposite Films

6.1 Introduction

In chapters 3–5, proton and ion conducting membranes were manufactured by pulsed plasmachemical deposition (and subsequent post-deposition reactions). These films showed conductivities, which were high enough for use in proton exchange membrane fuel cells—both low temperature ($<$100 °C) and intermediate temperature (100–200 °C). The potential scaleup opportunities presented by vapour-phase deposition processes would be increased if other parts of the proton exchange membrane could also be deposited in this way. These other parts include the catalytic layer present at both anode and cathode of a fuel cell (see Figure 1.2, page 14). The catalytic layer at either electrode must conduct protons, but also electronic conductivity is required (unlike the proton exchange membrane where electronic conductivity would cause a short circuit). Finally, the catalytic layer must contain moieties able to catalyse the oxidation and reduction reactions. In this chapter, therefore, organometallic precursors are used in a plasmachemical deposition to fabricate inorganic nanostructures within an organic matrix. The platinum-containing films fulfil the criteria of being able to conduct protons and electrons, which combined with platinum's known catalytic ability (it is currently used in commercially produced fuel cells), mean that the nancomposite layers could be used in proton exchange membrane fuel cells.

Metal-containing nanocomposite layers are highly sought after for many applications including catalysis,[1–3] photonics,[4,5] proton exchange membranes,[6] batteries,[7] vapour sensors,[8] data storage,[9] biosensing,[10] cell imaging[11] and thermoresponsive materials.[12]

The most common approaches for producing such nanocomposite materials and films involve sol-gel synthesis,[2] in-situ photocuring,[13] layer-by-layer deposition,[14,15] self-assembly,[5,9,16] surface initiated polymerization[17] and electrochemical deposition.[18] These tend to be wet-chemical

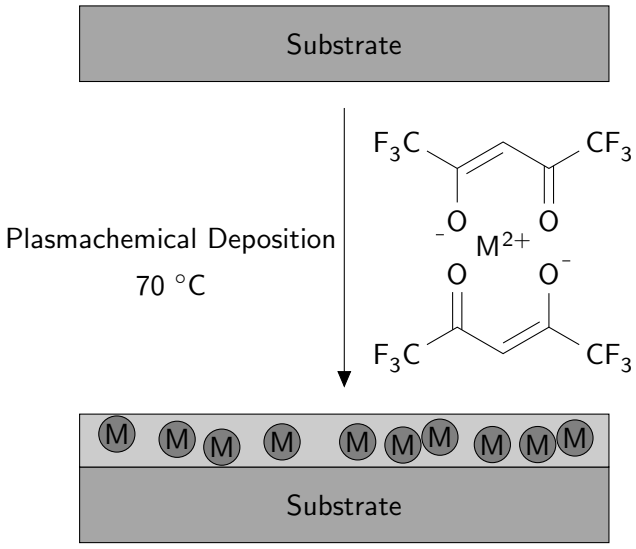

Scheme 6.1: Plasmachemical deposition of metal-containing nanocomposite films.

methods and suffer from a number of drawbacks such as the requirement for multiple steps,[14] or potential damage to substrates arising from high processing temperatures.[2] Dry (solventless) approaches, such as plasma enhanced chemical vapour deposition combined with rf sputtering from an inorganic target to produce catalytic, metal-containing nancomposite films are also known,[19] however, composition can be difficult to control and the high input power levels required to induce sputtering often cause damage to temperature-sensitive substrates. The high temperatures necessary for chemical vapour deposition techniques place similar limitations.[20]

Non-isothermal plasmachemical deposition is an attractive alternative method for preparing nanocomposite functional thin films requiring much lower processing temperatures. It utilizes a glow discharge to effect precursor activation (via VUV irradiation or ion and electron bombardment), which culminates in film growth.[21] The level of chemical functionality can be carefully tailored by varying the average power density.[22] In this investigation the plasmachemical deposition of metal-containing nanocomposite films using platinum(II) and copper(II) hexafluoroacetylacetonate at temperatures of 70 °C, which concurrently display ionic and electronic conductivities, is described, Scheme 6.1. This is accomplished by careful choice of plasma process parameters and metal ligands. Such multifunctional nanocomposite films are highly sought after for electrochemical device components, e.g. batteries[23] and fuel cells.[3] This is the first example of a single-step synthesis of metal-containing nanocomposite materials displaying such properties.

6.2 Experimental

6.2.1 Plasmachemical Deposition of Nanocomposite Layers

Plasmachemical deposition was carried out in an electrodeless cylindrical glass reactor as described in section 2.1 (page 27). The chamber was contained within an oven set at 70 °C. Substrates used for coating were silicon (100) wafer pieces (Silicon Valley Microelectronics Inc.), polypropylene sheet (capacitor grade, Lawson Mardon Ltd.) with two evaporated gold electrodes (5 mm length and 1.5 mm separation) for conductivity testing and poly(tetrafluoroethylene) (Goodfellow Cambridge Ltd.) for transmission electron microscopy. Platinum(II) hexafluoroacetylacetonate (+98%, Strem Chemicals Ltd.) and copper(II) hexafluoroacetylacetonate (Aldrich Ltd.) precursors were loaded into separate sealable glass tubes and dried under vacuum. The reactor was then purged with precursor vapour for 5 min at a pressure of 0.1 mbar prior to electrical discharge ignition. Upon plasma extinction, the precursor vapour was allowed to continue to pass through the system for a further 3 min, in order to quench any remaining free radical sites within the films, and then the chamber was pumped back down to base pressure. Following deposition, the coated substrates were rinsed in deionized water for 16 h in order to test for film stability and adhesion (as well as to remove any unbound precursor).

6.2.2 Film Characterization

Film thicknesses were measured using a spectrophotometer (nkd-6000, Aquila Instruments Ltd.) as described in section 2.4 (page 33). Typical film growth rates were 3–6 nm min^{-1}.

Surface elemental compositions were determined by X-ray photoelectron spectroscopy (XPS) using a VG ESCALAB Mk II electron spectrometer as described in section 2.2 (page 28). Experimentally determined instrument sensitivity (multiplication) factors were taken as C(1s): O(1s): F(1s): Pt(4f): Cu(2p) equals 1.00: 0.34: 0.26: 0.05: 0.05.

Elemental depth profiling measurements of platinum concentration through the deposited layer were undertaken by the Rutherford backscattering technique (RBS) using a $^4He^+$ ion beam (5SDH Pelletron Accelerator) in conjunction with a PIPS detector at 19 keV resolution (carried out by Dr Richard Thompson).

Infrared spectra were acquired using a FTIR spectrometer (Perkin-Elmer Spectrum One) as described in section 2.3 (page 31).

Transmission electron microscopy images were obtained using a Phillips CM100 microscope. Coated PTFE squares were embedded into an epoxy resin and then cross-sectioned using a cryogenic microtome. The cross-sections were then mounted onto copper grids prior to electron microscopy analysis.

For ion-conductivity values, impedance measurements across the 10 Hz–13 MHz frequency range were carried out at 20 °C using coated polypropylene substrates with an LF impedance analyser (Hewlett-Packard, model 4192A) whilst submerged in ultra high purity water (resistivity

Plasma power/W	Pt content/atom % XPS	Pt content/atom % RBS	Ionic conductivity/ mS cm^{-1}	Electronic conductivity/ 10^{-6} mS cm^{-1}
2	5.3±0.3	4.3±0.7	120±10	12±2
5	5.2±0.3	4.3±0.7	95±8	31±1
10	5.7±0.4	4.9±0.7	120±10	8±4

Table 6.1: Platinum content and ionic and electronic conductivity of plasmachemically deposited platinum(II) hexafluoroacetylacetonate films as a function of plasma power.

greater than 18 MΩ cm, organic content less than 1 ppb, Sartorius Arium 611) as described in section 2.6 (page 35).

Electrical conductivity values were determined for the coated polypropylene substrates by measuring the variation in electrical current across the 0–200 V range (Keithley 2400 SourceMeter).

6.3 Results

6.3.1 Plasmachemical Deposition of Metal-Containing Nanocomposite Layers

XPS analysis following the plasmachemical deposition of platinum-containing layers indicated the absence of Si(2p) signal, which confirmed coverage of the underlying silicon substrate. The concentration of platinum measured by XPS was found to be consistent with the Rutherford backscattering depth profiling studies (which confirmed constant level of metal content throughout the depth of the films), Table 6.1. Retention of the precursor trifluoromethyl (CF_3) groups within the deposited layers was evident by the distinct C(1s) XPS shoulder at 293.0 eV,[24] Figure 6.1. This feature diminishes in intensity as plasma power is raised, which can be attributed to greater fragmentation and ablation of the precursor arisng from more energetic plasma excitation.[21] The broad, unresolvable C(1s) shoulder at 288–289 eV is consistent with C=O group incorporation into the functional layers.[25]

Similarly, XPS analysis of plasmachemically deposited copper-containing layers indicated the absence of Si(2p) signal, which confirmed coverage of the underlying silicon substrate and the concentration of copper measured by XPS was found to be consistent with the Rutherford backscattering depth profiling studies, Table 6.2. A trifluoromethyl (CF_3) component within the C(1s) spectra was evident along with a broad, unresolvable shoulder corresponding to C=O centres, Figure 6.2.

Infrared spectroscopy provided further evidence for the degree of structural retention within the nanocomposite films, Figures 6.3 and 6.4. For the platinum(II) hexafluoroacetylacetonate precursor, the following assignments can be made:[26,27] a mixture of C=C and C=O stretches (1581 cm^{-1} and 1532 cm^{-1}, denoted A), chelate C−H deformation (1434 cm^{-1}, denoted B), CF_3 stretches (1346 cm^{-1}, 1196 cm^{-1} and 1146 cm^{-1}, denoted C) and C=C chelate stretch (1255 cm^{-1},

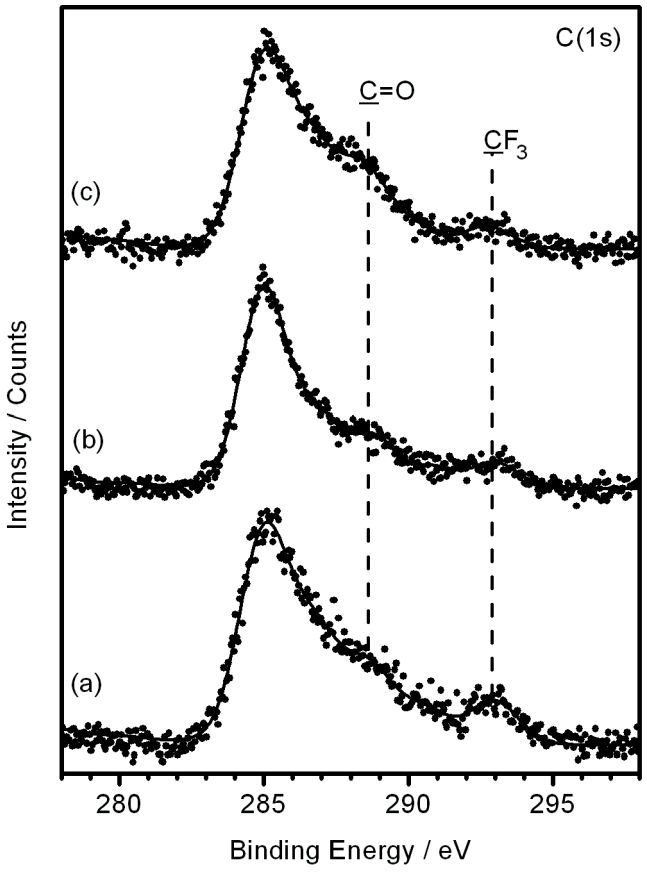

Figure 6.1: XPS C(1s) spectrum for plasma deposited platinum(II) hexafluoroacetylacetonate at plasma input powers of: (a) 2 W, (b) 5 W and (c) 10 W.

	Cu content/atom %		
Plasma power/W	XPS	RBS	Ionic conductivity/mS cm^{-1}
2	3.5±0.8	2.6±0.6	50±10
5	2.3±0.4	1.5±0.9	34±9
10	<0.5	—	130±10

Table 6.2: Copper content and ionic conductivity of plasmachemically deposited copper(II) hexafluoroacetylacetonate films as a function of plasma power.

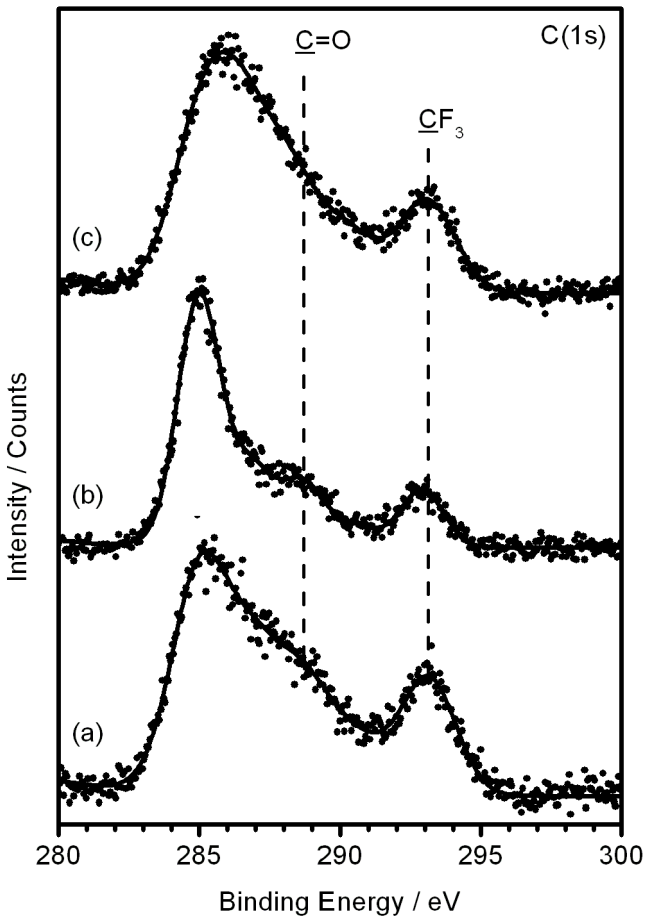

Figure 6.2: XPS C(1s) spectrum for plasma deposited copper(II) hexafluoroacetylacetonate at plasma input powers of: (a) 2 W, (b) 5 W and (c) 10 W.

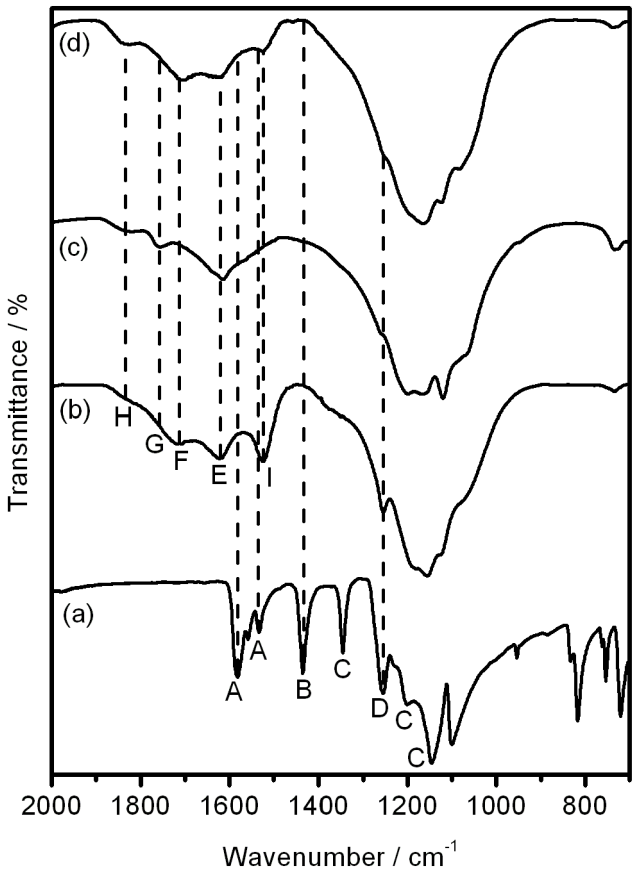

Figure 6.3: FTIR spectra of: (a) platinum(II) hexafluoroacetylacetonate precursor and plasma deposited platinum(II) hexafluoroacetylacetonate at plasma powers of (b) 2 W, (c) 5 W and (d) 10 W.

denoted D). For the plasmachemically deposited platinum(II) hexafluoroacetylacetonate layers, the carbonyl C=O stretches split into several regions including the original beta-diketonate stretches (A), beta-diketone stretch (1620 cm^{-1}, denoted E), carboxylic acid dimer stretch (1705 cm^{-1}, denoted F), carboxylic anhydride antisymmetric stretch (1754 cm^{-1}, denoted G) and carboxylic anhydride symmetric stretch (1826 cm^{-1}, denoted H).[28] For all the platinum-containing plasma deposited films, the C−H deformation (B) is shifted to 1524 cm^{-1} (denoted I), which is consistent with a new environment for the chelate unit (i.e. unbound precursor is absent).[27] The plasma deposited films also show broad stretches over the 1400–1100 cm^{-1} region, which corresponds to CF_x stretches, and there is retention of the shoulder at 1255 cm^{-1} attributable to C=C chelate stretching (D). Although the different plasma deposited films appear similar in nature, some key differences include the more intense chelate C−H deformation and C=C stretch (D and I) peaks for the case of 2 W input plasma power (corresponding to less plasma induced fragmentation at lower energies[21]). There is also a significant loss of the carboxylic acid dimer peak (F) for the 5 W plasma deposition.

Infrared spectra for the copper(II) hexafluoroacetylacetonate similarly showed C=O stretches

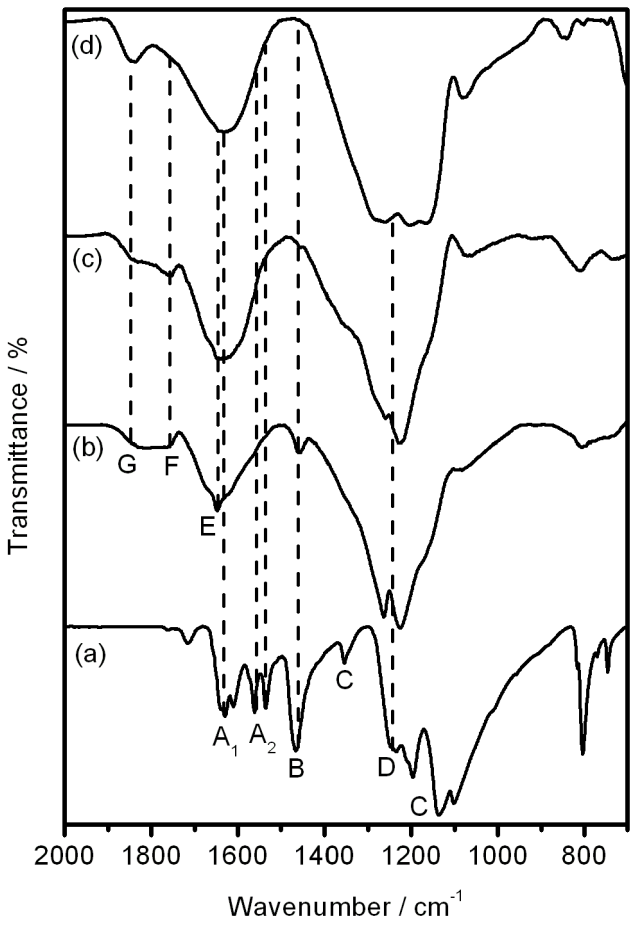

Figure 6.4: FTIR spectra of: (a) copper(II) hexafluoroacetylacetonate precursor and plasma deposited copper(II) hexafluoroacetylacetonate at plasma powers of (b) 2 W, (c) 5 W and (d) 10 W.

at 1638 and 1629 cm^{-1} (denoted A_1), a mixture of C=C and C=O stretches (1560 cm^{-1} and 1534 cm^{-1}, denoted A_2), chelate C−H deformation (1464 cm^{-1}, denoted B), CF_3 stretches (1354 cm^{-1}, 1195 cm^{-1} and 1132 cm^{-1}, denoted C) and C=C chelate stretch (1233 cm^{-1}, denoted D), Figure 6.4.[27] The plasmachemically deposited copper(II) hexafluoroacetylacetonate layers had less well-defined infrared spectra than the platinum(II) analogues, however broad peaks corresponding to a variety of C=O environments can be seen (E denotes beta diketone stretch, F denotes carboxylic acid dimer stretch and G denotes carboxylic anhydride stretch).[28]

Transmission electron microscope images of the plasma deposited copper- and platinum-containing films show homogeneous films for deposition at 2 W and 10 W, Figure 6.5. For both metal-containing layers deposited at plasma power of 5 W, however, distinct nanoparticles are visible within the films. The metal-containing nanoparticles within both films are all significantly less than 10 nm in size. The organic matrix can be clearly seen around the nanoparticles.

6.3.2 Ionic and Electronic Conductivity of the Metal-Containing Nanocomposite Layers

Ionic conductivity measurements of the plasmachemically deposited nanocomposite films whilst immersed in ultrahigh purity water yielded high values exceeding 100 mS cm^{-1}, Tables 6.1 and 6.2. This can be attributed to the presence of fluorinated carboxylic acid moieties within the films, as evidenced by infrared spectroscopy. Such strong acidic groups can be expected to give rise to a high degree of acid dissociation under fully hydrated conditions, which in turn manifests in good proton conductivity.[29] Ionic conductivity values were found to be lower for the films deposited at 5 W, which correlates to the weaker acidic infrared absorbances (in the case of platinum), Figure 6.3.

The plasmachemically deposited, platinum-containing nanocomposite films also exhibit significant electronic conduction, Table 6.1. This conductivity is greater by a factor greater than 2 in the case of the 5 W plasma-deposited film (3.1×10^{-5} mS cm^{-1}), and is seen to coincide with the decrease in acid-containing groups (as shown by FTIR). Given the small particle sizes within the 5 W plasma-deposited films, the observed atomic percentage of platinum within the films is high enough (5 atom %) for percolation behaviour to take place, whereby conducting particles within an insulating medium are close enough for electron tunnelling and therefore the film conducts.[30] The copper-containing films exhibited no electronic conductivity which is attributed to the lower metal contents as evidenced by XPS and RBS, Table 6.2.

In contrast to earlier studies, where plasmachemically deposited nanocomposite layers were unstable in water, the present films did not display any deterioration in performance upon hydration.[31]

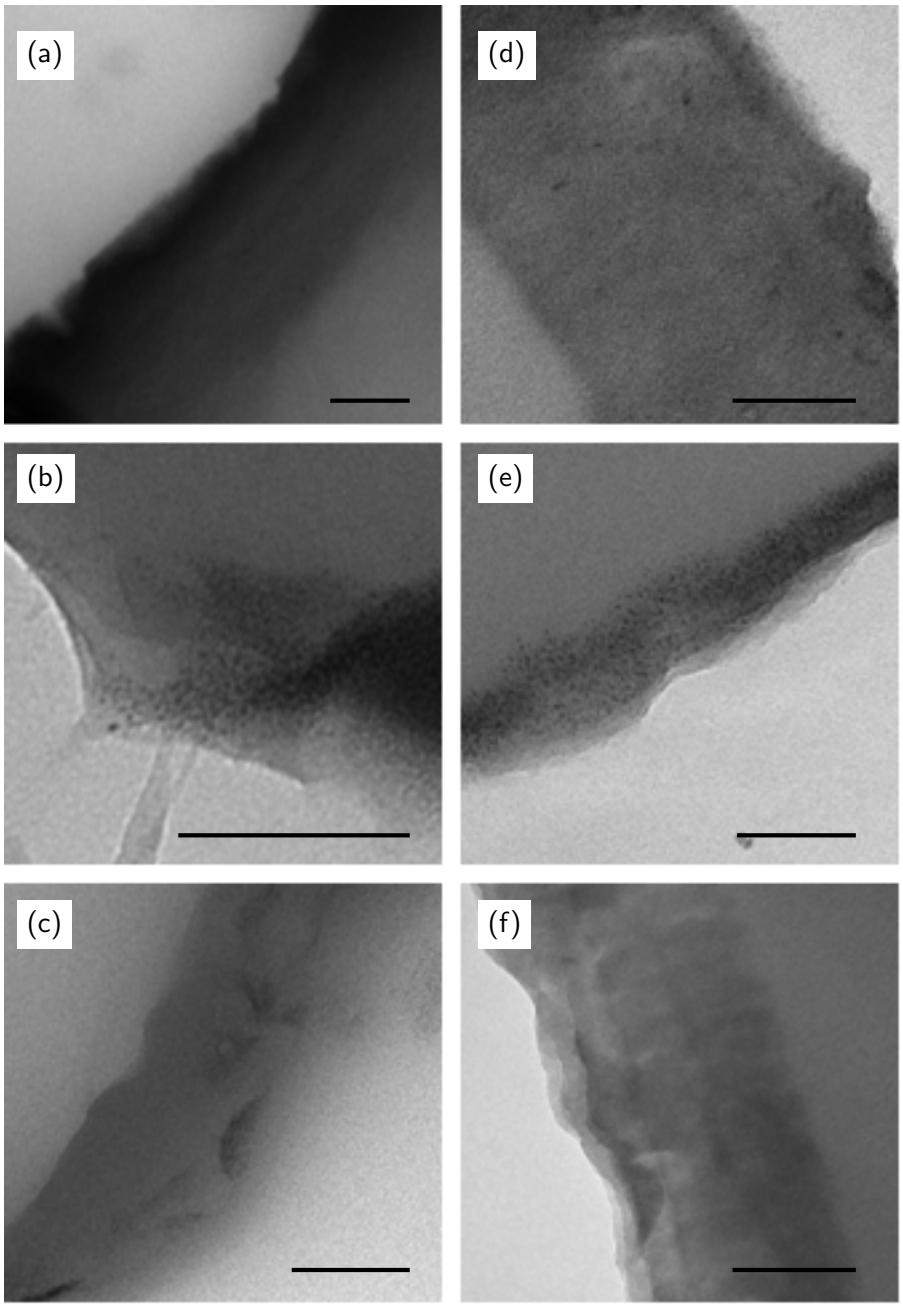

Figure 6.5: Transmission electron microscope images of plasma deposited (a–c) platinum(II) hexafluoroacetylacetonate films (plasma power = 2 W, 5 W and 10 W respectively) and (d–f) copper(II) hexafluoroacetylacetonate films (plasma power = 2 W, 5 W and 10 W respectively). Scale bar = 100 nm in all images

6.4 Discussion

Mixed ionic-electronic conductors are desirable for use as electrode materials in solid state batteries,[32] fuel cells,[33] electrochemical reactors[34] and light-emitting electrochemical cells.[35] They can comprise inorganic crystalline materials,[36] conjugated polymers[37] or heterogeneous polymeric systems and copolymers (i.e. mixtures of ion-conducting and conjugated, electron-conducting parts).[38] All of these systems require separate steps for manufacture and incorporation into an electrochemical device (usually via solution casting or spin coating in the case of polymer based systems). In this study it has been shown that one-step plasmachemical deposition using platinum(II) hexafluoroacetylacetonate gives rise to ion- and electron-conducting nanocomposite films. The conformal nature of the deposited films means that the manufacturing step can be easily applied to coating electrochemical device components (e.g. carbon cloth).

By careful tuning of the plasma power, metal-containing nanoparticles can be created within the organic matrix. The formation of nano-sized metal-containing structures within the film requires a certain degree of precursor fragmentation, which also explains the greater homogeneity observed at lower powers, Figure 3.[39] The host organic matrix, within which the metal-containing nanoparticles are located, is responsible for ionic conductivity together with good stability under hydrated conditions. This should be contrasted to nanocomposite films previously manufactured via plasmachemical deposition which have either produced unstable organic matrices,[31] or required high plasma powers (temperatures) in order to induce sputtering from an inorganic target.[19]

Previously metal hexafluoroacetylacetonates have been used to deposit inorganic-only films via chemical vapour deposition methods especially for use in microelectronic devices.[40] The current plasmachemical deposition approach allows a functional organic layer to also be retained. The specific trifluoromethyl groups present in the metal(II) hexafluoroacetylacetonate precursors serve a dual purpose: firstly they give the precursor a higher vapour pressure (thus enabling lower temperature deposition)[41] and secondly, when the precursor breaks up within the plasma (forming carboxylic acid groups), fluorination provides an electron-withdrawing effect, which is known to produce stronger acid groups (therefore resulting in higher proton conductivity when immersed in water).[42] This is the first example where plasmachemical deposition using a single precursor under mild conditions yields a robust, metal-containing, nanocomposite film, exhibiting both ionic and electronic conductivity.

The current commercial manufacturing process for proton exchange membrane fuel cell catalyst layers involves making a catalyst ink, whose components comprise Nafion, platinum nanoparticle-embedded carbon black particles and an appropriate solvent. This ink is then applied to the gas diffusion layer (typically carbon cloth) and then left to dry as the solvent evaporates (this technique is known as solvent casting). Other methods for producing catalytic nanoparticles on a surface, such as metal sputtering, still require the separate step of adding Nafion (or another suitable proton exchange membrane). The method outlined in this chapter attempts to combine all of these separate steps into one deposition process. By using a similar reactor to the work

carried out in chapters 3–5 (with the small modification of heating the deposition chamber), one can envisage an all-in-one deposition process where the platinum(II) hexafluoroacetylacetonate precursor is introduced and deposited followed by deposition of the proton exchange membrane without any intermediate steps. Since the plasmachemical deposition process is conformal, the application of the films directly onto carbon cloth/carbon black can be easily achieved.

6.5 Conclusions

Low power plasmachemical deposition has been utilized to fabricate platinum- and copper-containing nanocomposite films. Careful tailoring of the plasma input power level leads to metal-containing nanoparticles embedded within a robust organic matrix. The obtained platinum-containing films exhibit both ionic and electronic conduction. This approach offers a single-step, low temperature method for conformally coating substrates with metal-containing nanocomposite layers.

6.6 References

[1] (a) Kidambi, S.; Dai, J.; Li, J.; Bruening, M. L. *J. Am. Chem. Soc.* **2004**, *126*, 2658; (b) Ding, Y.; Chen, M.; Erlebacher, J. *J. Am. Chem. Soc.* **2004**, *126*, 6876; (c) Li, H.; Bian, Z.; Zhu, J.; Huo, Y.; Li, H.; Lu, Y. *J. Am. Chem. Soc.* **2007**, *129*, 4538; (d) Liang, Y.; Zhang, H.; Tian, Z.; Zhu, X.; Wang, X.; Yi, B. *J. Phys. Chem. B* **2006**, *110*, 7828.

[2] Subramanian, V.; Wolf, E. E.; Kamat, P. V. *J. Am. Chem. Soc.* **2004**, *126*, 4943.

[3] Bashyam, R.; Zelenay, P. *Nature* **2006**, *443*, 63.

[4] Zhang, J.; Coombs, N.; Kumacheva, E. *J. Am. Chem. Soc.* **2002**, *124*, 14512.

[5] Oh, H. S.; Liu, S.; Jee, H.; Baev, A.; Swihart, M. T.; Prasad, P. N. *J. Am. Chem. Soc.* **2010**, *132*, 17346.

[6] Zhang, W.; Li, M. K. S.; Yue, P.-L.; Gao, P. *Langmuir* **2008**, *24*, 2663.

[7] Park, C.-M.; Sohn, H.-J. *Chem. Mater.* **2008**, *20*, 3169.

[8] Cioffi, N.; Losito, I.; Torsi, L.; Farella, I.; Valentini, A.; Sabbatini, L.; Zambonin, P. G.; Bleve-Zacheo, T. *Chem. Mater.* **2002**, *14*, 804.

[9] Srivastava, S.; Samanta, B.; Jordan, B. J.; Hong, R.; Xiao, Q.; Tuominen, M. T.; Rotello, V. M. *J. Am. Chem. Soc.* **2007**, *129*, 11776.

[10] (a) Miranda, O. R.; Li, X.; Garcia-Gonzalez, L.; Zhu, Z.-J.; Yan, B.; Bunz, U. H. F.; Rotello, V. M. *J. Am. Chem. Soc.* **2011**, *133*, 9650; (b) Liu, Y.; Feng, X.; Shen, J.; Zhu, J.-J.; Hou, W. *J. Phys. Chem. B* **2008**, *112*, 9237.

[11] Wang, X.; Wang, C.; Cheng, L.; Lee, S.-T.; Liu, Z. *J. Am. Chem. Soc.* **2012**, *134*, 7414.

[12] Shimada, T.; Ookubo, K.; Komuro, N.; Shimizu, T.; Uehara, N. *Langmuir* **2007**, *23*, 11225.

[13] Lee, S.; Lee, B.; Kim, B. J.; Park, J.; Yoo, M.; Bae, W. K.; Char, K.; Hawker, C. J.; Bang, J.; Cho, J. *J. Am. Chem. Soc.* **2009**, *131*, 2579.

[14] Lu, C.; Dönch, I.; Nolte, M.; Fery, A. *Chem. Mater.* **2006**, *18*, 6204.

[15] Andres, C. M.; Kotov, N. A. *J. Am. Chem. Soc.* **2010**, *132*, 14496.

[16] Frankamp, B. L.; Boal, A. K.; Rotello, V. M. *J. Am. Chem. Soc.* **2002**, *124*, 15146.

[17] Dong, H.; Zhu, M.; Yoon, J. A.; Gao, H.; Jin, R.; Matyjaszewski, K. *J. Am. Chem. Soc.* **2008**, *130*, 12852.

[18] (a) Horch, R. A.; Golden, T. D.; D'Souza, N. A.; Riester, L. *Chem. Mater.* **2002**, *14*, 3531; (b) Toledano, R.; Mandler, D. *Chem. Mater.* **2010**, *22*, 3943.

[19] (a) Dilonardo, E.; Milella, A.; Palumbo, F.; Capitani, G.; d'Agostino, R.; Fracassi, F. *Plasma Processes Polym.* **2010**, *7*, 51; (b) Dilonardo, E.; Milella, A.; Palumbo, F.; Thery, J.; Martin, S.; Barucca, G.; Mengucci, P.; d'Agostino, R.; Fracassi, F. *J. Mater. Chem.* **2010**, *20*, 10224; (c) Zanna, S.; Saulou, C.; Mercier-Bonin, M.; Despax, B.; Raynaud, P.; Seyeux, A.; Marcus, P. *Appl. Surf. Sci.* **2010**, *256*, 6499.

[20] Palgrave, R. G.; Parkin, I. P. *J. Am. Chem. Soc.* **2006**, *128*, 1587.

[21] Yasuda, H. *Plasma Polymerization*; Academic Press: New York, 1985.

[22] Ratcliffe, P. J.; Hopkins, J.; Fitzpatrick, A. D.; Barker, C. P.; Badyal, J. P. S. *J. Mater. Chem.* **1994**, *4*, 1055.

[23] Débart, A.; Bao, J.; Armstrong, G.; Bruce, P. G. *J. Power Sources* **2007**, *174*, 1177.

[24] Holmes, S. A.; Thomas, T. D. *J. Am. Chem. Soc.* **1975**, *97*, 2337.

[25] Moulder, J. F.; Stickle, W. F.; Sobol, P. E.; Bomben, K. D. In *Handbook of X-ray Photoelectron Spectroscopy*; Chastain, J., Ed.; Perkin-Elmer Corporation: Minnesota, 1992.

[26] Nakamoto, K.; McCarthy, P. J.; Martell, A. E. *J. Am. Chem. Soc.* **1961**, *83*, 1272.

[27] Winter, S.; Weber, E.; Eriksson, L.; Csöregh, I. *New J. Chem.* **2006**, *30*, 1808.

[28] Lin-Vien, D.; Colthup, N. B.; Fateley, W. G.; Grasselli, J. G. *The Handbook of Infrared and Raman Characteristic Frequencies of Organic Molecules*; Academic Press: London, U.K., 1991.

[29] Kreuer, K. D. *Chem. Mater.* **1996**, *8*, 610.

[30] Jing, X.; Zhao, W.; Lan, L. *J. Mater. Sci. Lett.* **2000**, *19*, 377.

[31] Duque, L.; Förch, R. *Plasma Processes Polym.* **2011**, *8*, 444.

[32] Riess, I. *Solid State Ionics* **2003**, *157*, 1.

[33] West, A. R. *J. Mater. Chem.* **1991**, *1*, 157.

[34] Steele, B. C. H.; Kelly, I.; Middleton, H.; Rudkin, R. *Solid State Ionics* **1988**, *28–30*, 1547.

[35] Pei, Q.; Yu, G.; Zhang, C.; Yang, Y.; Heeger, A. J. *Science* **1995**, *269*, 1086.

[36] Porat, O.; Rosenstock, Z.; Shtreichman, I.; Reiss, I. *Solid State Ionics* **1996**, *86–88*, 1385.

[37] Deslouis, C.; El Moustafid, T.; Musiani, M. M.; Tribollet, B. *Electrochim. Acta* **1996**, *41*, 1343.

[38] (a) Riess, I. *Solid State Ionics* **2000**, *136–137*, 1119; (b) Javier, A. E.; Patel, S. N.; Hallinan, J., D. T.; Srinivasan, V.; Balsara, N. P. *Angew. Chem. Int. Ed.* **2011**, *50*, 9848.

[39] Park, S. Y.; Kim, N. *J. Appl. Polym. Sci. Polym. Appl. Symp.* **1990**, *46*, 91.

[40] (a) Cohen, S. L.; Liehr, M.; Kasi, S. *Appl. Phys. Lett.* **1991**, *60*, 50; (b) Awaya, N.; Ohno, K.; Arita, Y. *J. Electrochem. Soc.* **1995**, *142*, 3173; (c) Lakshmanan, S. K.; Gill, W. N. *J. Vac. Sci. Technol.* **1998**, *A16*, 2187; (d) Erhardt, M. K.; Nuzzo, R. G. *Langmuir* **1999**, *15*, 2188.

[41] Jones, A. C.; Aspinall, H. C.; Chalker, P. R. In *Chemical Vapour Deposition: Precursors, Processes and Applications*; Jones, A. C., Hitchman, M. L., Eds.; Royal Society of Chemistry: London, 2008; Chapter Chemical Vapour Deposition of Metal Oxides for Microelectronics Applications, pp 357–412.

[42] Elguero, J.; Yranzo, G. I.; Laynez, J.; Jiménez, P.; Menéndez, M.; Catalán, J.; de Paz, J. L. G.; Anvia, F.; Taft, R. W. *J. Org. Chem.* **1991**, *56*, 3942.

Chapter 7

Atomized Spray Plasma Deposition of Bioactive Layers

7.1 Introduction

In chapters 3–6, plasmachemical deposition has been shown to be an effective method of fabricating proton exchange membranes and catalytic nanocomposite layers which could be used in proton exchange membrane fuel cells. Whilst there are many advantages to plasmachemical deposition (and indeed other vapour-phase deposition techniques), a major shortcoming, which would potentially block industrial scaleup, is the low deposition rates. For example, in chapter 3, the deposition of anhydride-containing polymer films under optimum conditions yielded a deposition rate of up to 6 nm min^{-1}. The time to build up even a 1 micron layer (fuel cell proton exchange membranes are typically betwee 10 and 100 microns in thickness) is over 2.5 hours. Strategies for increasing the deposition rate could be to increase the duty cycle (i.e. a shorter off time or longer on time) or the peak power of the pulsed plasma. This, however, leads to the unwanted loss of structural retention within the polymer—that is, a lower density of anhydride groups with a corresponding loss of proton conductivity once hydrated. Plasmachemical deposition also has the limitation of requiring a precursor with a significant vapour pressure. These drawbacks are overcome in this chapter by the use of a spray delivery system (ultrasonic nozzle) which introduces a fine mist of precursor into the plasma reactor chamber. As a proof of concept, this chapter focuses on alkyl acrylate layers and an *N*-acryloyl based ester. The functionality of the polymer coatings is proven by measuring their bioactive properties.

The field of bioactive surfaces is becoming increasingly important as there exist large interests in the fabrication of biomedically compatible implants,[1] as well as for the study of biological processes[2] and for the prevention of biofouling.[3] The manufacture of phospholipid-containing, surface-immobilized layers has been previously used to create biofunctionalized coatings,[4] which can be used for biosensing,[5] biomimesis,[6] separation,[7] vesicle binding,[8] biocompatibility[9] and enzyme immobilization.[10] Conversely, protein-resistant layers which resist bioadhesion are highly

desirable for marine antifouling applications[11] and cell-resistant medical devices.[12]

Bioactive phospholipid layers have been attached to surfaces in the past using graft polymerization[13,14] or via interaction with self-assembled monolayers of alkanethiols,[15] thiolipids[16] or silanes[17] to form lipid bilayers. Similarly, protein-resistant surfaces (which usually comprise poly(ethylene glycol),[18,19] polyacrylamide[20] or polysaccharide[21] layers) have been produced by utilization of self-assembled monolayers,[18,22] physisorption,[23] graft polymerization[24,25] or plasmachemical deposition.[26,27]

Many of the above methods have distinct disadvantages: self-assembled monolayers require specific substrates[28] and can be moisture sensitive (e.g. silanes[29]) or unstable in oxidative chemical environments (e.g. thiols[30]); physisorption is by its very nature reversible and therefore limited in application; and graft polymerization requires deposition of an initiator layer[31] or surface modification prior to the grafting step.[13,24]

In contrast to the aforementioned techniques, plasmachemical deposition is a solventless, substrate-independent method for thin film production.[32] High levels of precursor retention can be obtained by pulsed plasmachemical deposition, which involves modulating an electrical discharge in the presence of precursor vapour on the microsecond-millisecond timescale.[33] An alternative approach to enhanced functional retention is to increase the pressure or flow rate of the precursor vapour within the reactor chamber, which also yields a decrease in average plasma power per precursor molecule.[32,34] Whilst high precursor vapour densities yield higher deposition rates and better structural retention, this method is inherently limited by plasma inhomogeneities (induced by the high precursor flow rates) which result in instabilities and eventual plasma extinction. These shortcomings, however, can be circumvented by the utilization of an atomized spray of the precursor.[35,36]

Reported in this chapter is the atomized spray plasma deposition (ASPD) of biocompatible poly(alkyl acrylate) layers and protein-resistant poly(*N*-acryloylsarcosine methyl ester) layers, Scheme 7.1. The deposition rates for these layers are increased by factors of over 20 compared to other vapour-phase deposition techniques.

7.2 Experimental

7.2.1 Atomized Spray Plasma Deposition of Bioactive Coatings

Plasmachemical deposition was carried out in an electrodeless, glass, T-shape reactor (volume 820 cm^3, base pressure of 3×10^{-3} mbar, and with a leak rate better than 2×10^{-9} mol s^{-1}) as described in section 2.1 (page 27). Substrates used for coating were silicon (100) wafer pieces (Silicon Valley Microelectronics Inc.), PTFE pieces (Goodfellow Cambridge Ltd.) and polypropylene pieces (Lawson-Mardon Ltd., capacitor grade); these were placed downstream from the atomizer nozzle. The precursor was loaded into a sealable glass tube and degassed using several freeze-pump-thaw cycles. Precursors used included n-hexyl acrylate (+98%, Sigma-Aldrich Ltd.), n-dodecyl acrylate

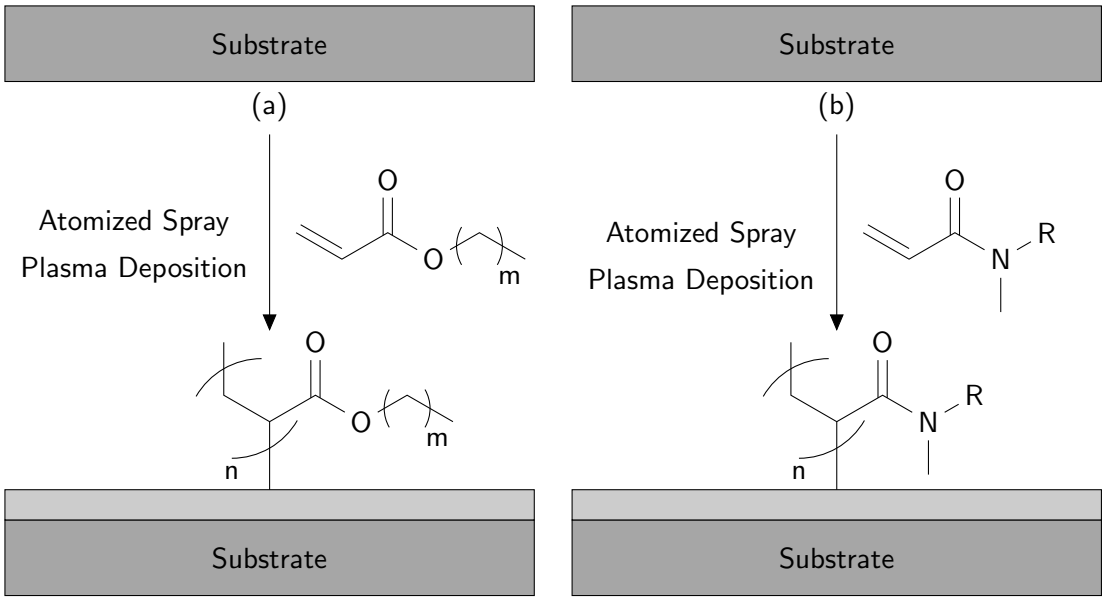

Scheme 7.1: Atomized spray plasma deposition (ASPD) of (a) poly(alkyl acrylate) layers (m = 5, 11, 17) and (b) poly(*N*-acryloylsarcosine methyl ester) layers (R = -CH_2COOCH_3).

(+90% Sigma-Aldrich Ltd.), n-octadecyl acrylate (+97%, Sigma-Aldrich Ltd., utilized as a 1:3 mixture with n-dodecyl acrylate) and *N*-acryloylsarcosine methyl ester (+97%, Alfa Aesar Ltd.). Precursor was introduced into the reactor at a flow rate of 0.02 mL s^{-1} (mediated by a low-flow metering valve) through an ultrasonic nozzle (Model no. 8700-120, Sono Tek Corp.) operating at 120 kHz. Deposition entailed running a continuous wave plasma at 50 W for 150 s in parallel to precursor spraying. Upon plasma extinction, the system was evacuated to base pressure before venting to atmosphere.

7.2.2 Film Characterization

Surface elemental compositions were determined by X-ray photoelectron spectroscopy (XPS) using a VG ESCALAB Mk II electron spectrometer as described in section 2.2 (page 28). Experimentally determined instrument sensitivity (multiplication) factors were taken as C(1s): O(1s): N(1s) equals 1.00: 0.36: 0.63.

Infrared spectra were acquired using a FTIR spectrometer (Perkin-Elmer Spectrum One) fitted with a liquid nitrogen cooled MCT detector as described in section 2.3 (page 31).

Sessile drop water contact angle measurements were performed at ambient temperature as described in section 2.5 (page 34).

Film thicknesses were measured using a spectrophotometer (nkd-6000, Aquila Instruments Ltd.) as described in section 2.4 (page 33).

7.2.3 Bioarray Production and Characterization

In the case of the alkyl acrylates, atomized spray plasma deposition was performed through a 100 mesh brass grid onto PTFE pieces, which were subsequently immersed briefly in successive solutions of 20 μg mL^{-1} phospholipid-biotin conjugate (KODE Biotech Ltd.) and 20 μg mL^{-1} avidin-FITC conjugate (Invitrogen Corp.) in phosphate buffer saline solution (Invitrogen Corp.). Between immersions the substrate was thoroughly rinsed with deionized water and washed in phosphate buffer saline solution.

For *N*-acryloylsarcosine methyl ester, atomized spray plasma deposition was carried out through a 1500 mesh nickel grid onto polypropylene pieces, which were immersed into a 50 μg mL^{-1} Protein A-FITC conjugate (Sigma-Aldrich Ltd.) in phosphate buffer saline solution, and subsequently thoroughly rinsed with deionized water and washed in phosphate buffer saline solution.

Fluorescence microscopy was performed using an Olympus IX-70 system (DeltaVision RT, Applied Precision Inc.) as described in section 2.7 (page 36).

7.3 Results

7.3.1 Atomized Spray Plasma Deposited Layer Production

A lack of any Si(2p) XPS signal showed that complete surface coverage of the substrate had been achieved by atomized spray plasma deposition, Table 7.1. For the atomized spray plasma deposited poly(alkyl acrylate) layers, there was good agreement between the carbon-to-oxygen elemental ratios expected theoretically and those obtained in practice, with a slight reduction in oxygen for each case. Angle-resolved XPS analysis revealed no significant change in these ratios, which indicates no surface ordering of the alkyl chains. For the atomized spray plasma deposited poly(*N*-acryloylsarcosine methyl ester) layers, there was a larger difference between the theoretical and experimental carbon-to-oxygen ratios, which was accompanied by a concurrent increase in nitrogen content at the surface, Table 7.1.

Atomized spray plasma deposited poly(alkyl acrylate) layers showed three distinctive components in the C(1s) XPS spectrum, Figure 7.1. These are a large hydrocarbon (C_xH_y) component at 285.0 eV and two smaller components corresponding to oxygenated carbon centres, C−O (at 286.6 eV) and O−C=O (at 288.9 eV) respectively. The decrease in the size of the oxygenated carbon component peaks with increasing alkyl chain length is in close agreement with that expected for theoretical poly(alkyl acrylate)s.

In the case of atomized spray plasma deposited poly(*N*-acryloylsarcosine methyl ester) layers, the XPS C(1s) spectrum displayed more complex features, which were fully consistent with the theoretically determined spectrum,[27] Figure 7.2. These consisted of components corresponding to C_xH_y/C−N (285.0 eV), N−C−COO (285.7 eV), C−O/N−C=O (286.7 eV), and O−C=O (288.6 eV). Therefore, despite the slight differences in XPS elemental ratios, the XPS spectra obtained for the atomized spray plasma deposited poly(*N*-acryloylsarcosine methyl ester) layers

Layer	%C	%O	%N
Theoretical poly(hexyl acrylate)	82	18	—
ASPD poly(hexyl acrylate)	84±1	16±1	—
Theoretical poly(dodecyl acrylate)	88.2	11.8	—
ASPD poly(dodecyl acrylate)	90±1	10±1	—
Theoretical poly(dodecyl acrylate-co-octadecyl acrylate)	89.3	10.7	—
ASPD poly(dodecyl acrylate-co-octadecyl acrylate)	92±1	8±1	—
Theoretical poly(*N*-acryloylsarcosine methyl ester)	64	27	9
ASPD poly(*N*-acryloylsarcosine methyl ester)	69±3	20±2	11±2

Table 7.1: Elemental XPS ratios for atomized spray plasma deposited layers.

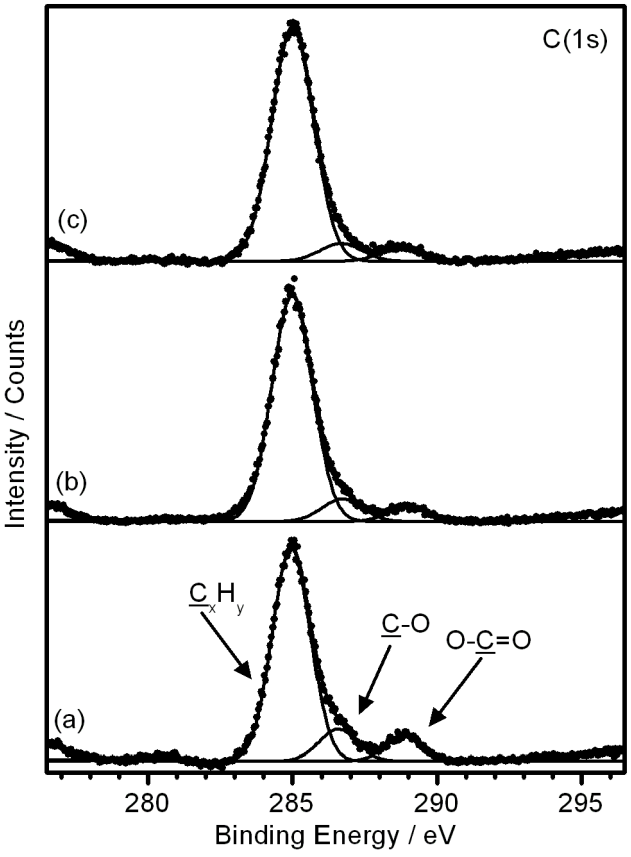

Figure 7.1: C(1s) X-ray photoelectron spectra of atomized spray plasma deposited: (a) poly(hexyl acrylate), (b) poly(dodecyl acrylate) and (c) poly(dodecyl acrylate-co-octadecyl acrylate).

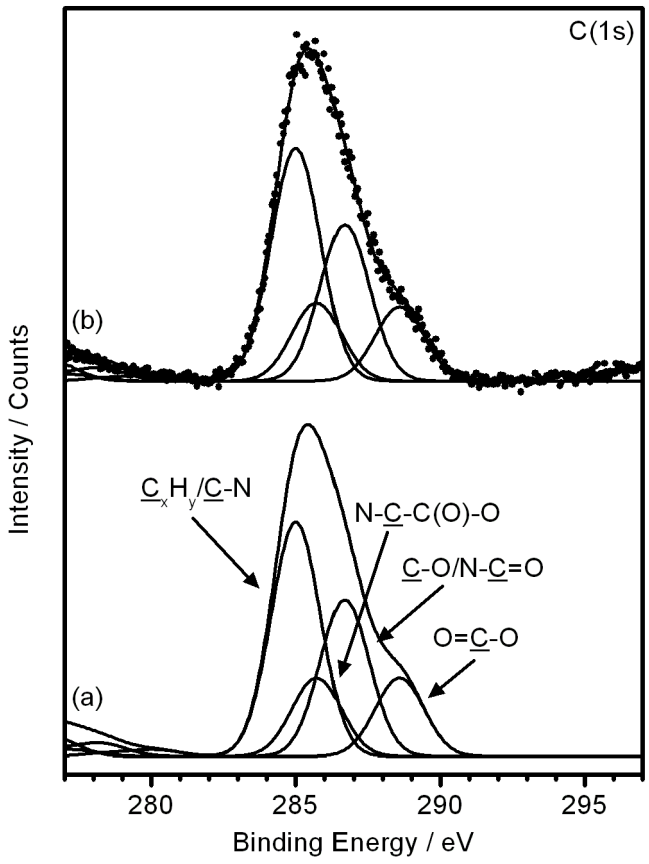

Figure 7.2: X-ray photoelectron spectra of: (a) theoretical poly(*N*-acryloylsarcosine methyl ester) and (b) atomized-spray-plasma deposited poly(*N*-acryloylsarcosine methyl ester).

were in good agreement with those expected theoretically.

Infrared spectra also provided evidence of high levels of structural retention throughout the atomized spray plasma deposited poly(alkyl acrylate) layers. Whilst stretches due to alkyl C−H and carbonyl C=O vibrations remained, there was a disappearance of stretches due to the C=C acrylate bond indicative of conventional polymerization having taken place within the layers, Table 7.2 and Figures 7.3, 7.4 and 7.5. For each layer, there was also an observed increase in the carbonyl C=O stretching of 10–18 cm^{-1}, which is consistent with a move from a conjugated carbonyl group (i.e. an acrylate) to an unconjugated carbonyl group (i.e. polymerization).[37]

Infrared spectroscopy also confirmed good structural retention within the poly(*N*-acryloylsarcosine methyl ester) films, Figure 7.6. The following bands can be assigned to the monomer: $\nu a(CH_3)$ stretch (2954 cm^{-1}), ν(C=O) carbonyl ester stretch (1743 cm^{-1}), ν(C=O) carbonyl amide stretch (1649 cm^{-1}), ν(C=C) vinyl stretch (1612 cm^{-1}), the ν(C−O) ester stretch (1201 cm^{-1}) and the $=CH_2$ twist (795 cm^{-1}).[27,37] The stretches due to the carbon-carbon double bond have disappeared in the atomized spray plasma deposited films, which is consistent with polymerization having taken place.

Contact angle analysis for the films showed that the atomized spray plasma deposited poly(alkyl

	Wavenumber observed / cm^{-1}					
Assignment	HA	ASPD-HA	DA	ASPD-DA	OA	ASPD-DA/OA
$\nu a(CH_3)$	2956	2958	2955	2954	2952	2953
$\nu a(CH_2)$	2930	2932	2922	2922	2917	2920
$\nu s(CH_3)$	2872	2872	2871	2871	2869	2871
$\nu s(CH_2)$	2860	2860	2853	2853	2848	2852
$\nu(C{=}O)$	1723	1741	1725	1735	1720	1730
$\nu(C{=}C)$	1637	—	1637	—	1633	—
	1620	—	1620	—		
=CH wag	984	—	983	—	976	—
$=CH_2$ wag	963	—	962	—	963	—
$=CH_2$ twist	809	—	809	—	814	—

Table 7.2: Infrared frequencies of alkyl acrylate monomers and the corresponding atomized spray plasma deposited polymer layers (HA = hexyl acrylate, DA = dodecyl acrylate, OA = octadecyl acrylate).

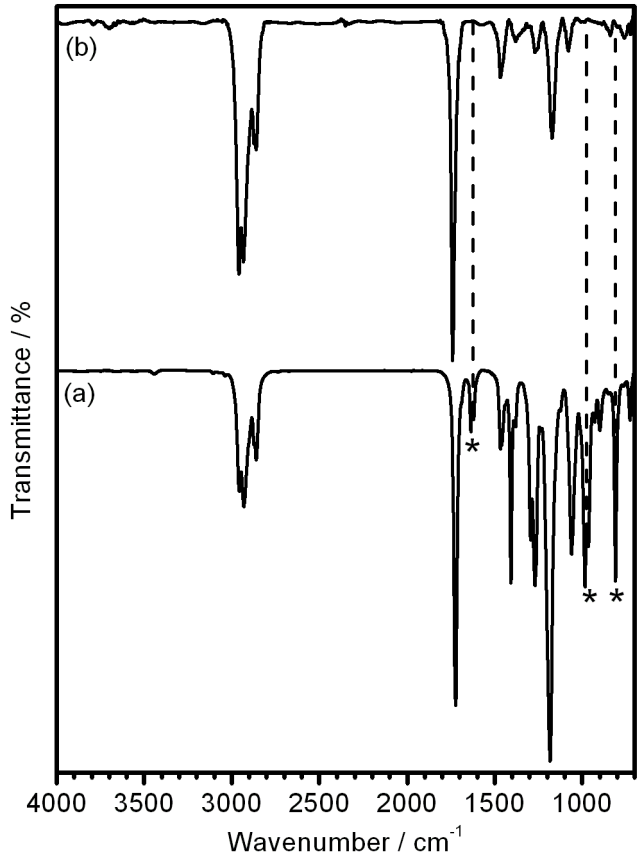

Figure 7.3: FTIR spectra of: (a) hexyl acrylate monomer and (b) atomized spray plasma deposited poly(hexyl acrylate). * Denotes stretches due to C=C double bond

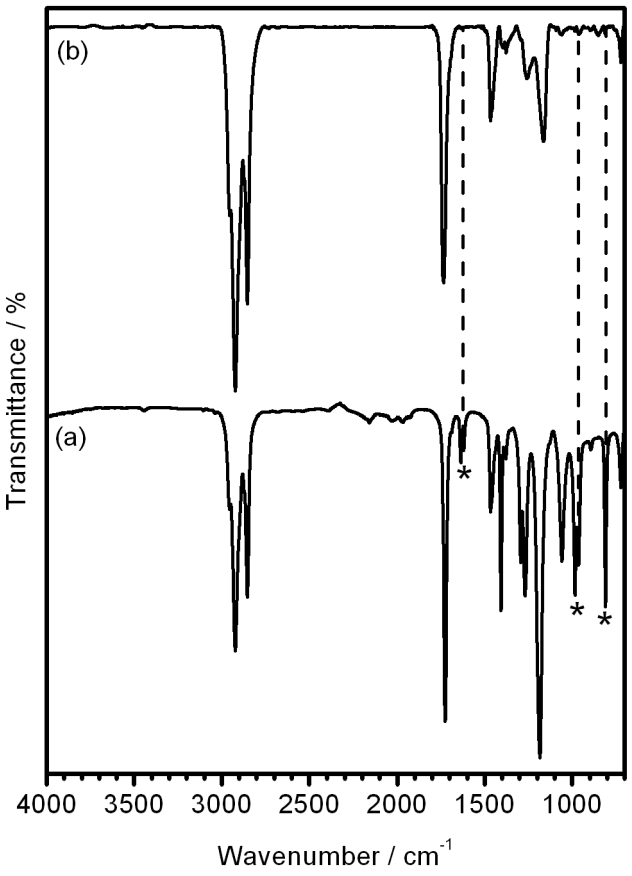

Figure 7.4: FTIR spectra of: (a) dodecyl acrylate monomer and (b) atomized spray plasma deposited poly(dodecyl acrylate). * Denotes stretches due to C=C double bond.

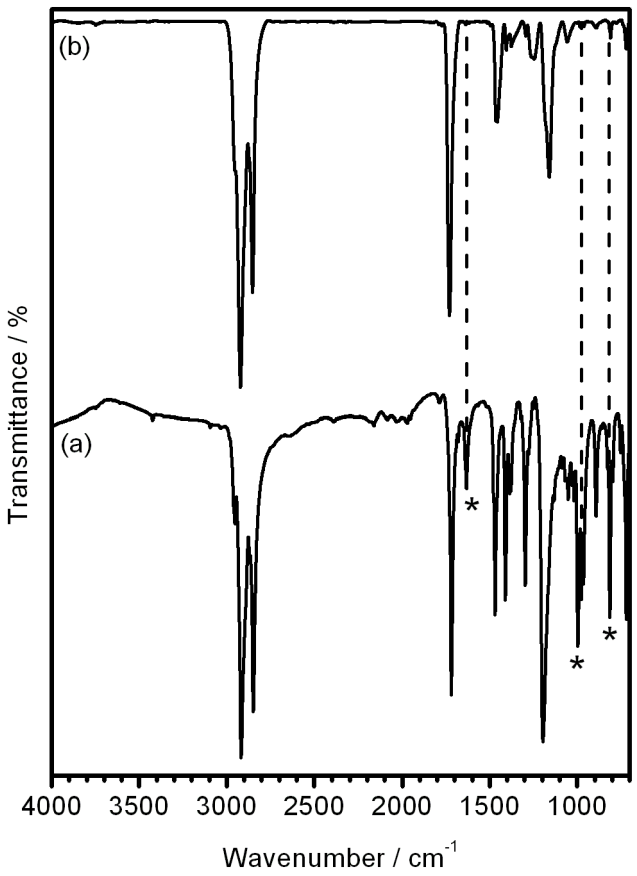

Figure 7.5: FTIR spectra of: (a) octadecyl acrylate monomer and (b) atomized spray plasma deposited poly(dodecyl acrylate-co-octadecyl acrylate). * Denotes stretches due to C=C double bond.

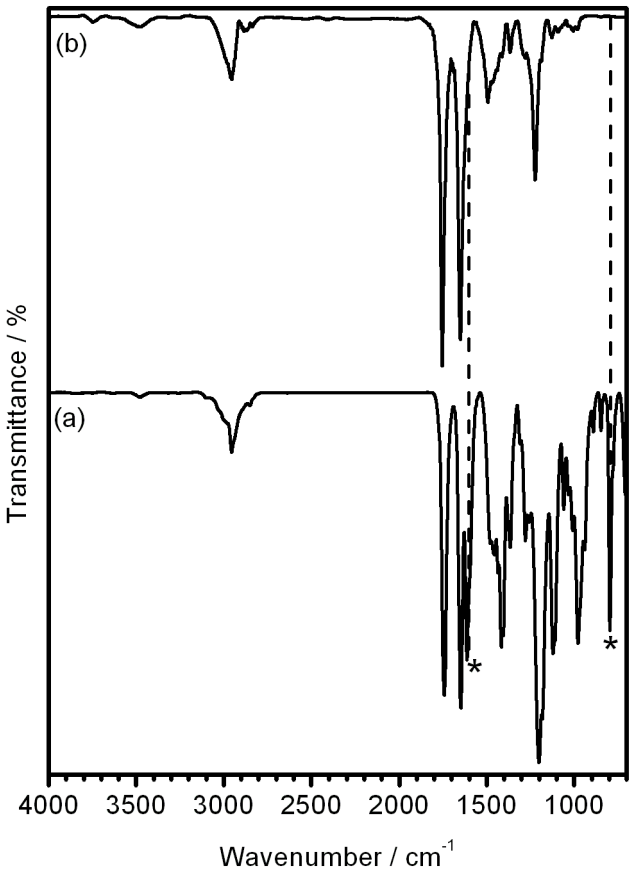

Figure 7.6: FTIR spectra of: *N*-acryloylsarcosine methyl ester and (b) atomized spray plasma deposited poly(*N*-acryloylsarcosine methyl ester). * Denotes stretches due to C=C double bond.

Layer	Contact angle/°	Deposition rate/nm min^{-1}
ASPD poly(hexyl acrylate)	80±1	4500±300
ASPD poly(dodecyl acrylate)	80±1	3500±200
ASPD poly(dodecyl acrylate-co-octadecyl acrylate)	80±1	3100±200
ASPD poly(*N*-acryloylsarcosine methyl ester)	53±1	195±9

Table 7.3: Equilibrium water contact angles and deposition rates for atomized spray plasma deposited layers.

acrylate) layers all had equilibrium water contact angles of 80°, which is consistent with the hydrophobic nature of the alkyl chain, Table 7.3.[38] The equilibrium water contact angle for atomized spray plasma deposited poly(*N*-acryloylsarcosine methyl ester) films was consistent with those previously observed for pulsed plasma deposited poly(*N*-acryloylsarcosine methyl ester) layers.[39] The observed hydrophilicity stems from the terminal ester group and the amide linkages within the polymer backbone.[27]

The deposition rates for all types of atomized spray plasma deposited films were large compared to similar films previously deposited using vapour-phase techniques (increased by a factor of above 20 in all cases), Table 7.3.[39,40] The deposition rate decreases with increasing alkyl chain length and is drastically reduced in the case of *N*-acryloylsarcosine methyl ester, which can be attributed to the increase in viscosity which results in decreased monomer spread over the atomizer nozzle tip becoming the rate-limiting step.

7.3.2 Bioarray Fabrication

Fluorescence micrographs of atomized spray plasma deposited poly(hexyl acrylate) and poly(dodecyl acrylate) films treated with phospholipid-biotin and avidin-FITC showed no significant fluorescence, Figures 7.7 and 7.8. In contrast, the poly(dodecyl acrylate-co-octadecyl acrylate) layer showed significant phospholipid binding, which can be attributed to the interdigitation of the 18-membered phosholipid alkyl groups with the 18-membered alkyl chains present in the octadecyl acrylate moiety.

Conversely, fluorescence micrographs of atomized spray plasma deposited poly(*N*-acryloylsarcosine methyl ester) films exposed to Protein A–FITC showed negative images, which shows that the layers are protein resistant, Figure 7.9.

7.4 Discussion

Bioactivity is defined as having an effect on living tissue, which on a chemical level implies interaction with biological molecules. Bioactivity in relation to surfaces can therefore be defined as

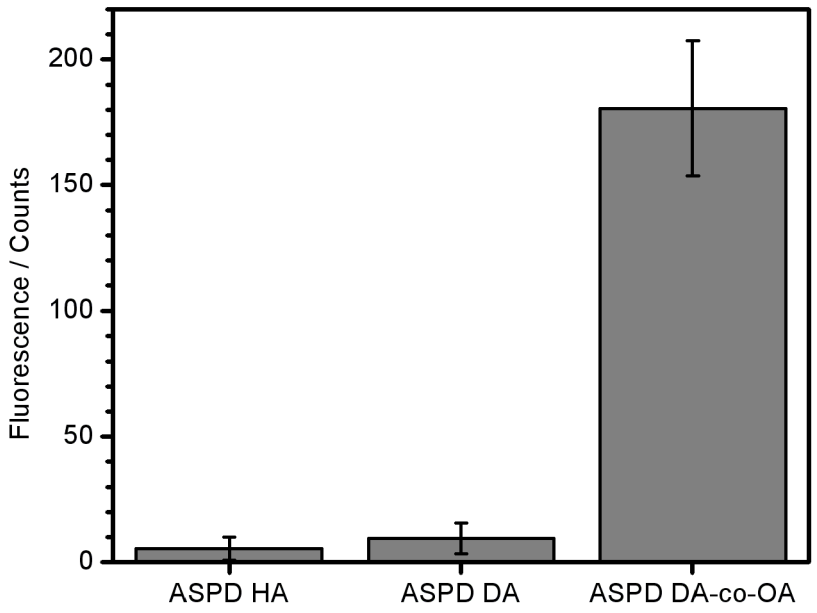

Figure 7.7: Fluorescence of atomized spray plasma deposited layers after exposure to phospholipid-biotin and avidin-FITC (HA = hexyl acrylate, DA = dodecyl acrylate, OA = octadecyl acrylate).

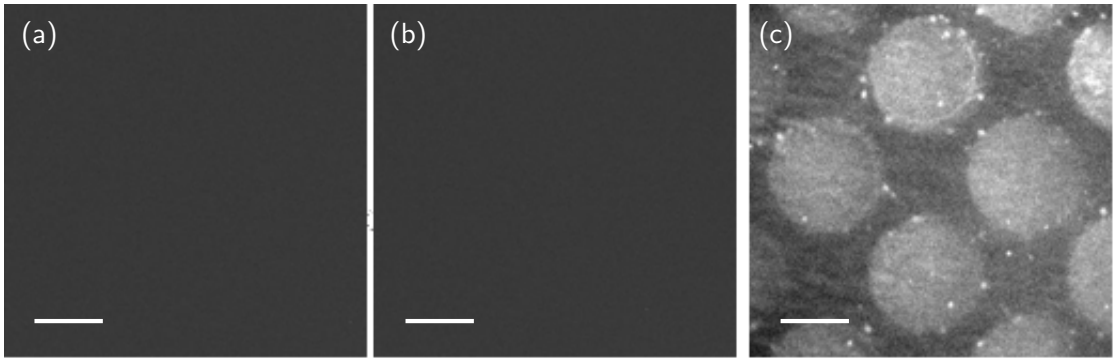

Figure 7.8: Fluorescence micrographs of phospholipid-biotin, avidin-FITC treated atomized spray plasma deposited: (a) poly(hexyl acrylate), (b) poly(dodecyl acrylate) and (c) poly(dodecyl acrylate-co-octadecyl acrylate). Scale bar is 100 μm in all images.

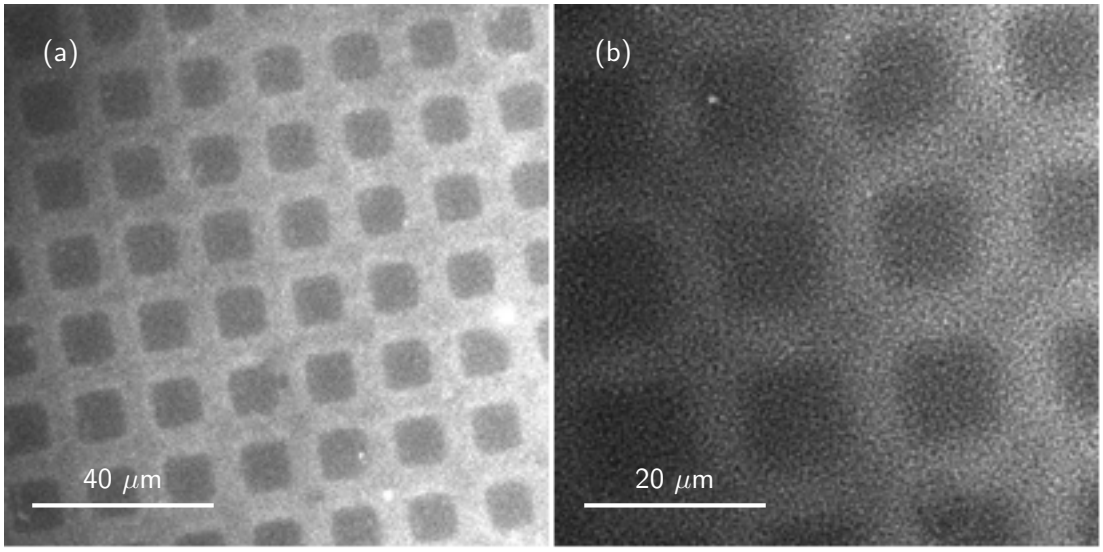

Figure 7.9: Fluorescence micrographs of atomized spray plasma deposited poly(*N*-acryloylsarcosine methyl ester) films exposed to Protein A–FITC at: (a) 20x magnification and (b) 40x magnification.

falling into three categories: (i) the ability to bind biomolecules or biological matter (i.e. immobilization); (ii) the ability to resist biomolecule or biological matter absorption (either chemisorption or physisorption—protein resistance and antifouling coatings would fall into this category); (iii) directly affecting biochemical processes (e.g. catalysis or inhibition). The coatings in this chapter fulfil the first two of these, specifically, the poly(alkyl acrylate)s are able to bind biomolecules (phospholipids) and the poly(*N*-acryloylsarcosine methyl ester) is able to resist biomolecule absorption (proteins).

Previously deposited alkyl-containing layers, which have been able to bind to phospholipids, have either required specific substrates[28] or multiple steps and solvents.[13,14] These limitations hold for the manufacture of protein-resistant surfaces as well. In contrast, atomized spray plasma deposition provides a substrate-independent, solventless technique to yield conformal poly(alkyl acrylate) and poly(*N*-acryloylsarcosine methyl ester) coatings. The deposition rates achieved using this methodology far exceed that of other vapour-phase deposition techniques such as initiated chemical vapour deposition (in the case of alkyl acrylates)[40] and conventional plasmachemical deposition (in the case of *N*-acryloylsarcosine methyl ester).[39] Also, use of the atomized spray means that the negligible vapour pressures of dodecyl acrylate and octadecyl acrylate are no longer a hindrance to deposition.

Additionally, unlike previously described atomized spray plasma deposition processes, the method described herein has no requirement of expensive diluent gases such as helium[35] and avoids plasma-induced damage of the growing film[41] by positioning of the substrates downstream from the atomizer nozzle.

The mechanics of how the ASPD process works to produce polymer coatings is slightly different from conventional plasma polymerization. Instead of a (relatively) uniform distribution of precursor molecules throughout the reactor in gaseous form, there are a large number of precursor-filled droplets (average size of around 20 microns). The monomer on the inside of these droplets is shielded from the plasma by monomer outside it, such that the only molecules to be activated (initiated) by the plasma are those on the droplet surface. As the droplet travels through the plasma, therefore, it acquires a large number of initated monomer species on its surface (depending on the plasma parameters), which begin to propagate as polymer chains. This mixture of monomer and propagating oligomers then hits the substrate surface, where, dependent on viscosity, it will spread and monomer still present will mix with active polymer chains. This results in the FTIR spectra observed for all the films where the C=C double bond stretches have completely disappeared.

A big advantage of the atomized spray deposition process is not only does it vastly increase the deposition rate of monomers which already have sufficient vapour pressure for conventional plasmachemical deposition (hexyl acrylate and *N*-acryloylsarcosine methyl ester[39]), but it also enables deposition of monomers with no vapour pressure (e.g. dodecyl acrylate, which has low vapour pressure ($<$0.1 mbar), and octadecyl acrylate, which is a solid and has negligible vapour pressure). As a result, previously unattainable plasma polymer films are achievable. This is particularly pertinent in view of the limited number of acid-bearing monomers that are commercially available with sufficient vapour pressure for conventional plasmachemical deposition. The ability of depositing liquid monomers with negligible vapour pressure (e.g. vinylphosphonic acid) represents a significant widening of the scope for plasmachemical deposition of proton exchange membranes (along with other fuel cell components).

The high deposition rates coupled with the structural and functional retention achieved by the atomized-spray-plasma methodology means potential use in high-throughput manufacturing such as utilization of roll-to-roll processes can be envisaged.

7.5 Conclusions

Both lipophilic and protein-resistant, conformal coatings have been prepared by use of atomized-spray-plasma deposition at room temperature. The use of atomized spray plasma deposition yields a substrate-independent coating process with high-throughput capabilities for the production of bioactive layers.

7.6 References

[1] (a) Hench, L. L.; Wilson, J. *Science* **1984**, *226*, 630; (b) Meyers, S. R.; Grinstaff, M. W. *Chem. Rev.* **2012**, *112*, 1615.

[2] Messersmith, P. B. *Science* **2008**, *319*, 1767.

[3] Statz, A. R.; Meagher, R. J.; Barron, A. E.; Messersmith, P. B. *J. Am. Chem. Soc.* **2005**, *127*, 7972.

[4] Sackmann, E. *Science* **1996**, *271*, 43.

[5] (a) Cornell, B. A.; Braach-Maksvytis, V. L. B.; King, L. G.; Osman, P. D. J.; Raguse, B.; Wieczorek, L.; Pace, R. J. *Nature* **1997**, *387*, 580; (b) Stora, T.; Lakey, J. H.; Vogel, H. *Angew. Chem. Int. Ed.* **1999**, *38*, 389.

[6] (a) Plant, A. L.; Gueguetchkeri, M.; Yap, W. *Biophys. J.* **1994**, *67*, 1126; (b) Naumann, C. A.; Prucker, O.; Lehmann, T.; Rühe, J.; Knoll, W.; Frank, C. W. *Biomacromolecules* **2002**, *3*, 27.

[7] van Oudenaarden, A.; Boxer, S. G. *Science* **1999**, *285*, 1046.

[8] (a) Stanish, I.; Santos, J. P.; Singh, A. *J. Am. Chem. Soc.* **2001**, *123*, 1008; (b) Zhang, L.; Hong, L.; Yu, Y.; Bae, S. C.; Granick, S. *J. Am. Chem. Soc.* **2006**, *128*, 9026.

[9] (a) Marra, K. G.; Winger, T. M.; Hanson, S. R.; Chaikof, E. L. *Macromolecules* **1997**, *30*, 6483; (b) Mornet, S.; Lambert, O.; Duguet, E.; Brisson, A. *Nano Lett.* **2005**, *5*, 281.

[10] Kallury, K. M. R.; Lee, W. E.; Thompson, M. *Anal. Chem.* **1992**, *64*, 1062.

[11] Omae, I. *Chem. Rev.* **2003**, *103*, 3431.

[12] Tria, M. C. R.; Grande, C. D. T.; Ponnapati, R. R.; Advincula, R. C. *Biomacromolecules* **2010**, *11*, 3422.

[13] Hsiue, G.-H.; Lee, S.-D.; Chang, P. C.-T.; Kao, C.-Y. *J. Biomed. Mater. Res.* **1998**, *42*, 134.

[14] Korematsu, A.; Takemoto, Y.; Nakaya, T.; Inoue, H. *Biomaterials* **2002**, *23*, 263.

[15] (a) Edinger, K.; Goelzhaeuser, A.; Demota, K.; Woell, C.; Grunze, M. *Langmuir* **1993**, *9*, 4; (b) Meuse, C. W.; Krueger, S.; Majkrzak, C. F.; Dura, J. A.; Fu, J.; Connor, J. T.; Plant, A. L. *Biophys. J.* **1998**, *74*, 1388; (c) Meuse, C. W.; Niaura, G.; Lewis, M. L.; Plant, A. L. *Langmuir* **1998**, *14*, 1604; (d) Terrettaz, S.; Stora, T.; Duschl, C.; Vogel, H. *Langmuir* **1993**, *9*, 1361.

[16] Lingler, S.; Rubinstein, I.; Knoll, W.; Offenhäusser, A. *Langmuir* **1997**, *13*, 7085.

[17] (a) Wagner, M. L.; Tamm, L. K. *Biophys. J.* **2000**, *79*, 1400; (b) Atanasov, V.; Knorr, N.; Duran, R. S.; Ingebrandt, S.; Offenhäusser, A.; Knoll, W.; Köper, I. *Biophys. J.* **2005**, *89*, 1780.

[18] Prime, K. L.; Whitesides, G. M. *Science* **1991**, *252*, 1164.

[19] (a) Dalsin, J. L.; Hu, B.-H.; Lee, B. P.; Messersmith, P. B. *J. Am. Chem. Soc.* **2003**, *125*, 4253; (b) Christman, K. L.; Schopf, E.; Broyer, R. M.; Li, R. C.; Chen, Y.; Maynard, H. D. *J. Am. Chem. Soc.* **2009**, *131*, 521.

[20] Huber, D. L.; Manginell, R. P.; Samara, M. A.; Kim, B.-I.; Bunker, B. C. *Science* **2003**, *301*, 352.

[21] (a) Chapman, R. G.; Ostuni, E.; Takayama, S.; Holmlin, R. E.; Yan, L.; Whitesides, G. M. *J. Am. Chem. Soc.* **2000**, *122*, 8303; (b) Luk, Y.-Y.; Kato, M.; Mrksich, M. *Langmuir* **2000**, *16*, 9604; (c) Ostuni, E.; Chapman, R. G.; Holmlin, R. E.; Takayama, S.; Whitesides, G. M. *Langmuir* **2001**, *17*, 5605; (d) Ostuni, E.; Chapman, R. G.; Liang, M. N.; Meluleni, G.; Pier, G.; Ingber, D. R.; Whitesides, G. M. *Langmuir* **2001**, *17*, 6336; (e) Kane, R. S.; Deschatelets, P.; Whitesides, G. M. *Langmuir* **2003**, *19*, 2388.

[22] (a) Chapman, R. G.; Ostuni, E.; Liang, M. N.; Meluleni, G.; Kim, E.; Yan, L.; Pier, G.; Warren, H. S.; Whitesides, G. M. *Langmuir* **2001**, *17*, 1225; (b) Jon, S.; Seong, J.; Khademhosseini, A.; Tran, T. N. T.; Laibinis, P. E.; Langer, R. *Langmuir* **2003**, *19*, 9989; (c) Gu, J.; Yam, C. M.; Li, S.; Cai, C. *J. Am. Chem. Soc.* **2004**, *126*, 8098; (d) Lasseter, T. L.; Clare, B. H.; Abbott, N. L.; Hamers, R. J. *J. Am. Chem. Soc.* **2004**, *126*, 10220.

[23] Groll, J.; Amirgoulova, E. V.; Ameringer, T.; Heyes, C. D.; Röcker, C.; Nienhaus, G. U.; Möller, M. *J. Am. Chem. Soc.* **2004**, *126*, 4234.

[24] Zhang, F.; Kang, E. T.; Neoh, K. G.; Wang, P.; Tan, K. L. *J. Biomed. Mater. Res.* **2001**, *56*, 324.

[25] Kingshott, P.; Thissen, H.; Griesser, H. J. *Biomaterials* **2002**, *23*, 2043.

[26] (a) Zhang, Z.; Menges, B.; Timmons, R. B.; Knoll, W.; Förch, R. *Langmuir* **2003**, *19*, 4765; (b) Shen, M.; Wagner, M. S.; Castner, D. G.; Ratner, B. D.; Horbett, T. A. *Langmuir* **2003**, *19*, 1692.

[27] Teare, D. O. H.; Schofield, W. C. E.; Garrod, R. P.; Badyal, J. P. S. *J. Phys. Chem. B* **2005**, *109*, 20923.

[28] (a) Bain, C. D.; Troughton, E. B.; Tao, Y. T.; Evall, J.; Whitesides, G. M.; Nuzzo, R. G. *J. Am. Chem. Soc.* **1989**, *111*, 321; (b) Tu, W.; Takai, K.; Fukui, K.-I.; Miyazaki, A.;

Enoki, T. *J. Phys. Chem. B* **2003**, *107*, 10134; (c) Stapleton, J. J.; Daniel, T. A.; Uppili, S.; Cabarcos, O. M.; Naciri, J.; Shashidhar, R.; Allara, D. L. *Langmuir* **2005**, *21*, 11061.

[29] Ulman, A. *Chem. Rev.* **1996**, *96*, 1533.

[30] Lee, M.-T.; Hsueh, C.-C.; Freund, M. S.; Ferguson, G. S. *Langmuir* **1998**, *14*, 6419.

[31] Teare, D. O. H.; Barwick, D. C.; Schofield, W. C. E.; Garrod, R. P.; Ward, L. J.; Badyal, J. P. S. *Langmuir* **2005**, *21*, 11425.

[32] Yasuda, H. *Plasma Polymerization*; Academic Press: New York, 1985.

[33] Ryan, M. E.; Hynes, A. M.; Badyal, J. P. S. *Chem. Mater.* **1996**, *8*, 37.

[34] Friedrich, J. *Plasma Processes Polym.* **2011**, *8*, 783.

[35] Ward, L. J.; Schofield, W. C. E.; Badyal, J. P. S.; Goodwin, A. J.; Merlin, P. J. *Chem. Mater.* **2003**, *15*, 1466.

[36] Ward, L. J.; Schofield, W. C. E.; Badyal, J. P. S.; Goodwin, A. J.; Merlin, P. J. *Langmuir* **2003**, *19*, 2110.

[37] Lin-Vien, D.; Colthup, N. B.; Fateley, W. G.; Grasselli, J. G. *The Handbook of Infrared and Raman Characteristic Frequencies of Organic Molecules*; Academic Press: London, U.K., 1991.

[38] Okouchi, M.; Yamaji, Y.; Yamauchi, K. *Macromolecules* **2006**, *39*, 1156.

[39] Harris, L. G.; Schofield, W. C. E.; Doores, K. J.; Davis, B. G.; Badyal, J. P. S. *J. Am. Chem. Soc.* **2009**, *131*, 7755.

[40] Lau, K. K. S.; Gleason, K. K. *Macromolecules* **2006**, *39*, 3688.

[41] Kolluri, O. S. PCT International Patent No. WO 98/10116, 1998.

Chapter 8

Atomized Spray Plasma Deposition of Polymer-Silica Nanocomposite Layers

8.1 Introduction

It was shown in the previous chapter that an atomized spray used in conjunction with plasma excitation forms an excellent method of increasing the deposition rate for plasmachemical polymer coatings. The ability to use precursors with no appreciable vapour pressure also opens up the opportunity to use solid precursors as long as they are combined with a liquid (in chapter 7 this is in the form of a solution). This capability is utilized in the current chapter to create nanocomposite coatings from a monomer precursor mixed with commercially available silica nanoparticles. This strategy is particularly pertinent with regard to improving proton exchange membrane properties, because silica is well known to improve the water retention of proton exchange membranes (meaning that performance does not deteriorate at temperatures higher than 100 °C) as well as helping increase the mechanical strength. The potential use of silica nanoparticles is exemplified in two different ways in this chapter—by adding to 2-hydroxyethyl methacrylate in order to improve mechanical properties and also to a di(ethylene glycol) precursor in order to promote amorphousness and therefore lithium ion conductivity.

Poly(2-hydroxyethyl methacrylate) coatings are used for a plethora of technological applications including heavy metal ion removal,[1] luminescent materials,[2,3] biomaterials,[4] nanostructures,[5] polymer electrolytes,[6] bioactivity,[7] tissue culture[8] and solar cells.[9] Furthermore, the inherent biocompatibility of poly(2-hydroxyethyl methacrylate)[10] makes it suitable as an adhesive for biomedical applications such as dentistry[11] and bone implants.[12] Nanocomposites can be formed by the addition of inorganic particles (e.g. zinc oxide,[2] calcium carbonate[13] or silica[14–16]) to the polymer, which can be utilized to improve the luminescent,[2] water uptake[16] or mechanical properties of materials.[13–15]

Poly(ethylene glycol) nanocomposite coatings are also used in many applications including photoinduced microstructures,[17] piezoelectric materials,[18] hydrogels,[19] biosensors,[20–22] drug de-

livery,[23,24] proton conducting membranes,[25,26] thixotropic cell support,[27] cell imaging,[28] photothermal therapy,[29] tissue engineering,[30] antibacterial coatings,[31,32] gas separation[33] and oxygen scavenging.[34] Poly(ethylene glycol)–ceramic nanocomposites have been used extensively for lithium-ion conducting membranes for solid-state battery applications;[35–38] ceramic fillers are used to improve mechanical[39] and interfacial[40] properties as well as to promote amorphousness within the electrolyte layers with a corresponding rise in ionic conductivity.[35]

Previous methods for preparing poly(2-hydroxyethyl methacrylate) nanocomposite layers have included sol-gel reaction,[2,14,15] free radical polymerization,[41] photopolymerization,[42] emulsion polymerization,[43,44] controlled radical polymerization,[45,46] in-situ reduction[47,48] and solution intercalation.[49] Such wet chemical approaches tend to require catalysts,[45] high temperatures,[15] multiple steps[2] or long reaction times.[14]

Similarly methods used previously to manufacture poly(ethylene glycol) nanocomposite coatings have included photopolymerization,[17,50] dendrimer mediated stabilization,[51] suspension polymerization,[18] coprecipitation,[21] sol-gel synthesis[25,27] and magnetron sputtering.[32] These methods can be expensive and time consuming,[21,24,51] require multiple steps,[21] yield a lack of fine control over coating thickness,[34] require a separate casting step[31] or utilize high power-inputs (leading to damage of the polymer film).[32]

Plasmachemical deposition of functional thin films is recognized as being a single-step, solventless technique, which provides conformal coatings.[52] It has previously been shown that where the electrical discharge is modulated in the presence of precursor vapour high levels of functional retention can be achieved.[53] An alternative approach for achieving such high levels of structural retention is to raise precursor vapour pressure within the reactor (i.e. increase the pressure/flow rate), such that the average plasma power per reactant molecule decreases.[52,54] However, in this case there exist limitations due to high precursor vapour pressures/flow rates leading to plasma instabilities/inhomogeneity and eventually extinction. Such shortcomings can be overcome by utilizing an atomized spray of the precursor.[55,56]

In this chapter the use of atomized spray plasma deposition (ASPD) of 2-hydroxyethyl methacrylate– or di(ethylene glycol) ethyl ether acrylate–silica nanoparticle slurry mixtures to form nanocomposite layers is described, Scheme 8.1. In the case of the 2-hydroxyethyl methacrylate precursor, application of this one-step plasmachemical deposition process to overlapping joints gives rise to excellent in-situ adhesion. For the case of the di(ethylene glycol) ethyl ether acrylate precursor, using mixtures with pre-dissolved lithium perchlorate yields layers which show lithium-ion conductivity at room temperature.

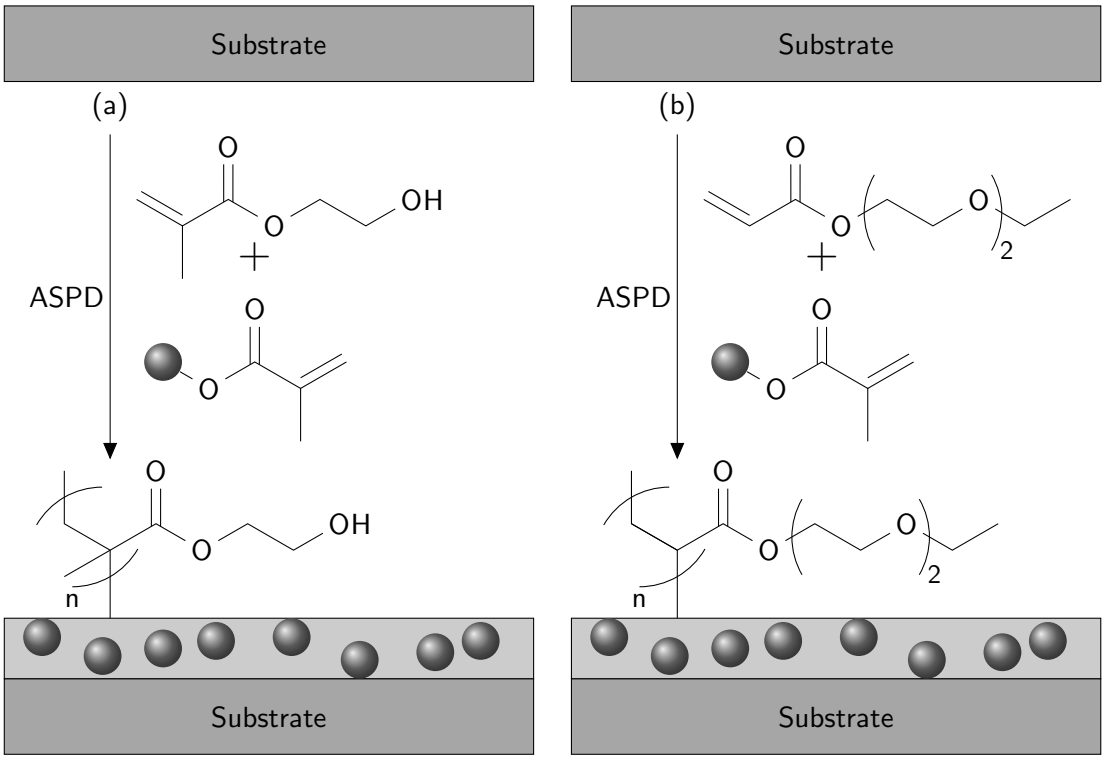

Scheme 8.1: Atomized spray plasma deposition of nanocomposite: (a) poly(2-hydroxyethyl methacrylate)–silica layers and (b) poly(di(ethylene glycol) ethyl ether acrylate)–silica layers.

8.2 Experimental

8.2.1 Atomized Spray Plasma Deposition of Nanocomposite Films

Atomized spray plasma deposition was carried out in an electrodeless, T-shape, glass reactor (volume 820 cm^3, base pressure of 3 x 10^{-3} mbar, and with a leak rate better than 2 x 10^{-9} mol s^{-1}), enclosed in a Faraday cage. The precursor inlet was surrounded by a copper coil (4 mm diameter, 7 turns). Substrates used for coating were silicon (100) wafer pieces (Silicon Valley Microelectronics Inc.), borosilicate glass microscrope slides (Smith Scientific Ltd.) and polypropylene pieces (capacitor grade, Lawson-Mardon Ltd., with two gold electrodes of 3.5 mm length, 1.5 mm width and 1.5 mm separation). They were placed downstream in line-of-sight from the atomizer nozzle (Model no. 8700-120, Sono Tek Corp.). Precursors comprised mixtures of 2-hydroxyethyl methacrylate (+97% Aldrich Ltd.) and methacrylsilane treated fumed silica particles (Aerosil R711, Evonik Industries AG) and di(ethylene glycol) ethyl ether acrylate (+90% Aldrich Ltd.) and lithium perchlorate (+99%, Alfa Aesar Ltd.) with silica particles. These were loaded into separate sealable glass delivery tubes and degassed using several freeze-pump-thaw cycles. Precursor was then introduced into the reactor at a flow rate of 0.02 mL s^{-1} through the ultrasonic nozzle operating at 120 kHz. Deposition entailed running a continuous-wave plasma at 50 W for 150 s in the presence of precursor atomization. Upon plasma extinction, the system

was evacuated to base pressure before venting to atmosphere.

8.2.2 Film Characterization

Surface elemental compositions were determined by X-ray photoelectron spectroscopy (XPS) using a VG ESCALAB Mk II spectrometer as described in section 2.2 (page 28). Experimental instrument sensitivity (multiplication) factors were C(1s): O(1s): Cl(2p) equals 1.00: 0.36: 0.39.

Infrared spectra were acquired using a FTIR spectrometer (Perkin-Elmer Spectrum One) as described in section 2.3 (page 31).

Transmission electron microscopy images were obtained using a Phillips CM100 microscope. This entailed embedding plasma coated polypropylene squares into an epoxy resin, and then cross-sectioning using a cryogenic microtome. The cross-sections were mounted onto copper grids prior to electron microscopy analysis.

Film thicknesses were measured by freezing coated silicon samples in liquid nitrogen followed by fracture to reveal a cross-section. These were then imaged using an optical microscope (Olympus BX40) fitted with a x20 magnification lens.

Penetration of the atomized spray plasma deposited poly(2-hydroxyethyl methacrylate)–silica coatings between two overlapping pieces of flat glass was examined using a Raman microscope (LABRAM, Jobin Yvon Ltd.). A He-Ne laser was employed as the excitation source (632.8 nm line, operating at 20 mW). The unattenuated laser beam was focused onto the sample using a x10 microscope objective and the corresponding Raman signals were collected by the same microscope objective in a backscattering configuration in combination with a cooled CCD detector system. The spectrometer diffraction grating (300 g/mm) was calibrated against neon light emission lines in the 600–700 nm range. The depth of penetration was measured by monitoring the relative intensity of the polymer C−C skeletal stretch peaks at 900–950 cm^{-1} with distance.

Adhesion testing of the ASPD coatings comprised depositing directly onto two overlapping borosilicate glass microscope slide pieces. Subsequently, lap shear adhesion tests (attributable to penetration of deposited material at the joint) were carried out using an Instron 5543 tensilometer operating at a crosshead speed of 1 mm min^{-1} as described in section 2.8 (page 36).

Impedance measurements across the 700 Hz–13 MHz frequency range were carried out using an LF impedance analyser (Hewlett-Packard 4192A) for atomized spray plasma deposited poly(di(ethylene glycol) ethyl ether acrylate) layers on polypropylene substrates at room temperature (20 °C). Impedance plots displayed a single arc which was used to extract the resistance of the deposited membrane layer, which was used to calculate lithium-ion conductivity as described in section 2.6 (page 35).

Layer	%C	%O	%Cl
Theoretical poly(2-hydroxyethyl methacrylate)	67	33	—
ASPD poly(2-hydroxyethyl methacrylate)	77±2	23±2	—
Theoretical poly(di(ethylene glycol) ethyl ether acrylate)	69.2	30.8	—
ASPD poly(di(ethylene glycol) ethyl ether acrylate)	69.1±0.3	30.9±0.3	—
ASPD poly(di(ethylene glycol) ethyl ether acrylate)–lithium perchlorate (1 wt %)	69.2±0.5	30.2±0.5	0.6±0.3
ASPD poly(di(ethylene glycol) ethyl ether acrylate)–lithium perchlorate (5 wt %)	65.1±0.8	32.9±0.8	2.0±0.5
ASPD poly(di(ethylene glycol) ethyl ether acrylate)–lithium perchlorate (10 wt %)	65.6±0.8	31.3±0.8	3.0±0.5

Table 8.1: Elemental XPS compositions of atomized spray deposited layers

8.3 Results

8.3.1 Atomized Spray Plasma Deposition of Nanocomposite Layers

The lack of any Si(2p) XPS signal confirmed coverage of the substrates by the nanocomposite films, Table 8.1. For the ASPD poly(2-hydroxyethyl methacrylate) layers the C(1s) spectra can be fitted to three components corresponding to: hydrocarbon C_xH_y (285.0 eV), singly bonded carbon-oxygen C−O (286.6 eV) and the carbonyl ester O−C=O (288.9 eV), Figure 8.1. There were no discernible differences in the C(1s) XPS spectra regardless of percentage silica content (up to the maximum loading of 2.4 wt %).

Atomized spray plasma deposited poly(di(ethylene glycol) ethyl ether acrylate) films showed three component peaks within the C(1s) XPS spectrum, which corresponded to hydrocarbon C_xH_y at 285.0 eV, C−O centres at 286.4 eV and O−C=O centres at 288.8 eV, Figure 8.2. These component envelopes have the ratio 3.2:4.7:1.1, which is close to the theoretical 3:5:1, therefore there is good structural retention within the nanocomposite layers. This is confirmed by the elemental ratio of carbon to oxygen for the atomized spray plasma deposited poly(di(ethylene glycol) ethyl ether acrylate) layers being the same as that of theoretical polymer, Table 8.1. Addition of lithium perchlorate led to the appearance of a Cl(2p) peak at 207.7 eV binding energy, which is characteristic of perchlorate environments.[57]

For the 2-hydroxyethyl methacrylate monomer, the following infrared assignments can be made:[58] antisymmetric CH_3 stretch (2953 cm^{-1}), antisymmetric CH_2 stretch (2928 cm^{-1}), symmetric CH_3 stretch (2881 cm^{-1}), carbonyl C=O stretch (1713 cm^{-1}), vinyl C=C stretch (1635 cm^{-1}), $=CH_2$ wag (941 cm^{-1}) and $=CH_2$ twist (814 cm^{-1}), Figure 8.3. Atomized spray plasma deposited poly(2-hydroxyethyl methacrylate) layers show similar absorbances except for the absence of peaks due to C=C double bonds (C=C stretch, $=CH_2$ wag and $=CH_2$ twist) which are

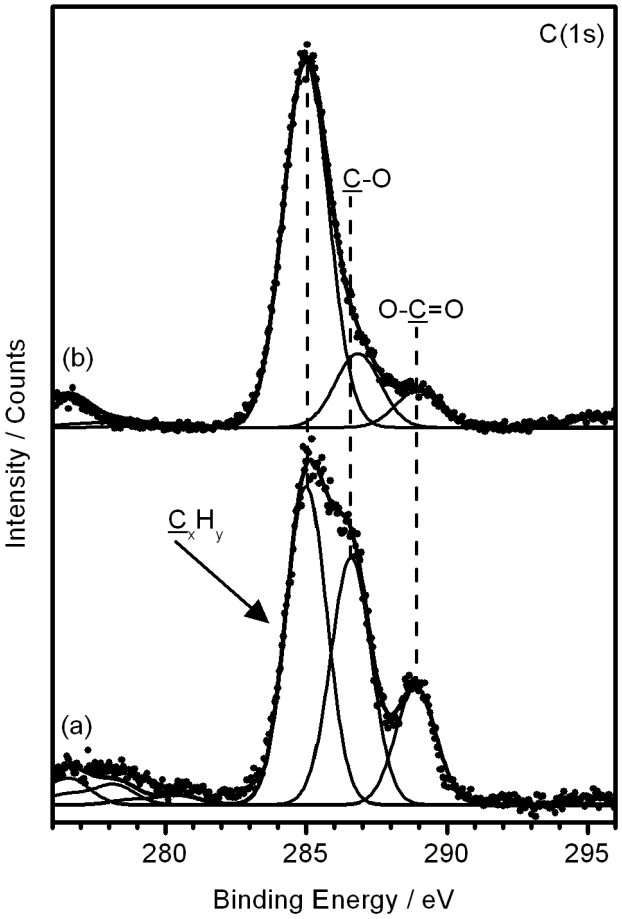

Figure 8.1: X-ray photoelectron C(1s) spectra of: (a) theoretical poly(2-hydroxyethyl methacrylate) and (b) atomized spray plasma deposited poly(2-hydroxyethyl methacrylate).

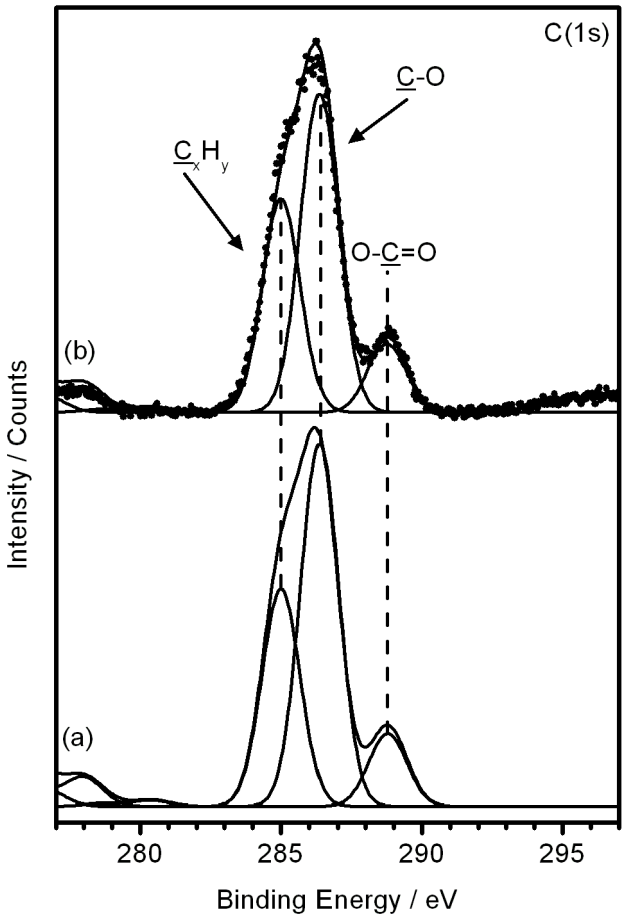

Figure 8.2: X-ray photoelectron C(1s) spectra of: (a) theoretical poly(di(ethylene glycol) ethyl ether acrylate) and (b) atomized spray plasma deposited poly(di(ethylene glycol) ethyl ether acrylate).

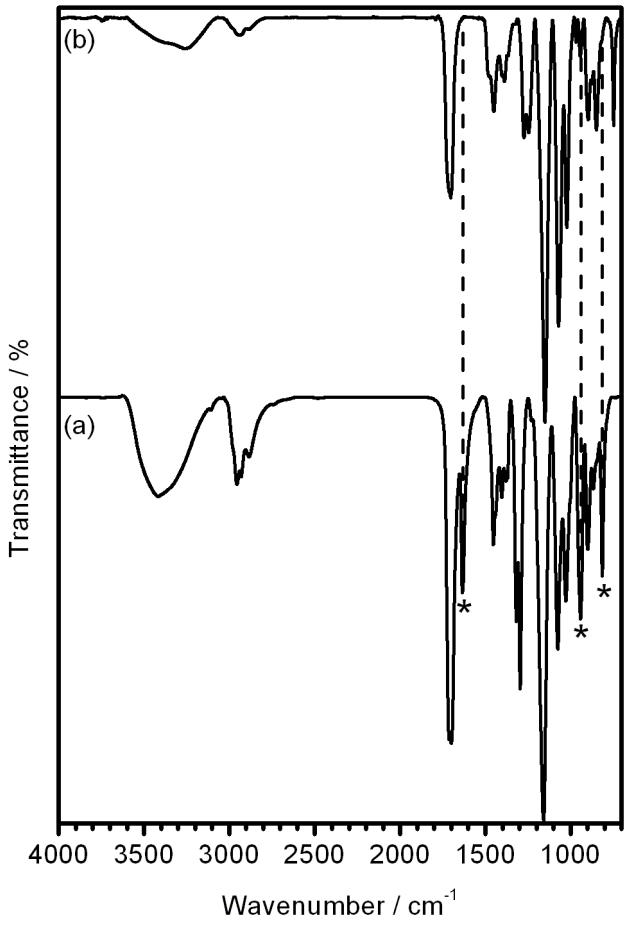

Figure 8.3: Fourier transform infrared spectra of: (a) 2-hydroxyethyl methacrylate monomer and (b) atomized spray plasma deposited poly(2-hydroxyethyl methacrylate) film. * Denotes absorbances due to polymerisable C=C double bond present in monomer.

replaced by a peak at 747 cm^{-1} attributed to -CH_2- twist. These changes are consistent with conventional polymerization taking place at the C=C double bond. As noted for XPS, there were no discernible differences in the infrared spectra for varying silica contents. The excellent bulk structural retention illustrated by the infrared spectra (which analyses the entire coating thickness) is consistent with residual plasma-induced modification/damage of the deposited film being limited to the surface (since XPS only probes the outermost 5 nm[59]).

The following assignments for the infrared spectrum of the di(ethylene glycol) ethyl ether acrylate monomer can be made:[58,60] CH_3 antisymmetric stretch (2974 cm^{-1}), CH_2 antisymmetric stretch (2928 cm^{-1}), CH_3/CH_2 symmetric stretch (2867 cm^{-1}), carbonyl C=O stretch (1721 cm^{-1}), vinyl C=C stretches (1637 and 1619 cm^{-1}), C−O−C ether antisymmetric stretch (1108 cm^{-1}), =CH wag (984 cm^{-1}), $=CH_2$ wag (965 cm^{-1}), C−O−C ether symmetric stretch (859 cm^{-1}) and $=CH_2$ twist (809 cm^{-1}), Figure 8.4. In the case of the atomized spray plasma deposited poly(di(ethylene glycol) ethyl ether acrylate) the methyl/methylene CH_3/CH_2 stretches and the ether C−O−C stretches remain, but the vinyl C=C stretches have disappeared along with the

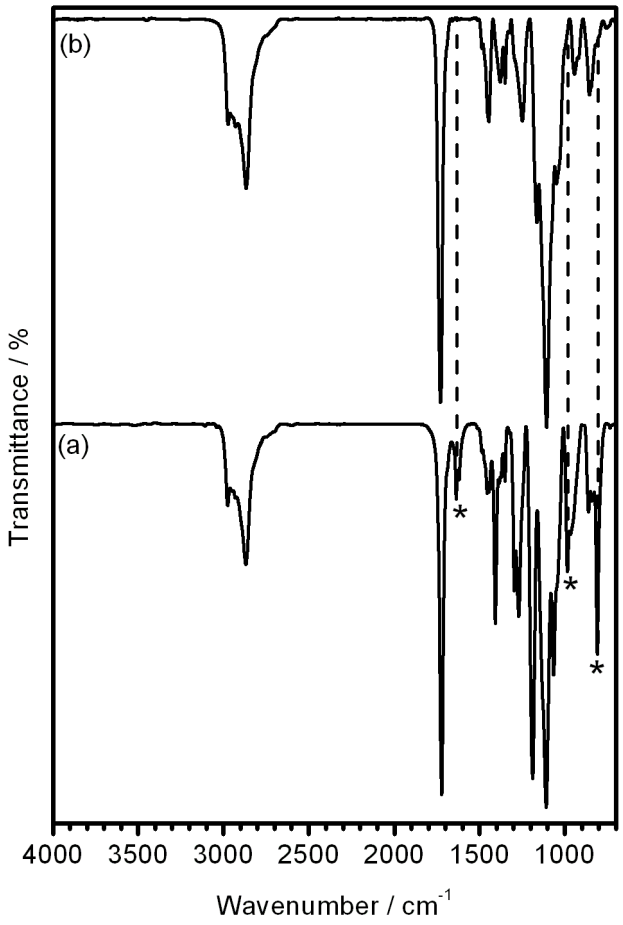

Figure 8.4: Fourier transform infrared spectra of: (a) di(ethylene glycol) ethyl ether acrylate monomer and (b) atomized-spray-plasma deposited poly(di(ethylene glycol) ethyl ether acrylate). * Denotes absorbances due to C=C double bond.

$=CH/=CH_2$ wags and $=CH_2$ twist. This is consistent with polymerization having occurred at the acrylate C=C double bond. There is also a shift in the C=O stretch from 1721 cm^{-1} in the monomer to 1729 cm^{-1} in the atomized spray plasma deposited polymer, which is consistent with a move from a conjugated double bond system (i.e. acrylate) to an unconjugated system (i.e. poly(acrylate)). Therefore good structural retention is observed by infrared throughout the atomized spray plasma deposited layers with retention of the ether moieties. The infrared spectra for polymers codeposited with lithium perchlorate and silica showed no significant differences. This is attributed to the distinctive perchlorate and silica absorbances both falling within the 1050–1150 cm^{-1} range (perchlorate at 1076 cm^{-1}, silica at 1107 cm^{-1})[58,61] which is dominated by the strong C−O−C ether antisymmetric peak of the polymer.

Transmission electron microscopy of the atomized spray plasma deposited 2-hydroxyethyl methacrylate/1 wt % silica mixture clearly shows clusters of silica nanoparticles (average diameter 15 nm) embedded within the poly(2-hydroxyethyl methacrylate) host matrix, Figure 8.5. Similarly transmission electron microscopy of the atomized spray plasma deposited poly(di(ethylene

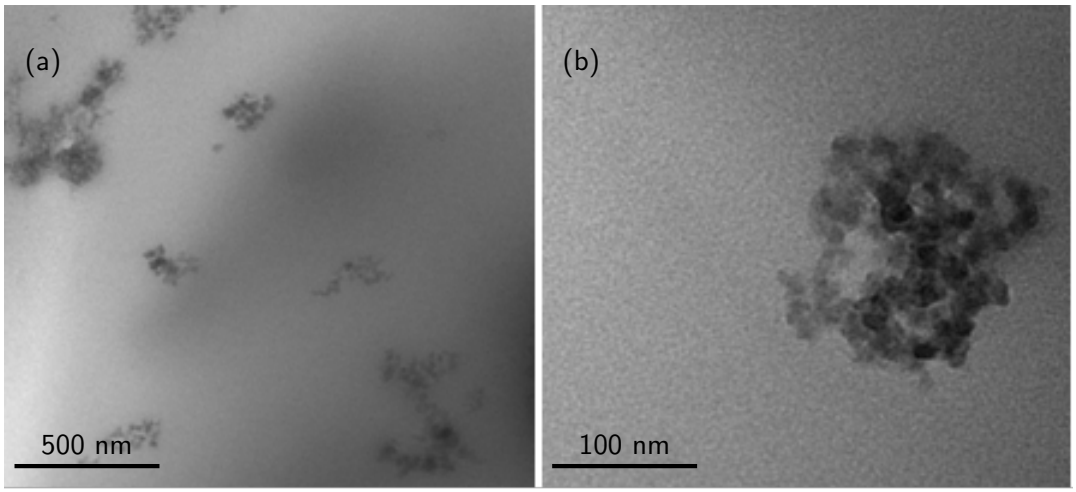

Figure 8.5: Transmission electron microscopy images for atomized spray plasma deposited poly(2-hydroxyethyl methacrylate)–1 wt % silica at (a) x25,000 and (b) x130,000 magnification.

glycol) ethyl ether acrylate)–silica layers clearly shows silica nanoparticles embedded within a host polymer organic matrix (albeit more evenly dispersed than the poly(2-hydroxyethl methacrylate)), Figure 8.6.

Deposition rates for the atomized spray plasma deposited poly(2-hydroxyethyl methacrylate)–silica layers were 3.7$\pm$0.4 μm min^{-1} and measured to be independent of silica loading. Precursor mixtures exceeding 2.4 wt % silica content were found to be too viscous to atomize, and therefore unable to be deposited. Similarly the deposition rates for atomized spray plasma deposited poly(di(ethylene glycol) ethyl ether acrylate)–silica layers were 4.0$\pm$0.3 μm min^{-1} independent of silica loading.

8.3.2 Adhesion of Overlapping Glass Joints Coated with Poly(2-Hydroxyethyl Methacrylate)–Silica Nanocomposite Layers

Raman spectroscopy showed that the atomized spray plasma deposited poly(2-hydroxyethyl methacrylate)–silica coatings are able to penetrate between two overlapping glass substrates to a depth of 743$\pm$53 μm, Figure 8.7. This phenomenon can be attributed to the liquid precursor droplets hitting the surface and wetting into the joint. Given that initiation of polymerization happens during the flight of the droplets through the plasma, then conventional polymerization mechanisms will continue to take place at the surface/joint interface.

The adhesive bond strength of the overlapping glass joints following atomized spray plasma deposition of poly(2-hydroxyethyl methacrylate) with no silica content was 5.1 MPa, which rose rapidly with increasing silica content to reach a maximum value of approximately 84 MPa at 0.5 wt % silica loading for which the adherent (bulk glass) failed, Figure 8.8. At lower silica loadings the weaker bond failure occurs due to cohesive failure (i.e. the coating itself breaking), whilst at

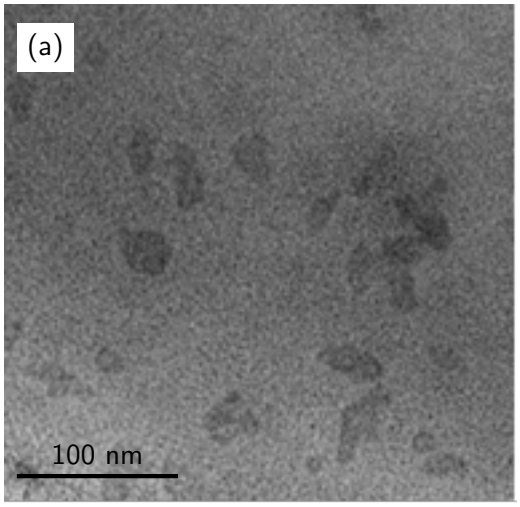

Figure 8.6: Transmission electron microscopy images for atomized spray plasma deposited poly(di(ethylene glycol) ethyl ether acrylate)–1 wt % silica.

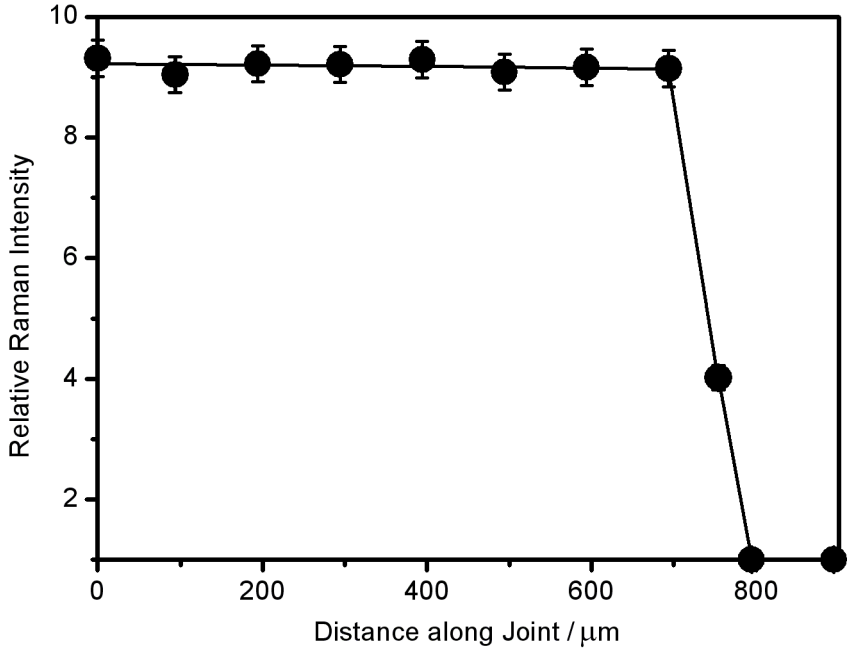

Figure 8.7: Raman intensity relative to background of the 900–950 cm^{-1} C−C skeletal stretch peaks versus the penetration distance of the atomized spray plasma deposited poly(2-hydroxyethyl methacrylate)–1 wt % silica coating for overlapping glass substrates.

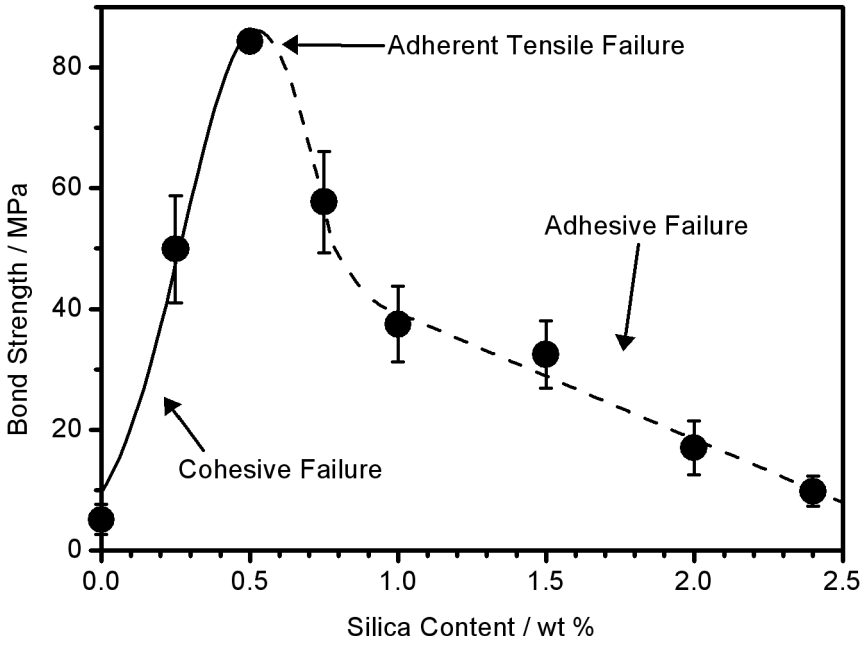

Figure 8.8: Shear bond strengths of atomized spray plasma deposited poly(2-hydroxyethyl methacrylate) bonded glass-glass overlap joints as a function of methacrylsilane treated silica nanoparticle loading. Solid line denotes cohesive failure and dashed line denotes adhesive failure.

higher silica content, the bond strength drops reaching 9.8 MPa at 2.4 wt % silica content, which is due to adhesive bond failure (i.e. the coating coming away from the glass-coating interface). This trend would be consistent with the methacryl modified silica particles acting as crosslinkers, which enhance the coating strength (i.e. a move from cohesive failure to adhesive failure—the coating coming away from the glass). Above 0.5 wt % silica content, the bond strength falls due to it becoming more difficult to form Si−O−C bonds between the hydroxyl groups present on the glass surface and those contained in the poly(2-hydroxyethyl methacrylate) coating via condensation reactions because the inherent bulk crosslinking causes a drop in polymer chain mobility.[62]

Shear moduli obtained from lap shear tests gave 0.35 GPa for atomized spray plasma deposited poly(2-hydroxyethyl methacrylate) coatings containing no silica, and the measured value rose linearly with silica content before levelling off at around 6 GPa for silica loading exceeding 1 wt %, Figure 8.9. This trend is also consistent with the methacryloyl modified silica particles inducing greater crosslinking within the films and therefore greater stiffness (shear modulus).

8.3.3 Lithium-Ion Conductivity of the Poly(Di(Ethylene Glycol) Ethyl Ether Acrylate)–Silica Nanocomposite Layers

The atomized spray plasma deposited nanocomposite layers showed lithium-ion conductivity at ambient temperature up to a value of 1.4×10^{-4} S cm^{-1} for the case of atomized spray plasma

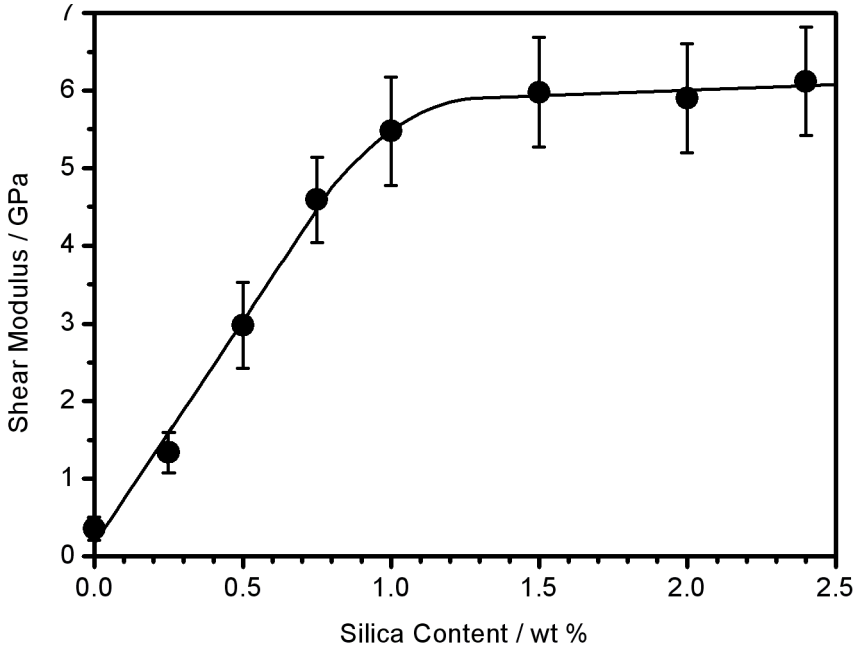

Figure 8.9: Shear moduli of atomized spray plasma deposited poly(2-hydroxyethyl methacrylate) onto glass-glass overlap joints as a function of methacrylsilane treated silica nanoparticle loading.

deposited 1 wt % silica in 10 wt % lithium perchlorate–di(ethylene glycol) ethyl ether acrylate, Figure 8.10. For the precursor mixtures with no silica, only that with 1 wt % lithium perchlorate showed lithium-ion conductivity. This is due to the 5 and 10 wt % lithium perchlorate/monomer precursor mixtures crystallizing at the tip of the ultrasonic nozzle, thus leading to limited deposition. This problem did not occur for the silica–lithium perchlorate–monomer precursor mixtures (attributed to the ceramic inhibiting crystallization). For all of the nanocomposite layers, the optimum silica content for lithium-ion conductivity was found to be 1 wt %. This can be attributed to two competing effects: firstly, addition of silica promotes amorphousness within the polymer which leads to increased ionic conductivity[35] (ethylene glycol-containing polymers without ceramic fillers tend to crystallize at temperatures below 70 °C[63]); secondly, the methacryloyl groups on the silica particles lead to crosslinking, which will limit polymer segmental motion thus reducing ionic conductivity. The precursor mixtures with 1 wt % silica therefore provide the crossover conditions of reduced regions of crystallinity combined with limited crosslinking for optimum lithium-ion conductivity given these two effects. The nanocomposite layers also showed increased peak lithium-ion conductivity with higher lithium perchlorate contents (up to a maximum at 10 wt %, which was the maximum amount of lithium perchlorate able to be dissolved into the precursor without the viscosity becoming too great for deposition).

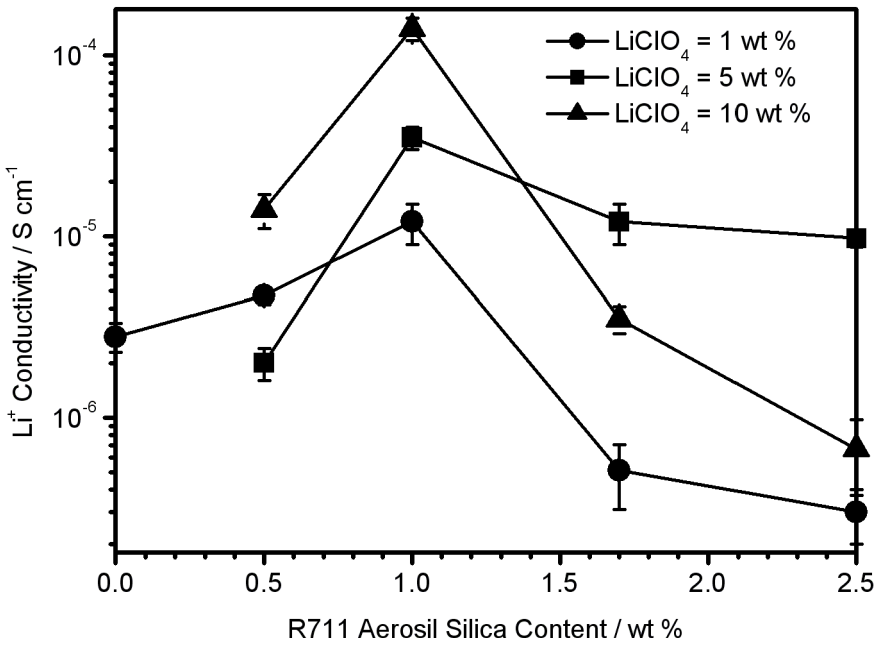

Figure 8.10: Lithium-ion conductivity of atomized spray plasma layers as a function of methacrylsilane modified silica nanoparticle content with different lithium perchlorate loadings.

8.4 Discussion

Previous approaches for preparing inorganic-polymer nanocomposites have entailed wet chemical syntheses, which involve multiple steps,[2] high temperatures[15] and normally require solvent extraction as well as a separate casting step.[44] In contrast, atomized spray plasma deposition (ASPD) utilizes a precursor-silica nanoparticle slurry mixture for a single-step direct application. An additional advantage of the atomized spray plasma is that deposition rates are vastly enhanced compared to conventional vapour-phase plasma polymerization (by a factor exceeding 250),[64] which is due to the high throughput of precursor delivery into the plasma zone.

The shear bond strength (84 MPa) of the optimum poly(2-hydroxyethyl methacrylate)–silica nanocomposite prepared in the present study by the atomized spray plasma deposition method exceeds those of conventional poly(2-hydroxyethyl methacrylate) based adhesives (10–45 MPa).[65] These high bond strengths for the ASPD nancomposite coating can be attributed to the poly(2-hydroxyethyl methacrylate) hydroxyl groups undergoing condensation reactions with glass surface hydroxyl groups to create Si−O−C bonds at the glass-coating interface.[62] In addition, the methacryloyl groups present on the silica particles help to enhance the adhesive bond strength by acting as crosslinkers within the bulk polymer thus raising its stiffness, which is confirmed by the increase in shear modulus of the coatings from 0.35 GPa to 6 GPa, Figure 8.9. These stiffness values are comparable to those reported previously for conventional poly(2-hydroxyethyl methacrylate) grafted from silica nanoparticles.[66]

Previous methods for the fabrication of poly(ethylene glycol)–ceramic nanocomposite coatings

have utilized alumina,[35,36] titanium dioxide[35] or silica[37] in order to introduce amorphousness and therefore improve lithium-ion conductivity. The atomized spray plasma deposited polymer–lithium perchlorate–silica coatings need much less silica by weight percentage than previous methods (i.e. 1 wt % optimum as compared to 5–10 wt %).[37] This can be attributed to the methacryloyl functionalization of the silica particles which are incorporated into the polymer chains thus inducing crosslinking which promotes amorphousness within the polymer nanocomposite layers. The values of lithium-ion conductivity reached with the atomized-spray-plasma deposited nanocomposite coatings described herein are comparable in magnitude to previous poly(ethylene glycol)–ceramic layers (i.e. 10^{-5}–10^{-3} S cm textsuperscript-1).[35–38]

The outlined atomized spray plasma deposition approach is capable of performing in-situ bonding at room temperature via penetration between overlapping substrates. This is far simpler and straightforward compared to existing methods for bonding glass or silicon (such as anodic bonding[67] requiring high substrate temperatures,[68] or the requirement for metallic interlayers[69]). Whilst previously reported nanocomposite fabrication methods may require multiple steps, removal of solvents or long processing times, atomized spray plasma deposition offers the advantages of being one-step, solventless, and yields large deposition rates. As a result, the use of the atomized spray plasma deposition method could be combined with industrial scale processes such as roll-to-roll to fabricate nanocomposite coatings with high throughputs onto electrochemical device components (e.g. carbon cloth or graphite).

The potential use of silica nanoparticles with acid-containing monomers to atomized-spray-plasma deposit robust, proton conducting films can now be envisaged. There are still some limitations experimentally, such as the requirement for silica particles to be well suspended within the liquid monomer. This suspension ability relies on the surface groups on the silica nanoparticle—for example, the methacrylsilane modified nanoparticles used in this chapter are only suspendable in methacrylate or acrylate precursors. However, when combined with the ability to concurrently dissolve salts (evidenced by lithium perchlorate in the current work), the dissolution of sulfonic acid containing monomer solids (e.g. sodium 4-styrenesulfonate) into an acrylate comonomer along with silica particles would render a coating with a combination of desirable properties.

8.5 Conclusions

Poly(2-hydroxyethyl methacrylate)–silica and poly(di(ethylene glycol) ethyl ether acrylate)–silica nanocomposite layers have been prepared by a single-step, solventless atomized spray plasma deposition process. For the former excellent adhesion and mechanical strength have been measured following in-situ application to overlapping joints and in the case of the latter, dissolution of lithium perchlorate into the precursor mixture yields coatings with significant lithium-ion conductivity at room temperature.

8.6 References

[1] Denizli, A.; Say, R.; Patır, S.; Arıca, M. Y. *React. Funct. Polym.* **2000**, *43*, 17.

[2] Hung, C.-H.; Whang, W.-T. *J. Mater. Chem.* **2005**, *15*, 267.

[3] Yu, Z.; Chen, L.; Chen, S. *J. Mater. Chem.* **2010**, *20*, 6182.

[4] (a) Stupp, S. I.; Braun, P. V. *Science* **1997**, *277*, 1242; (b) Song, J.; Saiz, E.; Bertozzi, C. R. *J. Am. Chem. Soc.* **2003**, *125*, 1236; (c) Song, J.; Malathong, V.; Bertozzi, C. R. *J. Am. Chem. Soc.* **2005**, *127*, 3366.

[5] (a) von Werne, T. A.; Germack, D. S.; Hagberg, E. C.; Sheares, V. V.; Hawker, C. J.; Carter, K. R. *J. Am. Chem. Soc.* **2003**, *125*, 3831; (b) Moran, I. W.; Briseno, A. L.; Loser, S.; Carter, K. R. *Chem. Mater.* **2008**, *20*, 4595.

[6] Bin Hasan Susan, M. A.; Kaneko, T.; Noda, A.; Watanabe, M. *J. Am. Chem. Soc.* **2005**, *127*, 4976.

[7] Heredia, K. L.; Bontempo, D.; Ly, T.; Byers, J. T.; Halstenberg, S.; Maynard, H. D. *J. Am. Chem. Soc.* **2005**, *127*, 16955.

[8] (a) Folkman, J.; Moscona, A. *Nature* **1978**, *273*, 345; (b) Schafer, Z. T.; Grassian, A. R.; Song, L.; Jiang, Z.; Gerhart-Hines, Z.; Irie, H. Y.; Gao, S.; Puigserver, P.; Brugge, J. S. *Nature* **2009**, *461*, 109; (c) Villa-Diaz, L. G.; Nandivada, H.; Ding, J.; Nogueira-de Souza, N. C.; Krebsbach, P. H.; O'Shea, K. S.; Lahann, J.; Smith, G. D. *Nat. Biotechnol.* **2010**, *28*, 581.

[9] Chung, M.-H.; Chen, C.-M.; Hsieh, T.-E.; Tang, R.-M.; Tsai, Y. S.; Chu, W.-P.; Liu, M. O.; Juang, F.-S. *Jpn. J. Appl. Phys.* **2009**, *48*, 04C177.

[10] Smetana, K.; Sulc, J.; Krcova, Z.; Pitrova, S. *J. Biomed. Mater. Res.* **1987**, *21*, 1247.

[11] Di Renzo, M.; Ellis, T. H.; Domingue, A.; Bertrand, L.; Sacher, E.; Stangel, I. *J. Adhes.* **1994**, *47*, 115.

[12] Young, A. M.; Ho, S. M.; Abou Neel, E. A.; Ahmed, I.; Barralet, J. E.; Knowles, J. C.; Nazhat, S. N. *Acta Biomater.* **2009**, *5*, 2072.

[13] Guvendiren, M.; Heiney, P. A.; Yang, S. *Macromolecules* **2009**, *42*, 6606.

[14] Ji, X. L.; Jiang, X. P.; Diu, X. P.; Dong, D. W.; Yu, D. H.; Jiang, B. Z. *J. Appl. Polym. Sci.* **2003**, *88*, 3168.

[15] Li, S.; Shah, A.; Hsieh, A. J.; Haghighat, R.; Praveen, S. S.; Mukherjee, I.; Wei, E.; Zhang, Z.; Wei, Y. *Polymer* **2007**, *48*, 3982.

[16] Costantini, A.; Luciani, G.; Silvestri, B.; Tescione, F.; Branda, F. *J. Biomed. Mater. Res., Part B* **2008**, *86B*, 98.

[17] Lavielle, L.; Turck, C.; Lougnot, D.-J. *J. Phys. Chem. B* **1998**, *102*, 7714.

[18] Miao, W.; Halloran, J. W.; Brei, D. E. *J. Mater. Sci.* **2007**, *42*, 8311.

[19] Wang, Q.; Mynar, J. L.; Yoshida, M.; Lee, E.; Lee, M.; Okuro, K.; Kinbara, K.; Aida, T. *Nature* **2010**, *463*, 339.

[20] Gulcev, M. D.; Goring, G. L. G.; Rakic, M.; Brennan, J. D. *Anal. Chim. Acta* **2002**, *457*, 47.

[21] Chandra, S.; Barola, N.; Bahadur, D. *Chem. Commun.* **2011**, *47*, 11258.

[22] Jirimali, H. D.; Nagarale, R. K.; Lee, J. M.; Saravanakumar, D.; Shin, W. *Electroanalysis* **2011**, *23*, 2109.

[23] (a) Liu, Z.; Robinson, J. T.; Sun, X.; Dai, H. *J. Am. Chem. Soc.* **2008**, *130*, 10876; (b) Lee, J. E.; Lee, N.; Kim, H.; Kim, J.; Choi, S. H.; Kim, J. H.; Kim, T.; Song, I. C.; Park, S. P.; Moon, W. K.; Hyeon, T. *J. Am. Chem. Soc.* **2010**, *132*, 552.

[24] Chandra, S.; Dietrich, S.; Lang, H.; Bahadur, D. *J. Mater. Chem.* **2011**, *21*, 5729.

[25] Honma, I.; Takeda, Y.; Bae, J. M. *Solid State Ionics* **1999**, *120*, 255.

[26] Chang, H. Y.; Lin, C. W. *J. Membr. Sci.* **2003**, *218*, 295.

[27] Pek, Y. S.; Wan, A. C. A.; Shekaran, A.; Zhuo, L.; Ying, J. Y. *Nat. Nanotechnol.* **2008**, *3*, 671.

[28] (a) Lim, Y. T.; Noh, Y.-W.; Cho, J.-H.; Han, J. H.; Choi, B. S.; Kwon, J.; Hong, K. S.; Gokarna, A.; Cho, Y.-H.; Chung, B. H. *J. Am. Chem. Soc.* **2009**, *131*, 17145; (b) Chan, Y.-S.; Ye, F.; Gallina, M. E.; Zhang, X.; Jin, Y.; Wu, I.-C.; Chiu, D. T. *J. Am. Chem. Soc.* **2012**, *134*, 7309.

[29] (a) Ji, X.; Shao, R.; Elliott, A. M.; Stafford, R. J.; Esparza-Coss, E.; Bankson, J. A.; Liang, G.; Luo, Z.-P.; Park, K.; Markert, J. T.; Li, C. *J. Phys. Chem. C* **2007**, *111*, 6245; (b) Wang, X.; Wang, C.; Cheng, L.; Lee, S.-T.; Liu, Z. *J. Am. Chem. Soc.* **2012**, *134*, 7414.

[30] Ma, G.; Yang, D.; Li, Q.; Wang, K.; Chen, B.; Kennedy, J. F.; Nie, J. *Carbohydr. Polym.* **2010**, *79*, 620.

[31] Arif Sher Shah, M. S.; Nag, M.; Kalagara, T.; Singh, S.; Manorama, S. V. *Chem. Mater.* **2008**, *20*, 2455.

[32] Chen, Q.; Yue, L.; Xie, F.; Zhou, M.; Fu, Y.; Zhang, Y.; Weng, J. *J. Phys. Chem. C* **2008**, *112*, 10004.

[33] (a) Patel, N. P.; Miller, A. C.; Spontak, R. J. *Adv. Mater.* **2003**, *15*, 729; (b) Shao, L.; Chung, T.-S. *Int. J. Hydrogen Energy* **2009**, *34*, 6492.

[34] Xiao-e, L.; Green, A. N. M.; Haque, S. A.; Mills, A.; Durrant, J. R. *J. Photochem. Photobiol., A* **2004**, *162*, 253.

[35] Croce, F.; Curini, R.; Martinelli, A.; Persi, L.; Ronci, F.; Scrosati, B.; Caminiti, R. *J. Phys. Chem. B* **1999**, *103*, 10632.

[36] Marcinek, M.; Bac, A.; Lipka, P.; Zalewska, A.; Żukowska, G.; Borkowska, R.; Wieczorek, W. *J. Phys. Chem. B* **2000**, *104*, 11088.

[37] Świerczyński, D.; Zalewska, A.; Wieczorek, W. *Chem. Mater.* **2001**, *13*, 1560.

[38] Chinnam, P. R.; Wunder, S. L. *Chem. Mater.* **2011**, *23*, 5111.

[39] Weston, J. E.; Steele, B. C. H. *Solid State Ionics* **1982**, *7*, 75.

[40] (a) Croce, F.; Scrosati, B. *J. Power Sources* **1993**, *43*, 9; (b) Peled, E.; Golodnitsky, D.; Ardel, G.; Eshkenazy, V. *Electrochim. Acta* **1995**, *40*, 2197.

[41] Xiang, Y.; Peng, Z.; Chen, D. *Eur. Polym. J.* **2006**, *42*, 2125.

[42] (a) Bosch, P.; Del Monte, F.; Mateo, J. L.; Levy, D. *J. Polym. Sci., Part A: Polym. Chem.* **1996**, *34*, 3289; (b) Liu, Y.-Y.; Liu, D.-M.; Chen, S.-Y.; Tung, T.-H.; Liu, T.-Y. *Acta Biomater.* **2008**, *4*, 2052.

[43] Du, Y.-Z.; Tomohiro, T.; Kodaka, M. *Macromolecules* **2004**, *37*, 803.

[44] Cao, Z.; Walter, C.; Landfester, K.; Wu, Z.; Ziener, U. *Langmuir* **2011**, *27*, 9849.

[45] Sun, L.; Dai, J.; Baker, G. L.; Bruening, M. L. *Chem. Mater.* **2006**, *18*, 4033.

[46] Oral, A.; Shahwan, T.; Güler, c. *J. Mater. Res.* **2008**, *23*, 3316.

[47] Gröhn, F.; Kim, G.; Bauer, B. J.; Amis, E. J. *Macromolecules* **2001**, *34*, 2179.

[48] Xiang, Y.; Chen, D. *Eur. Polym. J.* **2007**, *43*, 4178.

[49] Benlikaya, R.; Alkan, M.; Kaya, I. *Polym. Compos.* **2009**, *30*, 1585.

[50] (a) Barichard, A.; Galstian, T.; Israeli, Y. *J. Phys. Chem. B* **2010**, *114*, 14807; (b) Barichard, A.; Galstian, T.; Israeli, Y. *Phys. Chem. Chem. Phys.* **2012**, *14*, 8208.

[51] Dietrich, S.; Schulze, S.; Hietschold, M.; Lang, H. *J. Colloid Interface Sci.* **2011**, *359*, 454.

[52] Yasuda, H. *Plasma Polymerization*; Academic Press: New York, 1985.

[53] Ryan, M. E.; Hynes, A. M.; Badyal, J. P. S. *Chem. Mater.* **1996**, *8*, 37.

[54] Friedrich, J. *Plasma Processes Polym.* **2011**, *8*, 783.

[55] Ward, L. J.; Schofield, W. C. E.; Badyal, J. P. S.; Goodwin, A. J.; Merlin, P. J. *Chem. Mater.* **2003**, *15*, 1466.

[56] Ward, L. J.; Schofield, W. C. E.; Badyal, J. P. S.; Goodwin, A. J.; Merlin, P. J. *Langmuir* **2003**, *19*, 2110.

[57] Morgan, W. E.; Van Wazer, J. R.; Stec, W. J. *J. Am. Chem. Soc.* **1973**, *95*, 751.

[58] Lin-Vien, D.; Colthup, N. B.; Fateley, W. G.; Grasselli, J. G. *The Handbook of Infrared and Raman Characteristic Frequencies of Organic Molecules*; Academic Press: London, U.K., 1991.

[59] Klasson, M.; Hedman, J.; Berndtsson, A.; Nilsson, R.; Nordling, C.; Melnik, P. *Phys. Scr.* **1972**, *5*, 93.

[60] Kumar, T. *Analyst* **1990**, *115*, 1597.

[61] Cohn, H. *J. Chem. Soc.* **1952**, 4282.

[62] Xu, P.; Wang, H.; Tong, R.; Iv, R.; Shen, Y.; Du, Q.; Zhong, W. *Polym. Degrad. Stab.* **2006**, *91*, 1522.

[63] Gray, F. M. *Solid Polymer Electrolytes—Fundamentals and Technical Applications*; VCH: Wenheim, Germany, 1991.

[64] Tarducci, C.; Schofield, W. C. E.; Badyal, J. P. S.; Brewer, S. A.; Willis, C. *Chem. Mater.* **2002**, *14*, 2541.

[65] (a) Stackhouse, J., J. A.; Kristol, D. S.; Von Hagen, S.; Rao, G. *J. Biomed. Mater. Res.* **1989**, *23*, 81; (b) Chigira, H.; Koike, T.; Hasegawa, T.; Itoh, K.; Wakumoto, S.; Hayakawa, T. *Dent. Mater. J.* **1989**, *8*, 86; (c) Causton, B.; Sefton, J. *Br. Dent. J.* **1989**, *167*, 308; (d) Perdigao, J.; Swift, J., E. J.; Heymann, H. O.; Malek, M. A. *Am. J. Dent.* **1998**, *11*, 207; (e) Chappelow, C. C.; Power, M. D.; Bowles, C. Q.; Miller, R. G.; Pinzino, C. S.; Eick, J. D. *Dent. Mater.* **2000**, *16*, 396; (f) Hussain, L. A.; Dickens, S. H.; Bowen, R. L. *Biomaterials* **2005**, *26*, 3973; (g) Walter, R.; Swift, J., Edward J.; Ritter, A. V.; Bartholomew, W. W.; Gibson, C. G. *Am. J. Dent.* **2009**, *22*, 215.

[66] Kaddami, H.; Gerard, J. F.; Hajji, P.; Pascault, J. P. *J. Appl. Polym. Sci.* **1999**, *73*, 2701.

[67] Pomerantz, D. I. U.S. Patent No. 3,397,278, 1968.

[68] Anthony, T. R. *J. Appl. Phys.* **1985**, *58*, 1240.

[69] Lang, J., G. F. U.S. Patent No. 3,316,628, 1967.

Chapter 9

Atomized Spray Deposition of Conducting Polymer Layers

9.1 Introduction

Throughout this thesis, the aim has been to realise a proton exchange membrane fuel cell which could be manufactured entirely by vapour-phase deposition techniques because of the advantages that would bring (controllable thickness, no requirements for solvents etc.). The plasmachemical vapour-phase deposition of proton exchange membranes and catalytic nanocomposite layers has been investigated, but there is still the question of the fuel cell electrodes themselves. The atomized spray deposition technique outlined in the previous two chapters enables the introduction of a large quantity of monomer into the reactor chamber. Thus far, the polymerization reactions used have used conventional monomers with carbon-carbon double bonds. In this chapter, however, the use of a monomer with no polymerizable carbon-carbon double bond is used. The method of polymerization is via oxidation of a thiophene ring in order to form an electronically conducting poly(thiophene) coating. The atomized spray is necessary in order to maximise the monomer input, but in this case the initiation is provided not by plasma but by an oxidising agent

Poly(3,4-ethylenedioxythiophene) (PEDOT) is an intrinsically conducting polymer which has found use in many applications including dye-sensitized solar cells,[1,2] supercapacitors,[3] light emitting diodes,[4] thin film transistors,[5] oxygen reduction catalysts,[6] photodetectors,[7] molecular wires,[8] memory storage[9] and antistatic coatings.[10]

Previous methods for the manufacture of PEDOT coatings have entailed photoelectrochemical deposition,[1] electropolymerization,[11] oxidative polymerization,[12] oxidative chemical vapour deposition,[13–15] vapour-phase polymerization,[6,16] emulsion polymerization[17] and suspension polymerization.[18] However, these approaches suffer from drawbacks such as the need of additional steps to remove solvents[12] and byproducts[6] and the requirement for conducting substrates[1] or high temperatures.[14,19]

In this chapter the use of an atomized spray precursor delivery system is described to deposit

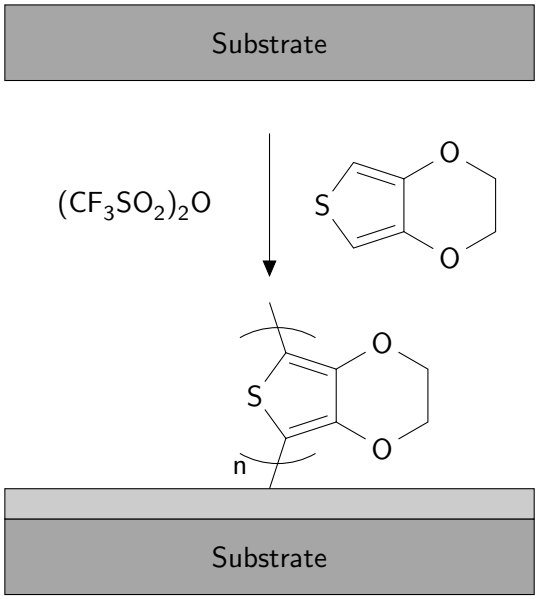

Scheme 9.1: Atomized spray deposition of PEDOT layers using EDOT precursor in the presence of triflic anhydride vapour.

PEDOT layers in the presence of triflic anhydride vapour, which acts as an oxidant in the following reaction, Scheme 9.1:[20]

$$2\,\mathrm{EDOT} + (CF_3SO_2)_2O \longrightarrow \mathrm{EDOT{-}EDOT} + CF_3SO_2H + CF_3SO_3H \qquad (9.1)$$

The oxidation of the EDOT monomer gives rise to polymerization, whereas the triflic anhydride is reduced to become triflic and triflinic acid. Since the deposition is carried out under vacuum, the triflic and triflinic acid moieties are removed due to their significant vapour pressures, which results in no acid damage to the growing polymer chain. As in other oxidation polymerizations for EDOT,[6,14,19] partial doping occurs in the form of remaining oxidant (triflate) anions. After the reaction is completed, any remaining reactant (either EDOT or triflic anhydride) is pumped away by the system.

9.2 Experimental

9.2.1 Atomized Spray Deposition of PEDOT Layers

Atomized spray deposition was carried out in an electrodeless, cylindrical, T-shape, glass reactor (volume 820 cm^3, base pressure of 3 x 10^{-3} mbar, and with a leak rate better than 2 x 10^{-9} mol s^{-1}). The chamber was pumped down using a 30 L min^{-1} rotary pump attached to a liquid nitrogen cold trap and a Pirani gauge was used to monitor system pressure. Prior to each deposition, the reactor was scrubbed using detergent, rinsed in propan-2-ol, and dried in an oven. Substrates used for coating were silicon (100) wafer pieces (Silicon Valley Microelectronics Inc.) and borosilicate

glass microscrope slide pieces (Smith Scientific Ltd.) with two evaporated gold electrodes (3 mm length, 1.5 mm width, separated by 1.5 mm). They were placed downstream from the atomizer nozzle (Model no. 8700-120, Sono Tek Corp.). 3,4-Ethylenedioxythiophene (+98%, TCI Europe NV) and triflic anhydride (+99%, Apollo Scientific Ltd.) were loaded into separate sealable glass tubes and degassed using several freeze-pump-thaw cycles. 3,4-Ethylenedioxythiophene precursor was then introduced into the reactor at a flow rate of 0.02 mL s^{-1} through the ultrasonic nozzle operating at 120 kHz, while triflic anhydride vapour was concurrently introduced via a leak valve at a pressure of 6 mbar. After deposition had occurred triflic anhydride vapour was allowed to pass through the system for a further 3 mins before subsequent evacuation to base pressure and venting to atmosphere.

9.2.2 Film Characterization

Surface elemental compositions were determined by X-ray photoelectron spectroscopy as described in section 2.2 (page 28). Experimental instrument sensitivity (multiplication) factors were C(1s): O(1s): S(2p): F(1s) equals 1.00: 0.36: 0.59: 0.24.

Infrared spectra were acquired using a FTIR spectrometer (Perkin-Elmer Spectrum One) fitted with a liquid nitrogen cooled MCT detector as described in section 2.3 (page 31).

Film thicknesses were measured by freezing coated silicon samples in liquid nitrogen followed by snapping to reveal a cross-section. These were then imaged using an optical microscope (Olympus BX40) fitted with a x20 magnification lens.

Electrical conductivity values were determined for the coated glass substrates by measuring the variation in electrical current across the 0–30 V range (Keithley 2400 SourceMeter) and applying the formula $\sigma = \frac{l}{R_S A}$, where σ is the conductivity, l is the separation of the electrodes, R_S is the resistance of the substrate/coating, and A is the cross-sectional area of the film being sampled.

9.3 Results

A lack of any XPS Si(2p) signal confirmed complete coverage of the substrates by the atomized spray deposition process, Table 9.1. The S(2p) spectrum contains two components corresponding to the thiophene ring C−S (163.7 eV)[21] and triflate SO_3CF_3 (168.3 eV),[22] Figure 9.1. The ratio of the areas of the S(2p) component peaks correspond to around one triflate or triflinate ion to every four EDOT monomer units. This ratio is confirmed by the presence of the F(1s) peak and corresponding adjustments in elemental XPS ratios of the atomized spray deposited PEDOT as compared to the theoretical (non-doped) polymer, Table 9.1.

Fourier transform infrared spectra of the EDOT monomer lead to the following absorbances being assigned:[23,24] =C−H ring stretch (3107 cm^{-1}), antisymmetric CH_2 stretch (2919 cm^{-1}), symmetric CH_2 stretch (2869 cm^{-1}), C=C aromatic out of phase stretch (1479 cm^{-1}), C=C aromatic in phase stretch (1444 cm^{-1}) and C−C deformation (1369 cm^{-1}), Figure 9.2. In the case

Layer	%C	%O	%S	%F
Theoretical PEDOT (undoped)	67	22	11	—
Atomized spray deposited PEDOT–triflic anhydride	54±1	24±1	11±1	11±1

Table 9.1: XPS elemental ratios for atomized spray deposited EDOT in the presence of triflic anhydride vapour.

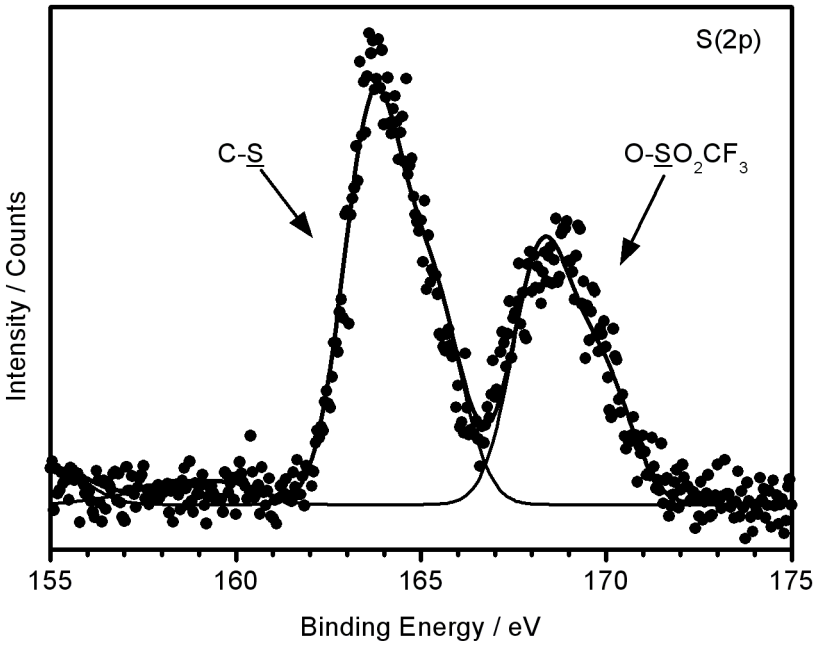

Figure 9.1: X-ray photoelectron S(2p) spectrum of atomized spray deposited PEDOT–triflic anhydride.

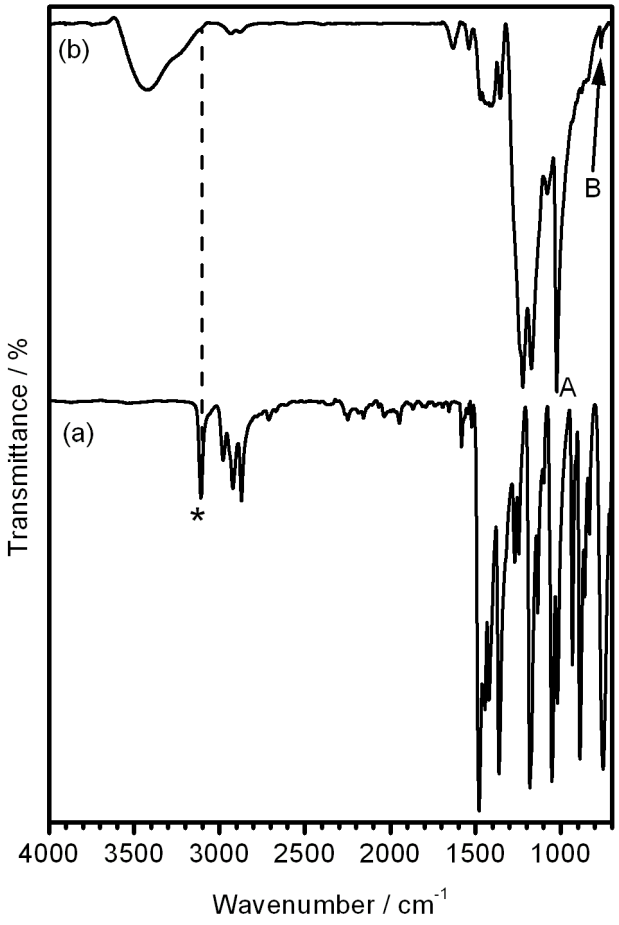

Figure 9.2: FTIR spectra of: (a) EDOT monomer and (b) atomized spray deposited PEDOT–triflic anhydride. * Denotes $=C-H$ ring stretch; A denotes SO_3 symmetric stretch; B denotes CF_3 symmetric stretch.

of the atomized spray deposited PEDOT–triflic anhydride coating: the $=C-H$ ring stretch has disappeared (which is consistent with polymerization via the 2-position on the thiophene ring); the CH_2 stretches remain confirming retention of the ethylenedioxy substituent; absorbances due to aromatic vibrations in the fingerprint region broaden out (which is consistent with a doped conjugated polymer system[25]); and absorbances due to triflate SO_3 symmetric stretch (1083 cm^{-1}, denoted A) and CF_3 symmetric stretch (762 cm^{-1}, denoted B) appear.[26]

Deposition rates for the atomized spray deposition of PEDOT–triflic anhydride films were measured to be 2.9 ± 0.4 μm min^{-1}.

Conductivity measurements for the atomized spray deposited PEDOT–triflic anhydride layers gave a value of 0.9 S cm^{-1} in conjunction with an ohmic response across the 0–30 V range.

9.4 Discussion

Previous vapour-phase deposition approaches for the polymerization of EDOT have utilized oxidants such as iron(III) chloride or iron(III) tosylate which require an extra washing step to remove the unwanted iron(II) salt byproduct.[6,14] Another approach is to use bromine vapour as the oxidant which alleviates the need for a washing step but still requires the monomer to be heated due to its low vapour pressure at room temperature.[19] In contrast the outlined atomized spray deposition approach requires no post-deposition washing step since any unwanted byproducts (triflic acid or triflinic acid) are pumped off, and there is no requirement for heating the monomer since it is introduced as a fine mist of droplets into the reactor. Therefore this approach is completely solventless and requires only ambient temperatures. This is the first time that triflic anhydride has been used as an oxidant for the vapour-phase production of conducting polymers. The conductivity of the films thus produced reaches a value of 0.9 S cm^{-1} which is high enough for use as an antistatic coating[27] or in electrochemical devices, such as capacitor electrodes.[28]

The ultrasonic nozzle provides small droplets (20 microns average diameter) of 3,4-ethylenedioxythiophene monomer into the reactor chamber (similar to previous chapters). In this case, however, there is not plasma to initiate reaction on the droplet surface but triflic anhydride vapour. Via a similar method to ASPD, therefore, the polymerization reaction is initiated at the droplet surface and carries on even after impact of the droplet onto the surface.

Vapour-phase depositions of many different conducting polymers could be envisaged via this oxidative vapour-phase polymerization mechanism. Monomer examples could also include pyrrole and aniline based compounds as well as thiophene. The use of conducting polymers as electrodes for fuel cells is particularly apt since not only do they provide electronic conductivity, but the dopant cation can provide proton conductivity (triflate is essentially the conjugate base of a strong acid and so is suited to this task). Additional to both of these properties, if the conducting polymer chain is very long then catalytic properties can emerge.[6] This atomized spray oxidative vapour deposition polymerization process could thus be used to not only produce electrodes for fuel cells but catalytic layers as well (after further optimization of parameters such as substrate temperature etc.).

The outlined atomized spray deposition approach can be used in conjunction with scalable processes such as roll-to-roll in order to yield high throughput, conformal, conductive polymer coatings.

9.5 Conclusions

The atomized spray deposition process provides a room temperature, solventless approach for production of conducting PEDOT–triflic anhydride coatings with no requirement for post-deposition steps.

9.6 References

[1] (a) Xia, J.; Masaki, N.; Lira-Cantu, M.; Kim, Y.; Jiang, K.; Yanagida, S. *J. Am. Chem. Soc.* **2008**, *130*, 1258; (b) Mozer, A. J.; Panda, D. K.; Gambhir, S.; Winther-Jensen, B.; Wallace, G. G. *J. Am. Chem. Soc.* **2010**, *132*, 9543.

[2] Tian, H.; Yu, Z.; Hagfeldt, A.; Kloo, L.; Sun, L. *J. Am. Chem. Soc.* **2011**, *133*, 9413.

[3] Liu, R.; Lee, S. B. *J. Am. Chem. Soc.* **2008**, *130*, 2942.

[4] Yan, H.; Lee, P.; Armstrong, N. R.; Graham, A.; Evmenenko, G. A.; Dutta, P.; Marks, T. J. *J. Am. Chem. Soc.* **2005**, *127*, 3172.

[5] Briseno, A. L.; Roberts, M.; Ling, M.-M.; Moon, H.; Nemanick, E. J.; Bao, Z. *J. Am. Chem. Soc.* **2006**, *128*, 3880.

[6] Winther-Jensen, B.; Winther-Jensen, O.; Forsyth, M.; MacFarlane, D. R. *Science* **2008**, *321*, 671.

[7] Gong, X.; Tong, M.; Xia, Y.; Cai, W.; Moon, J. S.; Cao, Y.; Yu, G.; Shieh, C.-L.; Nilsson, B.; Heeger, A. J. *Science* **2009**, *325*, 1665.

[8] Akkerman, H. B.; Blom, P. W. M.; de Leeuw, D. M.; de Boer, B. *Nature* **2006**, *441*, 69.

[9] Möller, S.; Perlov, C.; Jackson, W.; Taussig, C.; Forrest, S. R. *Nature* **2003**, *426*, 166.

[10] Jonas, F.; Morrison, J. T. *Synth. Met.* **1997**, *85*, 1397.

[11] (a) Randriamahazaka, H.; Noël, V.; Chevrot, C. *J. Electroanal. Chem.* **1999**, *472*, 103; (b) Du, X.; Wang, Z. *Electrochim. Acta* **2003**, *48*, 1713; (c) Liu, K.; Hu, Z.; Xue, R.; Zhang, J.; Zhu, J. *J. Power Sources* **2008**, *179*, 858.

[12] Kim, T. Y.; Park, C. M.; Kim, J. E.; Suh, K. S. *Synth. Met.* **2005**, *149*, 169.

[13] Lock, J. P.; Im, S. G.; Gleason, K. K. *Macromolecules* **2006**, *39*, 5326.

[14] Im, S. G.; Gleason, K. K. *Macromolecules* **2007**, *40*, 6552.

[15] Im, S. G.; Olivetti, E. A.; Gleason, K. K. *Appl. Phys. Lett.* **2007**, *90*, 152112.

[16] Winther-Jensen, B.; West, K. *Macromolecules* **2004**, *37*, 4538.

[17] (a) Kudoh, Y.; Akami, K.; Matsuya, Y. *Synth. Met.* **1998**, *98*, 65; (b) Lei, Y.; Oohata, H.; Kuroda, S.-I.; Sasaki, S.; Yamamoto, T. *Synth. Met.* **2005**, *149*, 211.

[18] Arbizzani, C.; Mastragostino, M.; Rossi, M. *Electrochem. Commun.* **2002**, *4*, 545.

[19] Chelawat, H.; Vaddiraju, S.; Gleason, K. K. *Chem. Mater.* **2010**, *22*, 2864.

[20] Maas, G.; Stang, P. J. *J. Org. Chem.* **1981**, *46*, 1606.

[21] Lindberg, B. J.; Hamrin, K.; Johansson, G.; Gelius, V.; Fahlman, A.; Nordling, C.; Siegbahn, K. *Phys. Scr.* **1970**, *1*, 286.

[22] Pârvulescu, A. N.; Gagea, B. C.; Pârvulescu, V.; Pârvulescu, V. I.; Poncelet, G.; Grange, P. *Catal. Today* **2002**, *73*, 177.

[23] Tran-Van, F.; Garreau, S.; Louarn, G.; Froyer, G.; Chevrot, C. *J. Mater. Chem.* **2001**, *11*, 1378.

[24] Lin-Vien, D.; Colthup, N. B.; Fateley, W. G.; Grasselli, J. G. *The Handbook of Infrared and Raman Characteristic Frequencies of Organic Molecules*; Academic Press: London, U.K., 1991.

[25] Yamamoto, T.; Alba, M. *Synth. Met.* **1999**, *100*, 237.

[26] Gejji, S. P.; Hermansson, K.; Lindgren, J. *J. Phys. Chem.* **1993**, *97*, 3712.

[27] (a) Matsuda, H.; Itou, T. U.S. Patent No. 4,785,217, 1988; (b) Clatanoff, W. J.; Chamberlain, C. S. U.S. Patent No. 5,409,968, 1995.

[28] Kirchmeyer, S.; Reuter, K. *J. Mater. Chem.* **2005**, *15*, 2077.

Chapter 10

Conclusions and Further Work

10.1 Conclusions

Plasmachemical deposition is a powerful technique for the manufacture of functional thin films. Pulsing the plasma yields a controllable polymerization process, which in turn leads to high levels of chemical functionality retention throughout the films. Chapters 3–4 used these properties in order to manufacture proton conducting films from carboxylic anhydride precursors. Maleic anhydride based monomers were particularly effective due to the polymerizable double bond and the fact that they could be hydrated simply to produce acid-containing films. Polymers which have a high density of carboxylic acids tend to absorb a large amount of water (e.g. poly(acrylic acid) based super absorbent polymers) or even dissolve under aqueous conditions. The use of a plasma to initiate polymerization bypassed this problem by ensuring a high enough level of crosslinking within the poly(anhydride) films to render them insoluble. The addition of a trifluoromethyl group to the maleic anhydride precursor further optimized the process, providing greater hydrophobicity (and subsequent stability in water), aiding the stabilization of radicals within the plasma (leading to faster deposition and better structural retention) and making the acid group stronger (i.e. a more labile oxygen-hydrogen bond). It was shown that during the plasmachemical deposition process radicals are temporarily trapped within the growing polymer film. These radicals were used for the graft-from polymerization reactions of a sulfonate salt monomer, which was then converted to acid form by ion exchange (washing in dilute acid). Both plasmachemically deposited film with and without the grafted sulfonic acid showed excellent proton conductivity, with the latter exceeding that of the industry benchmark, Nafion.

Membranes that did not require water for their conduction mechanism were manufactured in chapter 5. It was shown that using an imidazole-containing monomer for pulsed plasmachemical deposition yielded films which, upon quaternization in the vapour phase, showed excellent ion conduction above 90 °C. Doping with acids would render these poly(ionic liquid) films able to conduct protons in the intermediate temperature range (100–200 °C for fuel cells).

In chapter 6 the focus moved to plasmachemical deposition of metal-containing nanocomposite

layers for use as catalytic layers in proton exchange membrane fuel cells. The twin requirements of proton conduction and electronic conduction were met in the platinum-containing film (the copper-containing film was able to conduct protons but not electrons due to its lower metal content). Combining these properties with the known catalytic ability of platinum nanoparticles and plasmachemical deposition has produced a viable candidate for fuel cell catalyst layers.

In chapters 7–8 the limitations of vapour phase plasma polymerization were addressed—to whit, the low deposition rates and the requirement for a precursor with sufficient vapour pressure. Both these were overcome by the use of an ultrasonic nozzle to introduce a higher quantity of monomer into the reactor in the form of a fine mist. Proof of concept was provided by deposition of lipophilic poly(alkyl acrylate) layers along with protein resistant poly(*N*-acryloylsarcosine methyl ester) films. The deposition rates for these films were in the order of 0.1–3 μm min^{-1} which represented a large increase over the 3–6 nm min^{-1} rates for conventional pulsed plasmachemical deposition in chapters 3–4. The atomized spray plasma deposition was further used for the deposition of nanocomposite polymer-silica layers, the silica nanoparticles serving to improve mechanical properties. Both higher depsition rate and the ability to deposite nanocomposite coatings from a premixed precursor would be desirable for the plasmachemical deposition of fuel cell layers.

Finally in chapter 9, the atomized spray process is used in combination with oxidant vapour (rather than plasma excitation) in order to fabricate conducting polymer coatings. These coatings show enough electrical conductivity to be used as electrochemical device electrodes (e.g. for fuel cell cathode and anode).

Overall, vapour-phase deposition processes (especially those that are plasma-initiated) have proved an effective means for fabricating parts of proton exchange membranes, including the proton exchange membrane, the catalytic layers and the electrodes. Use of an atomized precursor spray in conjunction provides greater scope for advancement of these techniques (as shown by the proof-of-concept coatings of chapters 7–8).

10.2 Further Work

Fuel cells represent harsh environments for polymer layers to survive with acidic conditions, high temperatures, strong reductants/oxidants and mechanical stress from swelling and contracting due to water uptake and loss. For proton exchange membrane fuel cells to become viable alternatives to current technology for portable applications (i.e. the combustion engine for vehicles and the lithium-ion battery for portable electronics) the proton exchange membranes themselves need to be cheap to manufacture, highly proton conducting and robust (that is, having long lifetimes). The most obvious future work arising out of chapters 3–4, therefore, is the testing of the anhdyride-containing polymer coatings in a fuel cell. Even if the results of such tests were negative, however, there are other applications for acid-containing polymer coatings, such as for humidity sensors or ion exchange materials (indeed, not included within this thesis, a study into the ion exchange

properties of the anhydride coatings was carried out with the suprising result of the coatings absorbing heavy metals such as cadmium and zinc selectively over the alkali and alkaline earth metals).

Further work is warranted into the poly(ionic liquid)s (chapter 5), which showed high ionic conductivity. Rather than changing the monomer (which was done with no further success), a study into the quaternization agents (e.g. the effect of alkyl chain length with different bromoalkanes on ionic conductivity) as well as investigation into how the degree of quaternization would affect ionic conductivity (one would expect an optimum level significantly below 100% which would unduly increase the chances of ion-ion pairs forming).

The work in chapter 6 on metal-containing nanocomposite layers represents an exciting new area to be developed. The only previous metal-containing nanocomposite layers formed by this method were zinc oxide nanoparticles in an organic matrix that disintegrated in water. By contrast the chemical functionality of the organic matrix in this thesis was an important boon to the usefulness of the nanocomposites. Platinum precursors, however, are expensive (platinum(II) hexafluoroacetylacetonate was bought at a cost of greater than £300 per gram). Therefore, cheaper precursors need to be investigated, or perhaps the mixing of precursor vapours in order to create core-shell nanoparticles.

The greatest scope for advancement of vapour-phase deposition of functional coatings lies in the atomized spray plasma deposition setup. From the examples presented in this thesis we can separate out five main areas of research. They comprise (i) the use of pure monomer (e.g. poly(*N*-acryloylsarcosine methyl ester) in chapter 7); (ii) the use of premixed monomers to form copolymers (e.g. poly(octadecyl-co-dodecyl acrylate) in chapter 7); (iii) the suspension of premade nanoparticles in a monomer to form an polymer-inorganic nanocomposite coating (e.g. the silica particles in chapter 8); (iv) the dissolution of salts in the monomer to form a dissolved salt–polymer composite (e.g. lithium perchlorate in chapter 8); (v) the concurrent introduction of co-reactant vapour (e.g. triflic anhydride in chapter 9). Potential applications could include the increased throughput of superhydrophobic plasma polymer perfluorinated coatings (conventional plasma polymerization's flagship application) or the use of dissolved salts in acrylic acid to form super-absorbent polymer coatings (e.g. sodium polyacrylate).

With all the methods presented within this thesis there is scope for going beyond fuel cell based applications into a wider plethora of coating uses. This is hinted at with the proof of concept studies in chapters 7 and 8. So in conclusion vapour-phase deposition provides a versatile range of techniques for the fabrication of functional coatings for use in proton exchange membrane fuel cells and a variety of other applications (including batteries, adhesives and bioactive surfaces).